Coventry University

DOCTOR OF PHILOSOPHY

Investigating the effect of top surface morphology on CO2 storage using numerical simulation

Ahmadinia, Masoud

Award date:
2021

Awarding institution:
Coventry University

Link to publication

Investigating the effect of top surface morphology on CO_2 storage using numerical simulation

By

Masoud Ahmadinia

2020

Coventry University

Certificate of Ethical Approval

Applicant:

Masoud Ahmadinia

Project Title:

Investigating the effect of top surface morphology on CO2 storage using numerical simulation

This is to certify that the above named applicant has completed the Coventry University Ethical Approval process and their project has been confirmed and approved as Low Risk

Date of approval:

04 March 2020

Project Reference Number:

P103108

Investigating the effect of top surface morphology on CO$_2$ storage using numerical simulation

By

Masoud Ahmadinia

A thesis submitted in partial fulfilment of the University's requirements for the Degree of Doctor of Philosophy

2020

Faculty of Engineering, Environment and Computing

Abstract

Geological carbon storage is a promising technology for reducing CO_2 emissions released into the atmosphere as one contribution to the Paris Agreement goals to limit the global temperature increase to $1.5°C$ (UNFCCC 2015). Among possible storage sites, deep saline aquifers have the largest storage capacity. Once injected into the aquifer, due to its smaller density compared to that of formation brine, the CO_2 in the free phase tends to migrate upwards and forms a thin layer below the caprock (a low permeable formation that prevents the free CO_2 plume from further upwards migration).

This work investigated the impact of the caprock morphology on CO_2 plume migration in the saline aquifer storage sites, especially in relation to elevation changes below the seismic detection range.. Several mathematical tools and methods have been employed throughout this work, such as analytical calculation, numerical simulation, vertical equilibrium (VE) modelling (MRST and EVE), and data analysis and optimisation. The impact of caprock morphology and aquifer boundary on the CO_2 storage process through 3D numerical simulation and analytical calculations were subsequently investigated. The effect of boundary conditions on the storage process shows that CO_2 dissolution in aquifers with one closed end (due to faults, salt walls, etc.) is higher than an open aquifer.

Moreover, the analytical approach shows promising performance for estimating the CO_2 storage capacity (and possibility), making it a suitable site-screening tool before performing numerical simulations. The results suggest that dissolution is strongly correlated with formation dip (the acute angle with a horizontal plane). In models with low vertical permeability, however, increasing the tilt angle resulted in a lower dissolution (opposite to what was observed in previous studies). The plume outline in VE and 3D models was found to be similar, and in terms of computational cost, MRST was found to outperform the rest significantly. The conventional 3D simulators could be computationally intractable for long-term geological CO_2 storage problems. Therefore, the feasibility of simplified, computationally inexpensive VE models in studying the CO_2 storage process was investigated over a wide range of scenarios with various caprocks. The results were compared with several full 3D simulation methods and show that the VE approach is an effective method to model the relevant physical effects of geological CO_2 storage.

An optimisation tool implemented using VE formulation was seen to improve the match between the observed and simulated plume outline in a synthetic model and the operational

Sleipner field storage site in Norway. The results show an improvement of around 8% in the Sleipner plume match resulting from an average absolute elevation change of 3.23 metres. Calibrating the porosity, permeability, CO_2 density and injection rate results in a 5% improvement in the match, and once caprock morphology is included in the optimisation process, the match improvement increases by 16%. Subsequently, and for the first time, the importance of caprock topography variations has been quantified in the Sleipner model in the presence of other uncertain parameters, including porosity, permeability, CO_2 density, injection rate and temperature, using data analysis tools. The results show that caprock morphology is the second most important parameter (after density) in controlling the CO_2 plume migration in the Sleipner field.

This work raises the scientific understanding of the complexity of the impact of the caprock morphology on CO_2 plume migration in a real field model for safe sequestration, such as the most recent Sleipner Benchmark simulation grid and implies that its impact on model predictions has previously been underestimated.

To my family

Acknowledgement

Foremost, I am heartily grateful to my supervisor Dr Seyed Shariatipour for offering me this PhD opportunity. His endless patience through my study and before arriving in the UK when he reserved the position for me while I was struggling to get a visa. I am thankful for his trust, encouragement, and thoughtful guidance and for keeping me always positive in the 'ups and downs'. I would like to express my sincere gratitude to my external supervisor Dr Odd Andersen for his continuous support and helpful scientific discussion and advice. I have learned a great deal from my supervisors and could not imagine having better supervisors than them.

I thank my colleagues and staff at the Centre for Fluid and Complex Systems, especially Dr Philip Costen and Dr Lorna Everall. It would not have been possible to conduct this research without their precious support and guidance. Although both have a busy schedule, they always take time to help. I also thank Doctoral College, UK CCS Research Centre and Centre for Global Engagement to support and provide the funding to attend conferences and visit other research centres.

My sincere thank also goes to SINTEF Digital and the computational geosciences research group, especially Dr Knut-Andreas Lie, Dr Halvor Nilsen, Dr Stein Krogstad and Dr Xavier Raynaud, for providing access to their facilities during my multiple visits and for their insightful comments and encouragements.

I would like to thank my parents, siblings, friends and acquaintances for their moral support, encouragement and motivation to accomplish my personal goals, including this PhD. Finally, my deepest gratitude to my caring, loving and supportive fiancée, Xiaojie. 我爱你.

Nomenclature

Symbols

Pc	Capillary pressure
P	Pressure
S	Saturation
S_{rw}	Irreducible water saturation
S_w	Wetting phase saturation
S_{nw}	Non-wetting phase saturation
$\bar{H}$	Effective aquifer height
ς_T	Aquifer top boundary
ς_B	Aquifer bottom boundary
ω_1	Angular frequency
θ	Aquifer tilt angle
c	Total molar concentration
k	Absolute permeability
k_r	Relative permeability
k_{rw}	Water relative permeability
k_{rg}	Gas relative permeability
W	Wavelength
λ	Fluid mobility
Λ	Upscaled fluid mobility
φ	Porosity
ρ	Fluid density
q	Volumetric flux,
u	Fluid velocity
μ	Fluid viscosity
g	Gravitational acceleration
ξ_B	Elevation of the bottom of the formation (surface)
ξ_I	Elevation at which two fluids are separated (surface)
f_g	Fractional flow function for gas phase
β	Regularization term
T_s	Seafloor temperature
Z_s	Seafloor depth

Subscripts

α	Fluid phase
w	Water
g	Gas
c	Capillary

Abbreviations

CCS	Carbon capture and storage
VE	Vertical equilibrium
EOR	Enhanced oil recovery
mD	milli-Darcy
SR	Structural relief
SDC	Sørensen–Dice coefficient
RM	Rate multiplier
DM	Density multiplier
MRST	Matlab reservoir simulation toolbox
KNN	K-nearest neighbours
DTree	Decision tree
RF	Random forests
SHAP	SHapley additive exPlanations
ST	Structural traps
LR	Linear regression
OFAT	One factor at a time
E100	ECLIPSE blackoil simulator
E300	ECLIPSE compositional simulator
EVE	ECLIPSE vertical equilibrium simulator
MVE	MRST vertical equilibrium simulator
HM	History matching

Table of contents

v: List of Tables

Chapter 1

Introduction

1.1. Geological carbon storage

Global warming, primarily caused by the rapid increase in carbon dioxide (CO_2) emissions from fossil fuel combustion, is one of the major issues of our time (Olivier, Schure and Peters 2017). One of the proposed solutions to tackle this problem is carbon capture and storage (CCS), which has the potential to decrease greenhouse emissions by up to 32% by 2060 (Abergel *et al.* 2017). The idea of CCS is to capture CO_2 emissions from large point sources, such as power plants or industrial facilities, transport it to a geological storage site, and inject it deep into the ground in a geological formation that can hold the CO_2 indefinitely. The best geological formations for safe and long-term CO_2 storage purposes are usually within sedimentary rock with an appropriate porosity and permeability to prevent the CO_2 from escaping. The injected CO_2 parameters, such as its volume, temperature and pressure and CO_2 solubility in brine (formation water), and the injection site environment, such as the reservoir caprock permeability, heterogeneity, formation thickness, the presence of reactive minerals, potential fault, stress regime, injectivity and fracture formation, should also be considered in any storage site selection process (Grataloup *et al.* 2009; Rodosta *et al.* 2011; Wei *et al.* 2013). Moreover, it is preferable to exploit a storage formation near the CO_2 emissions source, such as a power plant or another energy-intensive industry, to lower transportation costs (Grant *et al.* 2018).

Currently, CCS is generally about carbon storage in geological formations, such as saline aquifers, or used as an enhanced oil recovery (EOR) agent in hydrocarbon reservoirs (Bui *et al.* 2018). Given this scenario the long-term security of the storage process should be investigated in which the selection, characterisation, and monitoring of the storage site needs to be carefully addressed. It is worth mentioning that although we have learnt a lot from various storage projects worldwide, the reality is that geological formations are generally heterogeneous, and their properties vary significantly with location. Studies show that even a small-scale internal heterogeneity in sedimentary formations can affect the CO_2 trapping potential by creating capillary barriers to CO_2 migration (Behzadi, Alvarado and Lynds 2012; Trevisan, Krishnamurthy and Meckel 2017).

Various trapping mechanisms prevent the CO_2 from further migration. The major ones are dissolution and residual trapping, structural closures, mineral trapping, stratigraphic pitchouts and hydrodynamic traps (Bachu, Gunter and Perkins 1994; Potdar and Vishal 2016; Zhang, D. and Song 2014b). The free phase CO_2 injected into a saline aquifer tends to migrate upwards due to buoyancy, as its density is lower compared to that of the resident brine and subsequently forms a thin layer beneath the sealing formation. Therefore, the topography variations of the reservoir's upper boundary play a significant role in the CO_2 plume's migration direction. Other factors controlling plume migration include the type (closed or open) of aquifer lateral boundaries, driving forces (flow is driven by hydrodynamic, capillary and buoyancy forces and opposed by viscous and sometimes capillary forces), fluid properties, displacement characteristics of the CO_2-water system in sedimentary rocks (irreducible saturation and capillary entry pressure of CO_2) and aquifer properties, such as thickness, porosity, permeability and heterogeneity (Al-Khdheeawi *et al.* 2017a; Al-Khdheeawi *et al.* 2017b; Bachu 2015; Li, B. and Benson 2015). Besides these factors, using various simulation tools may also result in differences in predicting CO_2 migration. For example, several simulators were employed by academic and industry experts to study three fundamental CO_2 storage problems. The results were not in general agreement, particularly for a problem relating to the upwards migration of the CO_2 plume in part of the Johansen formation in Norway (Class *et al.* 2009).

High vertical grid resolution would be required to represent the vertical phase distribution of the thin CO_2 plume beneath the caprock (Nilsen, Lie and Andersen 2016a). Moreover, the lateral grid resolution direction should be sufficiently high for two main reasons: first, to retain the small-scale topography variations in the geological model, which can retard the plume migration and divert its path; and second, to resolve the unstable dynamics of convective dissolution which may retard and limit the plume migration (which also requires high vertical resolution). Conventional 3D reservoir simulators are frequently computationally impractical to address long-term CO_2 storage problems for high-resolution models (Nilsen, Lie and Andersen 2016a). It is, however, possible to model most of the relevant physical aspects of long-term CO_2 storage using dimensionally reduced models, as has been investigated in previous studies (Bandilla, Karl and Celia 2019; Gasda, Sarah E., Nordbotten and Celia 2009; Nilsen, Lie and Andersen 2016b; Nordbotten, Jan Martin and Celia 2011). Using a model based on the assumption of vertical equilibrium, the problem dimension can be reduced from 3D to 2D. This significantly reduces the number of unknowns that need to be solved in the equation system, reducing the computational cost considerably. Consequently, it is possible to increase

lateral grid resolution beyond what would be practical in full 3D simulations. The full 3D model can be reconstructed from the 2D one (Nilsen, Lie and Andersen 2016b) as a post-processing step.

The impact of caprock morphology on CO_2 storage in saline aquifers, however, has previously been underestimated. General seismic surveys are proficient in detecting large-scale features in the caprock, including domes, traps and spill points. Their detection level, however, does not cover rugosity (the variation in structural relief below 10 m). LiDAR scanning of outcrops with a typical resolution between 0.1 to 1 metres, can provide evidence of geological features not evident in the seismic investigation. LiDAR is a technique for determining the distance to an object by transmitting a laser beam and measuring the time the light takes to return to the transmitter (Jackson *et al.* 2010). Sine-wave shaped structures present in the natural geological setting influence the CO_2 storage process (Ambrose *et al.* 2008). It is necessary to quantify and find the sources of uncertainty in the data representing the geological model as if this is not undertaken, it introduces errors into the simulation process.

This work shows that implementing realistic caprock characteristics will lead to a better prediction of plume migration and trapping, which is essential for screening and planning optimal storage sites. Most of the previous studies undertaken on CO_2 storage employed a one factor at a time (OFAT) approach (Allen, R. et al. 2018), where the response to one parameter is investigated, and the rest are kept at their initial value. The current work shows the limitation of the OFAT approach in the most recent Sleipner Benchmark model. This study introduces a more reliable method to simultaneously analyse the impact of six uncertain parameters, including porosity, permeability, CO_2 density, caprock morphology, reservoir temperature and pressure, by running one million sets of simulations. Moreover, this is one of the most comprehensive studies comparing the performance of a wide range of mathematical tools including full 3D and vertical equilibrium-based simulation approaches (E100, E300, EVE and MVE), analytical methods and adjoint-based optimisation tool to study the impact of caprock morphology, with the focus on small scale topography changes, on CO_2 storage migration in saline aquifers.

1.2. CO₂ Storage in saline aquifers

Among the proposed options for CO_2 storage projects, previous research shows that deep saline aquifers have the greatest storage potential (Benson et al. 2005; Gasda, S. E., Nilsen and Dahle 2013; Nilsen, Lie and Andersen 2016a). A promising, generic aquifer for CO_2 storage purposes would be located at depths more than 800m at which CO_2 can be in the supercritical phase

(Chadwick, A. *et al.* 2008; Gunter, William D., Bachu and Benson 2004). A saline aquifer has a considerably higher temperature than found at the surface, as the average thermal gradient of the earth is about 25-30 °C/km (Vandenberghe *et al.* 2000; Wolfson and Wissler 2007). Depending on the geothermal gradient, at depths below 800–1000 m, CO_2 becomes supercritical and has a liquid-like density of around 500–800 kg/m^3 (Metz *et al.* 2005). Supercritical CO_2 behaves in a similar manner to liquids and gases in terms of density and compressibility, respectively (Perera *et al.* 2011) and occupies a much lower volume than CO_2 in the gaseous phase (Haghbakhsh *et al.* 2013). In this form, CO_2 has a lower buoyancy force which increases storage efficiency with increasing depth (Bachu 2002). On the other hand, as higher injection pressures are required for deep aquifers to tackle hydrostatic pore pressures, it is important to find an aquifer at an optimum depth to minimize the operational costs (Bachu 2015). Current and previous operational CO_2 storage projects in saline aquifers are listed in Table 1.1.

Table 1.1. List of current and previous worldwide operational CO_2 storage in saline aquifers.

Project	Location	Scale[*]	Start	Status	Injection rate (Mt/year)	Reference
In Salah	Algeria	C	2004	Suspended in 2010	1.3	(Kelemen et al. 2019; Riddiford et al. 2005; White, J. A. et al. 2014)
Quest	Canada	C	2015	In operation	1.1	(Ajayi, Gomes and Bera 2019; Brydie *et al.* 2014; Bui *et al.* 2018)
Aquistore	Canada	P	2012	In operation	0.146	(Michael *et al.* 2009; Worth *et al.* 2017; Worth *et al.* 2014)
Ordos	China	P	2010	Ended in 2015	1	(Ajayi, Gomes and Bera 2019; Li, C. *et al.* 2016)

Ketzin	Germany	P	2008	In operation	0.06	(Ajayi, Gomes and Bera 2019; Schilling *et al.* 2009)
Minami-Nagaoka	Japan	P	2002	In operation	0.015	(Ajayi, Gomes and Bera 2019)
Sleipner	Norway	C	1996	In operation	0.9	(Allen, D. J. and Brent 2010; Furre, A-K *et al.* 2019; Furre, Anne-Kari *et al.* 2017; Hansen, H., Eiken and Aasum 2005)
SnØhvit	Norway	C	2008	In operation	0.7	(Furre, A-K *et al.* 2019; Hansen, O. *et al.* 2013; Maldal and Tappel 2004)
Frio	USA	P	2004	Ended	0.065	(Ajayi, Gomes and Bera 2019)
Decatur	USA	C	2011	Ended in 2014	1	(Ajayi, Gomes and Bera 2019; Finley 2009; Hnottavange-Telleen, Krapac and Vivalda 2009; Kelemen et al. 2019; Leetaru, Couëslan and McBride 2009)
Cranfield	USA	P	2009	In operation	1-1.5	(Ajayi, Gomes and Bera 2019; Lu, J. *et al.* 2013; Lu, Jiemin *et al.* 2012)
Citronelle	USA	P	2011	Ended in 2013	0.25	(Ajayi, Gomes and Bera 2019; Haghighat *et al.* 2013)
Teapot Dome	USA	P	2006	Ended	0.062	(Ajayi, Gomes and Bera 2019; Friedmann and Stamp 2006)

Sleipner in Norway is the first CO_2 storage project in a saline aquifer at a commercial scale (Ghosh, Sen and Vedanti 2015; Torp and Gale 2004). The project started in 1996 using a saline aquifer located at a depth between 800 m to 1,000 m beneath the sea, with the CO_2 provided by a nearby natural gas processing field (Arts *et al.* 2004; Head *et al.* 2004). The Sleipner field of the Utsira storage formation is late Cenozoic, a 200-250 m thick sandstone that has stored 17.8 Mt of CO_2 by 1 January 2019 (Furre, A-K *et al.* 2019), while the caprock formation is a Nordland shale with a thickness of 200-300 m (Nooner *et al.* 2007). About three years after the start of the project, the plume migrated through several thin layers of mudstone within the sandstone formation and stopped beneath the Nordland shale caprock. These layers help the dissolution process as they increase the interaction time between the brine and the CO_2. The risk of leakage through all stages of the storage process has been managed (Arts *et al.* 2004), and no leakage of CO_2 has been detected from this storage formation. The injected CO_2 into this layer is limited from further upwards migration by thick shale caprock. The seismic studies show that the mudstone layers physically trap the CO_2 within the sand formation (Ringrose and Oldenburg 2018).

The Snøhvit gas field is located in the Barents Sea 150 km from the coast and has been operated by Equinor since 2007. The produced gas contains 5-8% CO_2, separated and transported back to the geological storage field (Chiaramonte, White and Trainor-Guitton 2015) via a 150 km pipeline. The Snøhvit CO_2 storage project is the second-largest offshore CCS project to date (Buscheck *et al.* 2016). The transported CO_2 has been injected into a saline formation (since 2008) at a depth of 2600 – 26700 m below sea level, located next to the field. By April 2011, the aquifer had stored 1.09 million tonnes of CO_2 (Buscheck *et al.* 2016).

1.3. CO_2 Trapping mechanisms in saline aquifers

Various physical and geochemical mechanisms take place to store the injected CO_2 in the saline aquifer securely. There are four major trapping mechanisms, identified below:

1.3.1. Mineral trapping

The geochemical reactions between the dissolved CO_2 in brine and the surrounding rock result in secondary minerals' precipitation (Gunter, WD, Wiwehar and Perkins 1997; Pruess, K. et al. 2001). The process depends on several parameters, including rock type, composition, porosity, available reactive surface area, etc. (De Silva, Ranjith and Perera 2015). For example,

the reaction of CO_2 with carbonate-rich rock is much higher than other types of grain, such as quartz, which consequently increases the amount of mineral trapping (Newell and Ilgen 2019).

1.3.2. Residual trapping

Both the CO_2 plume and the displaced formation brine migrate away from the point of injection. During the post-injection period, however, the CO_2 and brine migration is strongly influenced by fluid density differences, and they move upwards and downwards, respectively. Therefore, the wetting phase (i.e. brine) displaces the CO_2 resulting in the disconnected CO_2 becoming trapped in the pores (Juanes *et al.* 2006; Kumar *et al.* 2005; Zhang, D. and Song 2014a).

1.3.3. Dissolution trapping

Dissolution trapping is regarded as the most effective storage mechanism, as it reduces the risk of buoyancy pressure and leakage effects on the caprock (Pruess, K. et al. 2001). The dissolution of CO_2 into the formation brine is controlled by the chemical potential, gravitational forces and density difference. Convective mixing (i.e. the transport of fluid driven by density differences), which generally occurs because the density of the CO_2-saturated water is about 1% greater than the unsaturated water density, is understood to be the dominant mechanism in the dissolution process (Pruess, K. et al. 2001; Riaz et al. 2006). The level of solubility depends on pressure, temperature, salinity and the type of formation. According to Hassanzadeh *et al.*, (Hassanzadeh, Pooladi-Darvish and Keith 2009), the solubility decreases for lower caprock tilt angles and higher permeability anisotropies. This is due to the retardation of the vertical plume migration and convective mixing. On the other hand, another study (Chen, Zeng and Shi 2013) reported that the dissolution mass is higher in heterogeneous aquifers, leading to increased storage capacity.

1.3.4. Structural and stratigraphic trapping

Stratigraphic traps result from changes in the depositional or diagenetic setting of the formation where the geometry of the depositional facies, together with its continuity, are the main parameters (Ambrose *et al.* 2008). Stratigraphic heterogeneities control the permeability distribution as they influence the inter-bedding between sandstones and mudstones. Moreover, the fluid's migration path is a strong function of the origin of the deposits, as it controls the stratigraphic structure in the formation (Galloway 1984; Morton, Jirik and Galloway 1988).

Structural traps, which play a key role in CO_2 storage, are geometries in folded shapes or permeability barrier faulted rocks (Richards *et al.* 2015). Following the injection of CO_2 within the aquifer, the structural trapping mechanism plays a role in keeping the plume within the storage formation (Newell and Ilgen 2019). The focus of the current work is on the structural trapping mechanism.

1.4. Thesis overview

1.4.1. Aims and objectives

This aim of this thesis is to determine the role of caprock morphology on CO_2 storage trapping and migration mechanisms in saline aquifers. The focal point of the analysis is the caprock elevation changes below the seismic detection range (~10m, referred to as rugosity), which are consequently not accurately represented in geological models employed in reservoir simulators. The research objectives to achieve the aim are as follows:

1. A study of the impact of caprock morphology on the CO_2 storage process.

2. An analysis of different simulation methods and a comparison of their performance in terms of accuracy and computational cost

3. A determination of whether considering the caprock morphology as a history matching parameter improves the final match between observed and simulated plume outline in a real case study.

4. A quantification of the importance of caprock morphology in a real CO_2 storage project in the presence of other uncertain parameters.

1.4.2. Research questions

The work addresses the following questions:

- What are the roles of numerical and analytical approaches in studying the impact of caprock morphology in a CO_2 storage project?

- What is the alternative (and possibly more efficient) computational method, besides full 3D simulations, to quantify the role of caprock morphology in long-term CO_2 storage?

- How does caprock morphology improve the match between an observed and simulated plume outline in a real case CO_2 storage site, such as Sleipner, if it is considered the only history matching variable?

- In a real case problem, how significant is an uncertainty in caprock morphology in the presence of other sources of model uncertainty?

The injected CO_2 plume might migrate several hundred kilometres in the lateral direction with minimal vertical movement. Therefore, a high resolution in the horizontal direction is essential in CO_2 storage problems to analyse the impact of caprock topography changes on plume trapping and migration behaviour. The first two research questions are focused on finding more

computationally tractable methods than full 3D simulators for CO_2 storage studies. Due to the significant difference in fluid densities, soon after the injection, the injected plume forms a continuous layer beneath the caprock. Therefore the shape and characteristics of the caprock can control the fate of an injected plume. The third and fourth research questions provide qualitative and quantitative assessments on the impact of caprock morphology on CO_2 storage.

1.4.3. Thesis structure

The thesis continues with the following chapters:

Chapter 2 presents the material synthesised from the available literature on the subject in an organised way. It provides information about the nature of caprock, followed by a critical analysis of previous work to find the gaps in current knowledge on the topic.

Chapter 3 looks at the impact of top surface morphology and the reservoir boundary on the CO_2 plume advancement, together with structural and dissolution trapping mechanisms, using numerical simulations and analytical calculations. Several models are synthesised using various equations to build-up an impression of the contact between the caprock and aquifer. The conditions under which structural trapping exists, together with its storage capacity, is calculated using analytical methods, and the results are later compared to those using a compositional simulator.

While the compositional simulator used in Chapter 3 showed promising results, its high computational cost restricts its use, e.g. increased lateral grid resolution beyond a limit. Therefore, **Chapter 4** looks for a more efficient simulation tool to study the impact of caprock morphology on CO_2 storage. For this purpose, the performance of four simulators, including ECLIPSE vertical equilibrium, ECLIPSE black-oil, ECLIPSE compositional and the Matlab reservoir simulation toolbox (MRST) vertical equilibrium, are compared. The aim is to find an approach with reasonable accuracy and low computational cost.

Chapter 5 aims to find the importance of considering the caprock morphology as a history matching parameter. For this purpose, after making sure about the performance of MRST in the previous chapter, an optimization tool is added to the simulation code implemented in MRST. The optimization tool is first tested on a synthetic model to find the match between observed and simulated plume outline. In the second part of the Chapter, the optimization tool is applied to the Sleipner model to minimize the mismatch between the data from seismology and simulation by changing the caprock morphology only.

So far in previous chapters, the importance of considering the uncertainties in caprock morphology in a CO_2 storage study in a saline aquifer are shown. **Chapter 6** quantifies the

importance of this uncertainty in the presence of other model uncertainties, such as in temperature, density, injection rate, porosity and permeability. For this purpose, the focus is on the CO_2 storage site, Sleipner in Norway. Data analysis tools are used to quantify the importance of caprock morphology in the presence of other uncertain parameters reported in the literature for the Sleipner model after running one million simulations.

Chapter 7 represents the main conclusions together with recommendations for future studies.

Chapter 2

Literature Review

2.1. Caprock properties

2.1.1. Caprock lithology

Caprock is a very low permeable geological unit that prevents the upwards migration of fluid, leading to the formation of a reservoir below. Considering the low permeability criteria and based on Figure 2.1 (Beauheim and Roberts 2002), caprock is often formed from shale or evaporite, which are different forms of sedimentary rock.
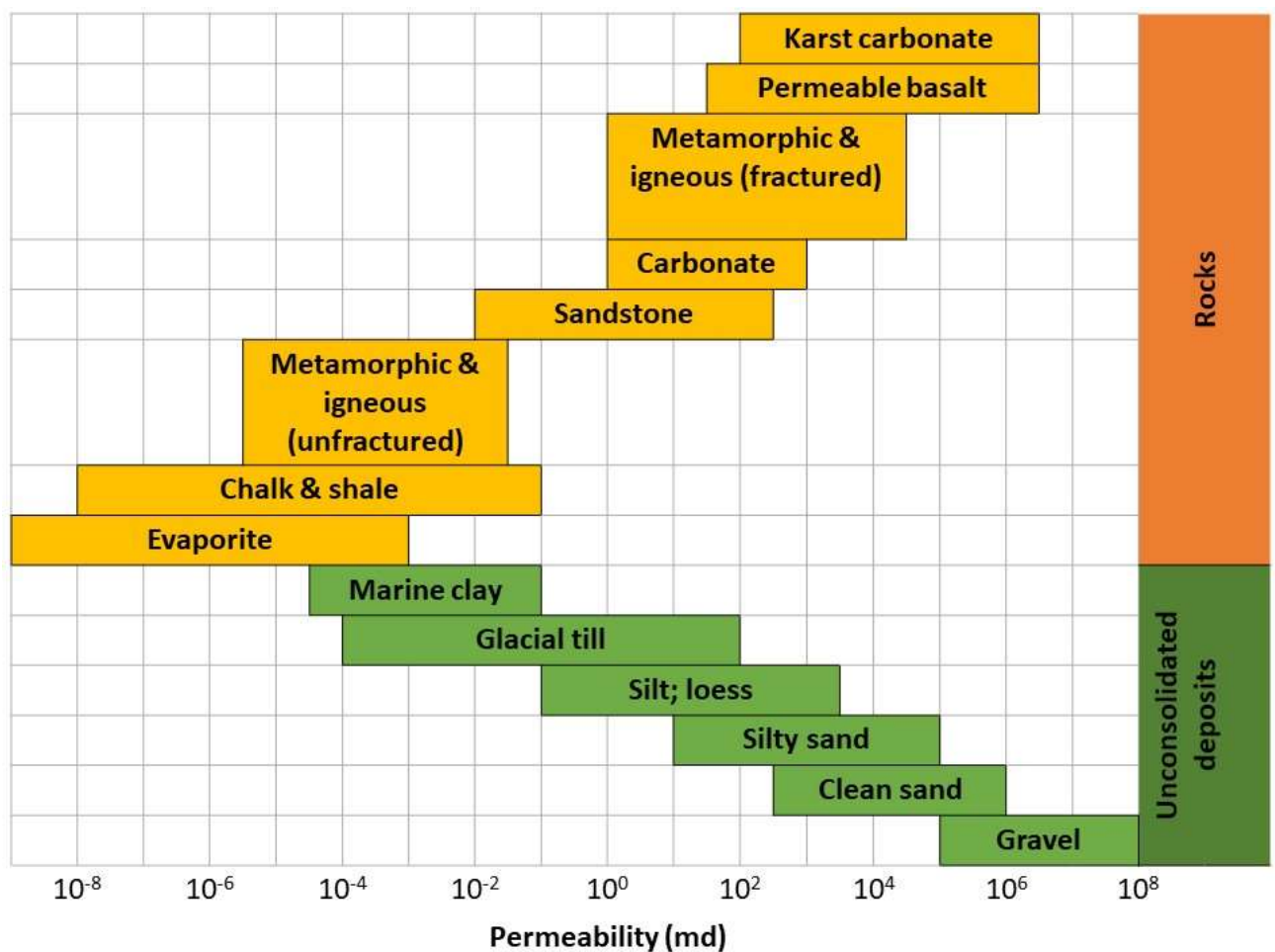
Figure 2.1. Relative ranking of permeability of various lithologies (Beauheim and Roberts 2002)

Shale is the most common sedimentary rock and is comprised of compacted mud containing clay and various minerals, including quartz, calcite, mica, etc. Shale is typically formed in slow deposition environments, such as lakes, swamps and ocean flow, through compaction. Heavier components sink first and eventually form sandstones and limestone, while fine particles

remain suspended in the water above (Schieber, Zimmerle and Sethi 1998; Vine and Tourtelot 1970).

Due to its small particle size, shale can serve as a caprock to block (or limit) the fluid flow as in the Melke and Spekk formations in Norway (the Viking group) which are interbedded with shale and mudstone (Bugge, Knarud and Mørk 1984).

Although evaporites are the least common sedimentary rocks, 14 and nine of the world's largest oil and gas fields, respectively, are sealed by them (Warren 2017). Even at shallow depths of a few hundred metres, they act as a pressure seal, (i.e. an impermeable rock, with zero transmissivity sustained over long periods of geologic time) which is not necessarily the case for thick shale layers (Warren 2017). The nature of the sealing in the Kalundborg CO_2 storage site in northern Denmark, for example, is evaporate. (Larsen *et al.* 2007).

2.1.2. Caprock morphology

Once injected into a saline aquifer, a portion of CO_2 will be securely stored through various processes, including structural, dissolution, residual and mineral trapping. At the same time, the remainder remains as a free phase. CO_2 is generally injected in a supercritical state (for space utilization purposes), and depending on the storage conditions, is stored as a gas, liquid or in a supercritical phase. Regardless of the phase, the injected CO_2 has a lower density than the formation water. Formation water is a mixture of originally trapped fluids, such as seawater and fluids, modified by rock–water interaction (hydration or dehydration reactions or crustal transport). Formation water exists naturally in the rock all along, before drilling. Consequently, shortly after the end of the injection period, most of the free phase CO_2 will migrate upwards due to buoyancy to lie beneath the seal. Therefore, the structural geometry of this low permeability seal may influence the long-term storage and plume migration of the CO_2. Figure *2.2* illustrates the caprock/ CO_2 interaction as well as the CO_2 migration and trapping process.
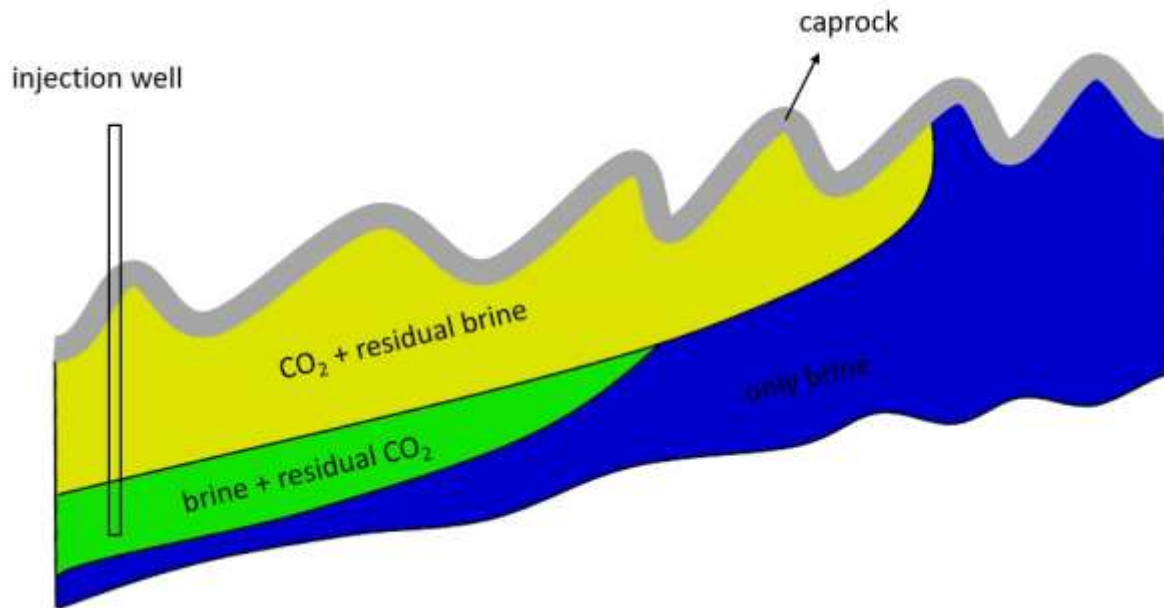
Figure 2.2. CO_2 and caprock interaction during the storage process

Most caprocks are sedimentary rocks, mainly deposited horizontally (Gasda, SE, Celia and Nordbotten 2008). However, they may become tilted over the long term, after the imposition of various tectonic forces. These structures, such as tilted beds, folds, etc., that we observe in the field are controlled by several processes such as pressure and temperature changes during the deformation of sedimentary rocks, which do not necessarily operate independently. Sinusoidal structures are formed throughout the deformation of strata and the deposition of sediments. They are common in sedimentary rocks and are observed at various scales, from microscopic to regional, of which the main types are folds and bedform (Tucker 2011).

Folds, which are known to be the largest type of sinusoidal features in geological settings, result from the non-isostatic pressure or so-called stress. There are three broad classes of folds, namely anticlines, synclines and monoclines (Fossen 2010). Table 2.1 illustrates the scales of sinusoidal structures observed in geologic environments (Han and Kim 2018a). As shown in Table *2.1*, folds occur along the entire geologic scale, from a thin section to the entire basin. Sinuous unfaulted symmetric folds are observed within numerous folds and thrust belts on a scale of hundreds of metres (Fossen 2010). In large scale basins (tens of kilometres), the caprock morphology is identified by domes and anticlines (Gasda, S. E. *et al.* 2012), which are in a seismic observation range greater than 10m (Jackson *et al.* 2010). The structural relief (SR) variation below 10 m is referred to as rugosity, which is not evident in current seismic investigations employed for deep geological storage formations but can be detected using

LiDAR scanning of outcrops and geostatistical earth models (Jones *et al.* 2009; Pringle *et al.* 2010).

Bedforms are geological features that are omnipresent in various environments, including eolian, fluvial etc. They are sine wave-shaped morphological features developed through the interaction of unconsolidated sediments and fluid flow (Miall 2013; Mountney 2012; Reading 2009). Bedforms are characterised based on their size and shape (Table 2.1), and their scale is regulated based on grain size, medium velocity (air or water) and flow depth. For instance, Eolian dunes, which are regularly spaced bedforms, have a wavelength between 5-250 m (Wilson 1972).

Table 2.1. The scale of different structures available in geological settings (Han and Kim 2018a).
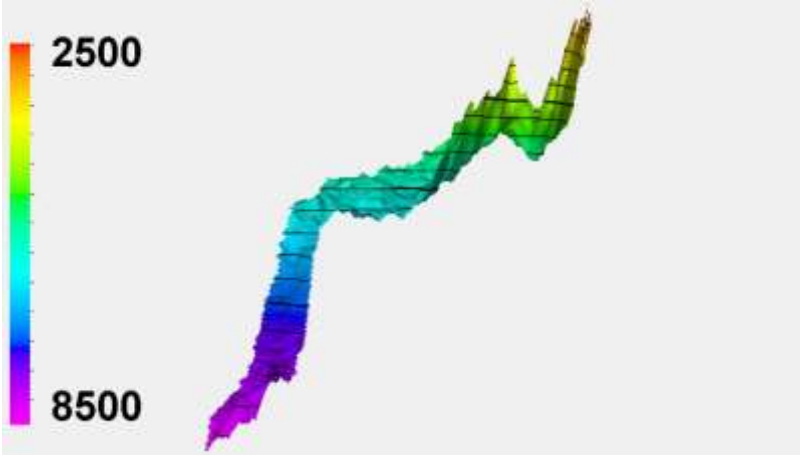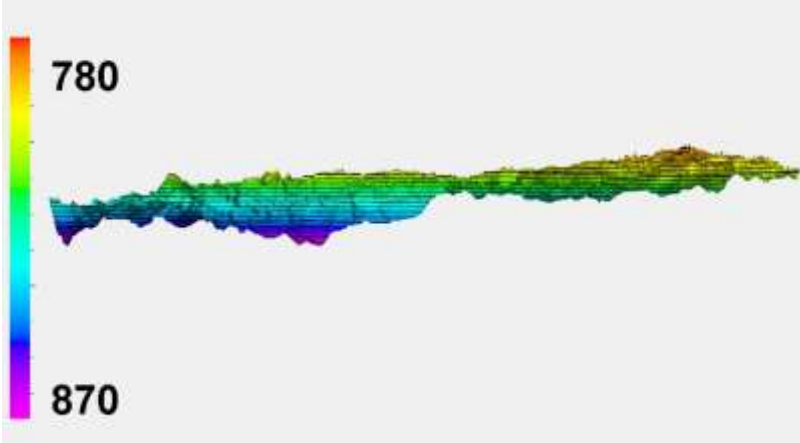
Type	Thin section (mm)	Hand sample (cm)	Outcrop (m)	Basin (km)
Structure folds	Folds			Antiforms / Synforms
Sedimentologic bedform		Ripples	Dunes	Draas

There have been numerous studies on CO_2 storage processes in dipping saline aquifers (Flett, Gurton and Weir 2007; Goater, Bijeljic and Blunt 2013; Jing et al. 2014; Wang et al. 2017). Formation dip has proven to significantly influence the storage process, including the residual and dissolution trapping (Kumar *et al.* 2005), up-dip migration and plume stabilization (Doughty and Pruess 2004). In some demonstration storage sites, the formation has preserved various dip angles from high ranges, such as Nagaoka in Japan (Mito, Xue and Ohsumi 2008) and Ketzin in Germany with 15° dip (Forster *et al.* 2006), Frio in Texas with 16°dip (Hovorka *et al.* 2006), to low ranges including the Vedder formation in California with a 7° dip (Doughty 2010). The dip angle is measured using geological basin maps and databases (Gasda, S. E. *et al.* 2012). The real case examples of these impacts also exist in the seismic survey of the plume migration in the Utsira Sand in Norway (Hermanrud, Christian *et al.* 2009).

The characteristic dip angle resulting from any regional uplift may be constant for hundreds of kilometres. However, the topography on a kilometre scale could change more and contain different types of antiform structures such as domes and anticlines that can be detected in

seismic surveys (Nilsen, Lie and Andersen 2016a). Table 2.2 summarises the structural properties of some saline aquifers, including their SR range, which are in a different development stage for real CO_2 storage projects.

Table 2.2. The structural properties of some real and potential storage sites. All figures are exaggerated by a factor of 25 in the z-direction.

Name	3D view (vertical axis represents the depth)	Location	SR range (m)	Status[*]
Captain X		North Sea	10-300	D
Sleipner		North Sea	5-10	O
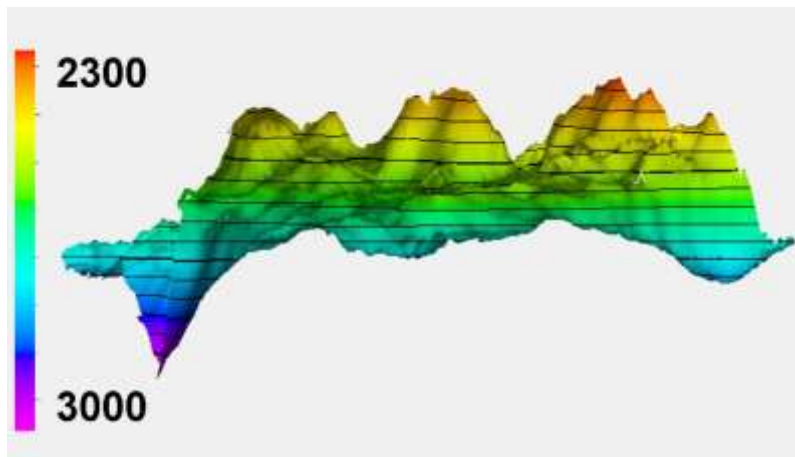
Forties 5 Site 1		North Sea	10-50	D
Johansen		West coast of Norway	10-50	D
Froan		Norwegian Sea	10-20	D
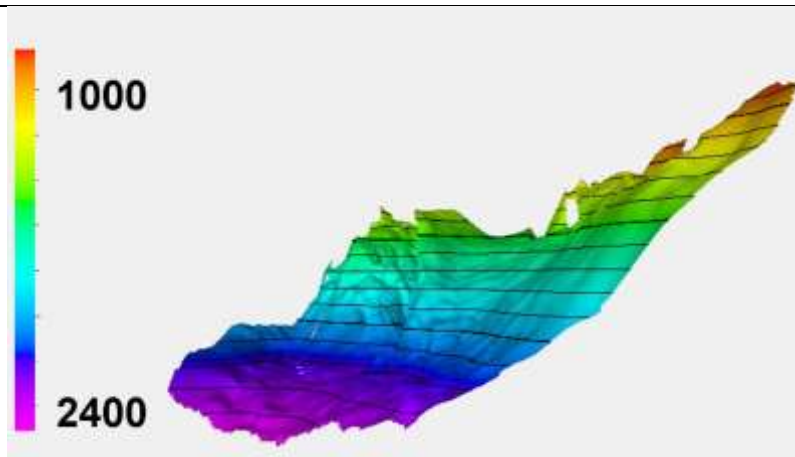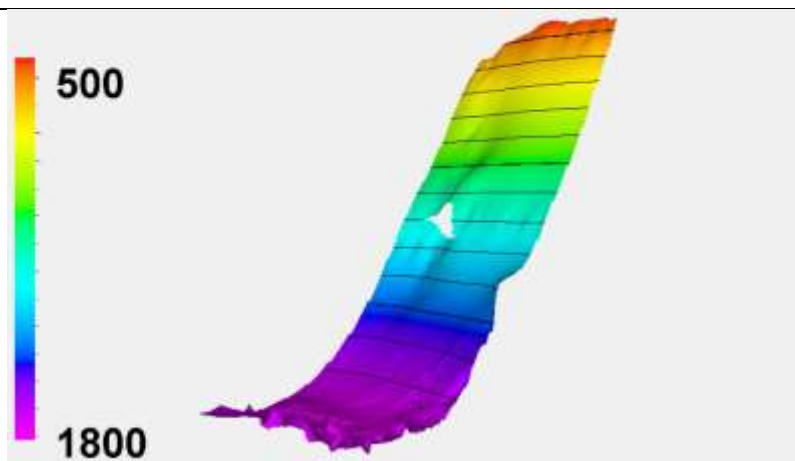
| Bunter Closure 36 | | North Sea | 200-700 | D |
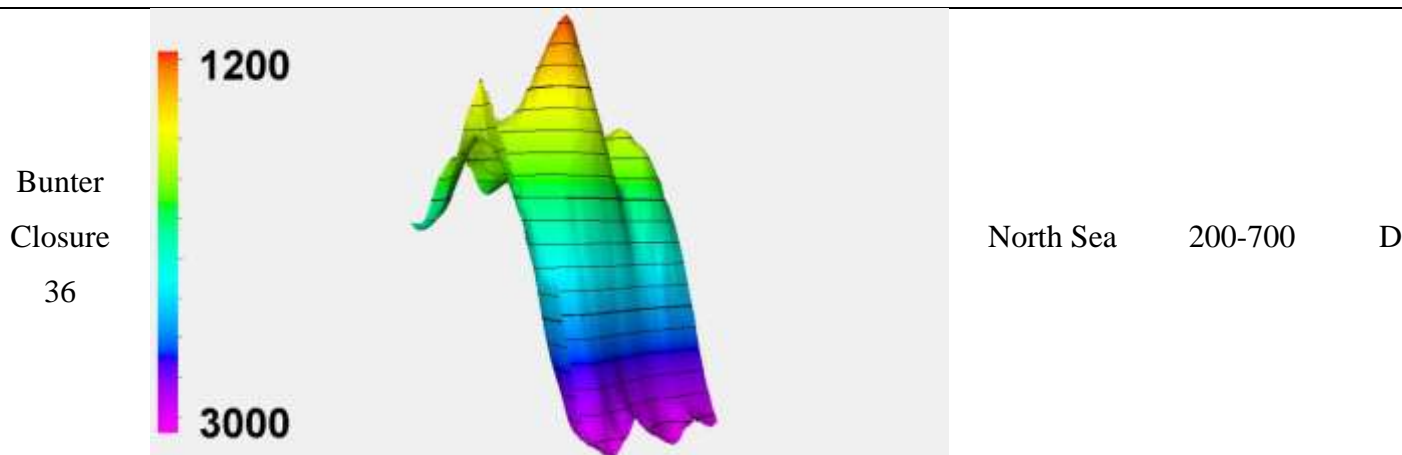
* D: developing; O: operating.

2.2. Literature review

Several research studies investigated the impact of caprock morphology on the CO_2 plume migration through numerical and analytical methods using realistic (Allen, R. et al. 2018; Nilsen et al. 2012) and synthetic models (Ahmadinia, M., Shariatipour and Sadri 2019; Han and Kim 2018a; Shariatipour, Seyed M., Pickup and Mackay 2016). It has been suggested that the nature of the caprock could be a source of the poor match between the observed and simulated plume outline in the Sleipner (Bandilla, Karl W., Celia and Leister 2014; Nilsen et al. 2017; Zhu et al. 2015). Some of the previous works on the importance of caprock morphology and slope on CO_2 storage are reviewed here.

The storage security of the site needs to be investigated carefully for long term CO_2 sequestration. The change of CO_2 from a free to a trapped gas, dissolved into the aqueous phase and precipitating on solid surfaces, is desirable and needs further investigation as this increases storage security. To fulfil this goal, Pruess and Nordbotton (Pruess, Karsten and Nordbotten 2011) performed numerical simulations using the TOUGH2-MP/ECO2N code for CO_2 storage in an aquifer with a tilted caprock. They considered a set of ideal fluid, rock and model properties. The aim was to focus on the fluid flow mechanisms, CO_2 migration and dissolution. Their results show that the buoyancy-driven plume migration dominates after injection ends, whereas, during the injection phase, the CO_2 pressure pushes the brine out of the pores. Although the plume thickness decreases as the CO_2 advances, the speed remains unaltered. The migration speed in the vertical equilibrium (VE)-based simulation model is higher than its actual value, which could be due to the vertical flow not being considered in the VE model. The permeability anisotropy acts as a resistance to the fluid path and thus slows the vertical flow. The results also showed a different mechanism in the cells located near the injection well,

where the plume displaces the water outwards due to its higher pressure. When it reaches the caprock, however, when the water displacement is mostly downward as the plume, due to its lower vertical pressure gradient, it has a higher tendency to move upward. The dissolution-diffusion-convection process increases the CO_2 dissolution sharply in the early injection stages, followed by a steadier state. The work could be improved by taking the heterogeneity, salinity, hysteresis (in relative permeability) into account.

Nilsen *et al.* (Nilsen et al. 2012) employed a systematic approach to investigate the effect of storage site properties and geometry on the carbon sequestration. They focused specifically on the top surface morphology and investigated the impact of geological heterogeneities on CO_2 capacity. Two types of the geological feature were considered in their study to apply the fold traps, namely offshore sand ridges (OSS) and a flooded marginal marine setting (FMM) built using a Gaussian random field. Three sets of configurations were investigated, namely a flat depositional topography with exclusively fault traps, an un-faulted system where there are only folded traps and a case with a combination of both. The structural trapping capacity was calculated through a spill-point (the structurally lowest point of the trap that can retain CO_2) approach and geometric analysis to reduce the computational cost. The CO2lab module of the Matlab Reservoir Simulation Toolbox (MRST) is a set of open-source simulation and workflow tools to study the long-term, large-scale storage of CO_2 (Lie 2019; Nilsen et al. 2015). Using the CO2lab module, they calculated the total available volumes (free, residually and structurally trapped) for all the models. The results showed the feasibility of the spill-point method in estimating the structural traps. While a simple volume analysis provides a good estimation of structural trapping, residual trapping must be calculated through detailed flow simulation.

Furthermore, regarding residual trapping, while using the flow simulation, not all the plume reached the top surface in OSS, which resulted in a smaller volume than the one resulting from the spill point method. The same statement applied to the FMM. The plume follows a single trail in the spill point for the flat case while it spreads laterally in the flow simulation method, resulting in a larger volume than the spill point method.

The impact of rugosity on plume migration using the static equilibrium upscaling was discussed by Gasda *et al.* (Gasda, S. E. *et al.* 2012). While some of the modelling studies employ computationally expensive approaches, such as local grid refinement (LGR) to include heterogeneity, they used the VE method to decrease the computational cost. They questioned the widespread application of a simplified top surface morphology on the CO_2 storage problem and showed that neglecting surface roughness in geological models generally leads to an

overestimation of the migration speed. Moreover, the roughness provides additional storage capacity for the CO_2. Their results also indicated that caprock topography could control the long-term CO_2 plume migration by reducing its maximum extent and trapping the CO_2 beneath the structural features. Top surface morphology also affects the dissolution trapping mechanism. The dissolution is expected to be higher in tilted reservoirs compared with flat ones, as the injected CO_2 has more space to migrate upwards and interacts with more formation brine. Large structural traps, such as sand ridges or anticlines, result in a lower dissolution as the CO_2 has less of an interaction with the formation brine.

In a later work (Gasda, S. E., Nilsen and Dahle 2013), the authors evaluated the importance of key structural parameters (including amplitude and wavelength of small scale structural traps) in controlling the CO_2 plume migration and trapping, compared with other mechanisms such as capillary trapping. While amplitude plays a significant role in the amount of structural trapping, the plume dynamics are mainly affected by the trap spacing, spill-points and formation dip angle. They also investigated the impact of topographic parameters on the up-scaling process and argued that the geological models characterised by shorter wavelengths are more suitable for up-scaling while those with longer wavelengths can be sufficiently resolved. They also showed that once CO_2 is flowing, the shape of an upscaled relative permeability curve is controlled by the structural characteristics that contribute to surface roughness, including structural relief, dip angle and spill point ratios. They defined the spill-point ratio to compare the distribution of spill-point depths over the area. A large ratio shows a more significant difference between the depth of the shallowest and deepest part of the trap and, consequently, higher surface roughness. Their work helps simplify the model and reduce the computational cost by effectively upscaling the topographical heterogeneity below the model resolution scale.

Goater et al. (Goater, Bijeljic and Blunt 2013) focused on the dynamic and spatially varying effects of CO_2 flow in dipping saline aquifers with no significant large-scale structural closure (such as domes or fault sealing traps). They improved the previous studies on the field as below: Gammer *et al.* (Gammer et al.) worked on the UK Storage Appraisal Project (UKSAP) considering the sensitivity of storage capacity in a dipping aquifer with a smooth top surface. Their work showed that aquifer permeability and formation dip were the main parameters affecting storage efficiency. Goater et al. (Goater, Bijeljic and Blunt 2013) improved their work by implementing top surface elevations into the models and showed that ignoring the caprock topography may underestimate storage capacity. As mentioned earlier, Nilsen et al. (Nilsen et al. 2012) used spill-point analysis and VE modelling to analyse the trapping in the top surface

structure of a dipping aquifer. Goater et al. (Goater, Bijeljic and Blunt 2013) improved their work by combining the effect of permeability, formation dip, top surface topography, injection rate, migration speed and pressure in their study.

Moreover, while other studies (Chadwick RA and Noy DJ. 2010; Jin et al. 2012; Pickup, Gillian Elizabeth et al. 2011) showed the importance of top surface morphology on the overall CO_2 plume migration, Goater *et al.* (Goater, Bijeljic and Blunt 2013) performed a systematic analysis of the impact of the top surface topography. They introduced four topographical features to smooth the models, including structural closures, and regions with a lower and higher dip than the model average and channels. Implementing structural closure and channels resulted in higher and lower storage efficiencies, respectively. The impact of higher and lower dip on storage efficiency was harder to explain and appeared dependant on the regime categorisation of the equivalent smooth model. For instance, a high dip region could decrease storage efficiency when the CO_2 plume in the equivalent smooth model was not limited by the migration velocity of the CO_2 nor its pressure.

Shariatipour et al. (Shariatipour, S. M., Pickup and Mackay 2016) studied the effect of tilt, rugosity and permeability anisotropy in CO_2 storage migration and trapping in a saline aquifer. They considered the domain's effect between the aquifer and the caprock (transition zone) on the CO_2 dissolution and movement, which was neglected in previous studies. Three sets of models were considered, with two created to investigate the aquifer/caprock morphology, where ridges were either parallel (para model) or perpendicular (perp model) to the tilt. Using impermeable interbedded shale layers, the effect of the transition zone was considered in the third set. Their results showed that the impact of the permeability anisotropy on migration speed was dominant during the injection phase.

In addition, while permeability anisotropy altered the migration distances in the post-injection phase, the tilt angle became the dominant parameter during this period. The trapping was limited in the tilted scenarios, and the authors derived a formula to find the maximum possible tilt for trapping. Their results also showed the opposite impact of the amplitude of rugosity in the perp and para models. While it increased the plume migration distance in the perp(endicular) mode, the same rugosity resulted in a smaller plume extension in the para(allel) model. The transition zone results showed an enhancement in the dissolution as the CO_2 has more contact with the brines as a result of the shale dispersing the plume over a wider area. Moreover, CO_2 was trapped beneath the shales, which increased its storage security.

Wang *et al.* (Wang *et al.* 2016) performed a systematic analysis of the impact of the formation slope on the CO_2 storage process in the Liujiagou formation in China. According to their

results, the plume will be symmetrical around the injection well. Moreover, the impact of dip on the CO_2 plume migration was negligible during the injection phase. They suggested that the dip angle, however, should be considered as one of the main criteria for long-term monitoring. While Nilsen *et al.* (Nilsen et al. 2012) demonstrated that topography changes straddling the scale of seismic resolution significantly retard the CO_2 plume up-dip migration, in another later work (Nilsen, Lie and Andersen 2016a), focussed on smaller-scale roughness and rugosity effects similar to the work done by (Gasda, S. E., Nilsen and Dahle 2013; Gasda, S. E. et al. 2012). They employed the CO2store module in MRST and used analytical and numerical up-scaling methods to resolve the small-scale structural features in a 1D model. They represented the caprock rugosity as layers with zero lateral permeability where the CO_2 plume becomes immobilized inside. Their results showed that residual and dissolution trapping reduces the plume thickness, while caprock rugosity retards the plume migration. The majority of the CO_2 near the tip of the plume was seen to be structurally trapped inside the small-scale structures (rugosity). Their results also showed that small-scale topography changes in the caprock would also affect the relative permeabilities.

Nilsen *et al.* (Nilsen et al. 2017) tried to match the observed plume outline from seismic data with the one from the simulation. They considered a wide range of parameters to calibrate it including top surface elevation, injection rate, porosity, permeability and CO_2 density. Their results suggested that the caprock morphology mainly controls the plume outline shape and that the CO_2-brine contact was governed by the CO_2 density. Later Allen et al. (Allen, R. et al. 2018) employed a one-factor-at-a-time (OFAT) approach and studied the sensitivity of estimating the storage to changes in porosity, permeability, caprock elevation and aquifer conditions (pressure and temperature) in the Utsira aquifer. For caprock elevation, the sensitivity analysis was also performed on a Geomodel of the Sandnes aquifer, and the results were compared against those for Utsira. Although the Utsira surface model is relatively smooth with sparsely distributed structural traps, the Sandnes aquifer contains dramatic slopes and a high degree of variation on the top surface. Their results showed that caprock elevation and permeability have the most significant impact on plume dynamics, which was also partially confirmed by Nilsen et al. (Nilsen et al. 2017). While average elevation changes of ± 8 m in the Sleipner model resulted in a significant change in plume outline and CO_2 storage capacity, a perturbation level of ± 30 m was not enough to produce any significant difference in the trapping structure of the Sandnes aquifer.

Han and Kim (Han and Kim 2018a) studied the impact of formation dip (2-10º) and the amplitude of structural relief and wavelength on CO_2 plume migration in a saline aquifer. The

contact boundary between the caprock and formation was chosen to be the same as in Shariatipour et al. (Shariatipour, S. M., Pickup and Mackay 2016). The speed of the plume front and amount of structural trapping was seen to be most sensitive to the formation dip and structural relief amplitude, respectively. The frontal speed showed a minor change with wavelength. Similar to the conclusion made by (Shariatipour, S. M., Pickup and Mackay 2016), the horizontal distance of the plume front and time showed a non-linear trend initially (representing the migration speed). The authors argued that this was due to the CO_2 plume's vertical migration before reaching the caprock (due to lower buoyancy). After the plume reaches the caprock and migrates mainly in the horizontal direction, the CO_2 plume in tilted models was seen to advance with a constant frontal speed, which confirms the results from previous studies (Pruess, Karsten and Nordbotten 2011).

Ahmadinia et al. (Ahmadinia, M., Shariatipour and Sadri 2019) performed a sensitivity analysis on the impact of caprock rugosity, aquifer slope and well location on CO_2 trapping mechanisms using sinusoidal geological models. In the highly tilted formations, the plume is dominated by the up-dip migration; therefore, to see the impact of rugosity, they considered a tilt angle of up to 3° only. Their results, similar to the previous studies (Gasda, Sarah E., Nordbotten and Celia 2012; Han and Kim 2018b), show that higher dip angles result in a higher dissolution and residual trapping but lower structural trapping. As the CO_2 plume migrates upward, it fills the traps by displacing the resident brine. Once the CO_2 and brine contact reaches the spill-point, the CO_2 plume moves to the neighbouring structure. Increasing the tilt angle results in a lower spill-point (therefore smaller structural traps), which results in a further upwards migration of the plume to contact the non-saturated brine, which eventually increases the residual and dissolution trappings. The results also indicated that in models with the highest rugosity values, the plume is less mobile, and residual trapping is minimal. In another work, they compared the results from the VE tool in MRST−CO2lab (MVE) against a number of simulators, including the ECLIPSE-black-oil (E100), ECLIPSE-compositional (E300) and ECLIPSE-VE (EVE) in a CO_2 storage study in an aquifer. They studied the impact of caprock morphology and aquifer slope on the CO_2 plume migration and dissolution. The results showed a good agreement between the approaches in terms of plume shape, although the amount of dissolved CO_2 in brine was different. While previous studies (Pruess, K. and Nordbotten 2011; Wang et al. 2016) showed that by increasing the tilt angle, the plume migrates further, which consequently results in a higher dissolution; Ahmadinia et al. argued that in tilted models, however, with limited vertical permeability, more CO_2 becomes trapped residually in the bottom layers which eventually results in a lower dissolution. Regarding the computational cost, MVE significantly

outperformed the rest. Table 2.3 summarises the model and methodology employed in previous studies on CO_2 storage. A list of equations representing the shape of the caprock-aquifer boundary is also presented in Table 2.4.

Table 2.3. Model comparison of previous work on CO_2 storage.

Shariatipour et al. (Shariatipour, S. M., Pickup and Mackay 2016)	Nilsen et al. (Nilsen et al. 2012)	Gasda et al. (Gasda, S. E. et al. 2012)	Pruess and Nordbotten (Pruess, K. and Nordbotten 2011)
3D	3D	3D	2D
8*8*0.1	30*60*0.1	10*10*0.1	10*0.2
80*80*100	300*600*20	?	Variable (local grid refinement) 7300 cells in total
0, 1,2 & 5	0.5	1	1.5
0.2	0.25	0.2	0.15
500	400-1000	100	500
E300-CO2STORE	EVE	VE based equations	TOUGH2-MP/ECO2N
Injection	Injection	?	Release
106	5000	1000	100
Yes	?	No	Considered
Yes	?	?	Considered

Work	Ahmadinia et al. (Ahmadinia, Masoud et al. 2019)	Ahmadinia et al (Ahmadinia, M., Shariatipour and Sadri 2019)	Han and Kim (Han and Kim 2018a)	Wang et al. (Wang et al. 2016)
Dim.	3D	3D	2D	2D
Scale (km)	40*40*0.1	15*15*0.1	0.4*0.1	10*0.291
Number of cells	201*201*9	101*101*4	400*100	101*50
Dip (°)	0 & 5	0, 0.5, 1, 2 & 3	2–10	0, 4, 8, 12, & 16
Porosity	0.2	0.2	0.1	~ 0.1
Permeability (mD)	50	500	20	~ 4
Simulator	MRST, E300, E100, EVE	E300	CMG's GEM	TOUGH2-ECO2N
Source	Injection	Injection	Release	Injection
Simulation time (yrs.)	1010	2000	10	120
Considered Pc	Yes	Yes	Yes	Yes
Considered	Yes	Yes	Yes	Yes

Table 2.4. Equations representing caprock morphology in previous studies.

Work	Equation
Gasda *et al.* (Gasda, S. E. et al. 2012)	symmetric sinusoidal surface: $\varsigma_T(x,y) = \bar{H}[1 + \alpha_1(sin\omega_1 x + sin\omega_1 y)]$ where $\bar{H}$= effective aquifer height $= \frac{1}{L}\int_0^L[\varsigma_T(x) - \varsigma_B(x)]dx$ $\varsigma_T \ and \ \varsigma_B$ represents reservoir top and bottom boundaries vertical locations $\alpha_1 = 0.1, \alpha_1 = 0.25, \omega_1 = angular \ frequency = \frac{2\pi}{W}$

asymmetrical system of staggered elliptical structures:

$\varsigma_T(x,y) = \bar{H}(1 + \alpha_2 e^{-\gamma})$

where

$\gamma = sin^2\omega_2(x - y) + sin^2\omega_2(x + y) + 2sin^2 2\omega_2 x$

Nilsen *et al.* (Nilsen et al. 2012)

surface in the form of $\frac{sinx}{x}$, Parameters:

Model	Short axis range	Long axis range	Standard deviation
OSS	1000	7000	13
FMM	200	7000	5

Nilsen *et al.* (Nilsen, Lie and Andersen 2016a)

$z(x) = D - L_1 sin\left(\frac{x}{W_1}\right)tan\theta + A\ sin\left(\frac{2\pi x}{W_2}\right)$

where

D = maximum depth

θ = aquifer tilt angle

W_1= characteristic length of the antiform structure

W_2= wavelength of the small-scale structures

A = amplitude of small-scale structures

Pruess and Nordbotten (Pruess, K. and Nordbotten 2011)	$z(x) = xsin\theta + 200cos\theta$ where θ = aquifer tilt angle
Shariatipour et al. (Shariatipour, S. M., Pickup and Mackay 2016)	$z(x) = z_0 + A\,sin(\omega x) + xtan\theta$ where A= amplitude $\omega = angular\ frequency = \dfrac{2\pi}{W}$ θ = aquifer tilt angle
Han and Kim (Han and Kim 2018a)	$z(x) = 20 + A\,sin(\omega x) + xtan\theta$ where A= amplitude $\omega = \frac{2\pi}{W}$ is the angular frequency θ = aquifer tilt angle
Ahmadinia et al. (Ahmadinia, Masoud et al. 2019)	$z(x,y) = A[sin(\omega_b x) + sin(\omega_b y)]$ $\qquad\qquad - R_x\,sin(\omega_c x) - R_y\,sin(\omega_c y) + x\,tan(\theta_x) + y\,tan(\theta_y)$ where $\omega = \frac{2\pi}{W}$ is the angular frequency A= amplitude of large-scale structures (domes) R = amplitude of small-scale structures (rugosity) θ = aquifer tilt angle

2.3. Software and tools

The following tools have been used throughout this study:

1. MATLAB Reservoir Simulation Toolbox (MRST)

2. ECLIPSE (E100, E300)

The majority of simulations in this work rely on MRST. This free, open-source software is available for public use for any purpose based on the GNU General Public License version 3 (GPLv3). This research tool aims to support studies on simulation and modelling of fluid in porous media. MRST provides a wide range of mathematical and plotting tools and computational methods that extends MATLAB in the direction of reservoir simulation. A collection of core functionalities is available as sets of add-ons to minimise the maintenance cost and make the software as flexible as possible. They offer a wide range of options, including (but not limited to) discretisation and solvers, simulators of incompressible and compressible flow, workflow tools such as flow diagnostics, grid coarsening, upscaling, and visualization of simulation output. In this study, the CO2lab module in MRST has been used to simulate CO_2 plume migration and trapping in saline aquifers. This module contains the results of more than a decade of research and development studies on CO_2 storage modelling, available in a unified and easy to use the toolbox. CO2lab module is in particular geared towards the long-term storage and trapping of CO_2 in a saline aquifer. It offers a wide range of computational methods and graphical use interphase to compute structural, residual and dissolution trapping and visualise their corresponding results. Moreover, it is equipped with an efficient simulator based on vertical equilibrium formulation to compute the plume migration path and detailed trapping inventories for various storage scenarios.

ECLIPSE is an oil and gas reservoir simulator owned and marketed by Schlumberger. Schlumberger is the world's leading provider of technology for reservoir characterisation, The ECLIPSE simulation package includes two separate simulators, ECLIPSE 100 and ECLIPSE 300. ECLIPSE 100 is a fully implicit simulator, which is specialised in black oil modelling and can simulate up to three-phase systems.

ECLIPSE 300 is a compositional simulator equipped with equations of state, pressure-dependent K-values, and the black oil model. It can be run in fully implicit, IMplicit Pressure Explicit Saturation (IMPES) and adaptive implicit (AIM) modes. In compositional simulation as the number of components and consequently, equations to be solved are large, the fully implicit mode's computational cost is significantly higher than ECLIPSE black oil. One approach to tackle this problem is to use the AIM mode by making cells implicit only where

necessary. Four equations of state are implemented in E300 including Redlich-Kwong, Soave-Redlich-Kwong, Peng-Robinson and Zudkevitch-Joffe. In this study, the CO2STORE option in ECLIPSE 300 is used to simulate CO_2 storage in saline aquifers. The CO2STORE option is a compositional reservoir simulator used for numerical simulations of CO_2 in geological formations (Schlumberger 2017). Three phases, including the CO_2 (gas phase), H_2O (liquid phase) and a solid phase, can be considered in the model. The Spycher and Pruess model (Spycher and Pruess 2005) is implemented in this simulator and is suitable for calculating the mutual solubility of CO_2 from 12 to 110 °C and H_2O from 15 to 100 °C and up to 600 bar.

2.4. Summary

This chapter summarises the existing knowledge on the impact of caprock morphology and reservoir slope on the CO_2 storage process as part of carbon capture and storage in saline aquifers. Discussions on the role of the caprock on CO_2 storage and its impact on various trapping mechanisms and plume migration are provided. Moreover, the published literature containing qualitative and quantitative findings on the importance of caprock is summarised with respect to its characterisation. The review provides the following crucial points as listed below:

- While the impact of dip on the CO_2 plume migration is negligible during the injection phase, it could be considered as one of the long-term monitoring criteria.
- Surface roughness (rugosity) in tilted models decreases the plume migration speed and provides additional storage capacity for the plume.
- Dissolution is expected to be higher with increasing tilt angle, resulting in further upwards migration of the plume and increased interaction with the formation brine. This is not always the case; studies show that in the models with limited vertical permeability, increasing the tilt results in more CO_2 becoming residually trapped in the bottom layers, which consequently decreases the dissolution.
- Using the VE models, the significant reduction of unknowns of the 2D system (compared to 3D), makes it possible to increase the lateral resolution beyond the practical limits in traditional 3D simulations, thus providing a better representation of the caprock morphology
- VE models show great potential for use in CO_2 storage problems, especially in cases with where the caprock topography is below the seismic resolution limit.

- Increasing the tilt angle results in a lower spill point and consequently smaller structural traps. This leads to further upwards migration of the plume (not necessarily in models with low vertical permeability), which increases the residual and dissolution trappings in the long run. On the other hand, the plume becomes less mobile in models with larger rugosity on the top surface, which results in lower residual trapping.

2.5. Contribution to knowledge

This research presented in this thesis aims to fill the current research gap through its aim of developing a better understanding the role of caprock morphology in the CO_2 storage process and quantifying its impact in the presence of other model uncertainties by employing efficient simulation and optimization tools. The novelty of this work lies in the following points:

- While previous studies are mainly focused on the impact of uncertain parameters separately, to the best of our knowledge, this is the first time that a study has focused on the joint effect of six of the most cited sources of uncertainties in a CO_2 storage problem. The uncertainty space on Sleipner 2019 Benchmark (Layer 9) is fully spanned using data-driven models. This work will enhance our scientific understanding of the complexity of the impact of the reservoir uncertainty on CO_2 plume migration in a real field model.

- For the first time, an optimization tool is applied to the Sleipner benchmark 2019 model, which resulted in an improved plume match by locally adjusting caprock elevation within seismic detection limits.

- This is the first benchmark studies on the impact of caprock morphology on CO_2 storage migration using a number of modelling approaches (E100, E300, EVE and MVE).

Chapter 3 [*]

Impact of caprock morphology on CO_2 migration and trapping

3.1. Introduction

This chapter focuses on carbon sequestration in saline aquifers to better understand CO_2 migration so that characterising the storage site becomes an essential consideration Several conditions need to be confirmed to verify the feasibility of a site for CO_2 storage, including the presence of a caprock, the possible CO_2 injection rate, the mechanical and flow properties of the reservoir and its storage capacity (Pruess, K. et al. 2001). The CO_2 migration distance depends on the relationship between the up-dip plume movement, residual trapping and the gas dissolution rate (Ennis-King, Jonathan and Paterson 2005). As the CO_2 plume eventually becomes distributed below the caprock, it is essential to study the site heterogeneities and the caprock's nature (Shariatipour, S. M., Pickup and Mackay 2016). An exemplary storage site candidate will have a secure and very low permeable caprock (extremely tight formation), a large pore volume, good permeability and good pressure connectivity over long distances so the injection will not result in a significant pressure build-up (Saripalli and McGrail 2002). Moreover, several parameters, including the presence and size of structural traps, the planned amount of injected CO_2, likely migration paths, and migration speed and pressure build-up, must be taken into account while characterising a potential storage reservoir.

Based on the site's structural characteristics, the lateral and vertical migration of the CO_2 can be predicted. Generally, two basic storage geometries are distinguishable, namely structural closure and open aquifer (Chadwick, A. et al. 2008). S*tructural closure* or the so-called anticlinal trap occurs when the vertical (and possibly lateral) migration of the free CO_2, is

---

[*] The content of this chapter is taken from the following paper:

Ahmadinia, M. and Shariatipour, M. (2020) A study on the impact of storage boundary and caprock morphology on carbon sequestration in saline aquifers. Greenhouse Gases: Science and Technology.

The candidate planned and developed the methodology, performed all the simulation and analysis, and wrote the manuscript. The co-author supervised the project and provided feedback on the manuscript.

limited by low permeability rocks. The advantage of this trapping mechanism is that it increases storage efficiency. There is, however, the possibility of a pressure build-up under the caprock as a result of a closed column of trapped buoyant fluid (Zhou *et al.* 2008). Another drawback is the small contact area between the gas and the water, limiting the dissolution between the two phases. In this type of trapping, the geometry of the anticlines and the down-dip flanks, where the dissolved CO_2 migrates in the long term, need to be analysed. The *open aquifer* is another storage geometry in which the CO_2 is free to migrate laterally as there are no laterally confining boundaries. After rising upwards due to its lower density, the injected CO_2 spreads beneath the caprock. The resulting large contact surfaces between the gas and water enhance the dissolution process. Due to the large plume extent, a larger area will need to be monitored, thus increasing the cost of monitoring the site and analysing the risk for the potential leakage pathways (Deng *et al.* 2017).

In order to better clarify the plume migration pattern and the potential storage capacity of the CO_2, it is crucial to characterise the structure of the storage site both locally and regionally. To fulfil this goal, the structure mapping of the depth to the top of the reservoir, reservoir thickness, and reservoir structural compartmentalisation need to be investigated carefully (Zhang, Z. and Huisingh 2017). The characteristics of the caprock may influence the plume migration and long-term CO_2 storage. For instance, they may result in complex flow paths, where the CO_2 travels in a tortuous, complex way through the rock column (Ambrose et al. 2008). Hesse et al. (Hesse et al. 2007), analysed the migration scale of the CO_2 plume after injection. Their results showed that the plume development has two stages, the first occurring in the full thickness of the aquifer and the second at the top of the site. They also addressed it in tilted models, where the residual trapping can play a dominant role. The demonstration case examples of these impacts exist in the seismic survey of the plume migration in the Utsira Sand in Norway (Hermanrud, Christian *et al.* 2009). Moreover, several studies have investigated the impact of the caprock on the overall carbon storage process in realistic (Goater, Bijeljic and Blunt 2013; Nilsen et al. 2011b; Nilsen et al. 2012) and synthetic (Ahmadinia, M. et al. ; Gasda, S. E. et al. 2012; Pruess, K. et al. 2001; Shariatipour, Seyed M., Pickup and Mackay 2016) models.

This chapter presents an investigation into the impact of the reservoir boundary and top surface morphology on the structural and dissolution trapping mechanisms through the aid of numerical simulations and analytical calculations in saline aquifers. Its intention is to provide

a better understanding of the impact of top surface morphology by performing qualitative and quantitative analyses of CO_2 plume behaviour under dipping and sinusoidal structures while considering the role of boundary conditions. In the first step, the impact of boundary conditions on the CO_2 plume migration and dissolution for horizontal and tilted planar models has been investigated. Subsequently, the widespread application of the simplified top surface in simulation models is questioned by focusing on the caprock shape's impacts on the CO_2 dissolution in the geological storage formations. For this purpose, ten models have been synthesized. Using the boundary conditions in the first part and based on the structural properties of several potential sites.

Moreover, similar to some previous work, such as (Han and Kim 2018b; Pruess, K. and Nordbotten 2011; Shariatipour, S. M., Pickup and Mackay 2016; Wang et al. *2016*), but with a wider range of top surfaces, the impact of the caprock morphology on plume advancement is studied. An analytical method has been developed for one of the models to determine the amount of structural trapping and the results have been validated through numerical simulations. This method would be useful for site screening before running any numerical simulation.

3.2. Methodology

It is computationally expensive and sometimes even impossible to run detailed 3D simulations on an entire CO_2 storage formation. Therefore, the model used in storage studies is sometimes part of a more extensive reservoir simulation. To represent the real case situation more accurately, the boundary of the sub-model needs to be evaluated carefully. One method to take the impact of removed pore volume into account is to multiply the porosity values of the sub-model edges by a factor (Shariatipour, S. M., Pickup and Mackay 2016). In the first part of this chapter, the impact of boundary conditions on the CO_2 plume migration and dissolution for horizontal and tilted planar (no added rugosity) models is investigated. Various quantities of pore volume multipliers are considered, and the pressures at the boundaries are monitored.

In Section 3.2.1, the numerical simulation model is described, followed by a summary of the role of the boundary conditions in the CO_2 plume migration and storage process (3.2.1.1). Section 3.2.2 provides details of the synthesised models using various caprock morphologies.

The application of analytical methods to study the possibility and the amount of structural trapping are explained in Section 3.2.3.

3.2.1. Numerical simulation

The CO2STORE option in ECLIPSE E300, a compositional reservoir simulator, is employed to perform the numerical simulations (Schlumberger 2017). Three phases, including the CO_2 (gas phase), H_2O (liquid phase) and a solid phase, are considered in the model. The Spycher and Pruess model (Spycher and Pruess 2005) is implemented in this simulator and is suitable to calculate the mutual solubility of CO_2 from 12 to 110 °C and H_2O from 15 to 100 °C and up to 600 bar.

The simulation is performed on a 2D cross-section of a synthetic gas-water reservoir with a grid resolution of $81 \times 1 \times 100$ and a cell size of 250 m $\times$ 8000 m $\times$ 1 m, which is considered to be constant throughout the study; except in Section 2.1.1. where the cell size is 175 m $\times$ 8000 m $\times$ 1 m. A single CO_2 injector is situated in the centre of the model operating under a constant flow rate of 1,368,603 cubic metres per day, roughly equivalent to a quarter of the CO_2 emission of a 500 MW coal-based power plant. The well is controlled by surface rate with a bottom-hole pressure limit of 220 bars. The total injected CO_2, however, in all the models is the same, as the pressure never reaches the assigned limit. The CO_2 is injected for 30 years, followed by a 1000-year post-injection period. The aquifer contains 100% brine in its initial condition with a mole fraction of 0.967 and 0.033 for H_2O and NaCl, respectively, and the salt is assumed to remain in the aqueous phase. The CO_2 plume migration beneath the caprock is mainly a drainage process; therefore, similar to the work done by (Pruess, K. and Nordbotten 2011; Wang *et al.* 2016) simulations are performed on a non-hysteretic model. The aquifer's static data, including porosity and permeability, is based on the Sherwood Sandstone Group (SSG, part of the CASSEM project) (Pickup, GE et al. 2011). The permeability is considered to be isotropic.

CO_2 dissolution in the aquifer is highly desirable due to the implication for increased storage safety. Studies have indicated the importance of molecular diffusion and its dominant role in CO_2 dissolution, especially in the early stages (Ennis-King, J. and Paterson 2003). Therefore, molecular diffusion option in ECLIPSE is considered in the simulations. The molar flux of component i per unit area per unit time, J_i is given by Fick's law,

$$J_i = -cD_i \frac{\partial x_i}{\partial d}$$

<div align="right">Equation 3.1</div>

where:

c is the total molar concentration

D_i is the diffusion coefficient of component i

x_i is the mole fraction of component i

$\frac{\partial}{\partial d}$ is the gradient in the direction of flow

The flux goes from high to low concentration regions, with a magnitude that is proportional to the concentration gradient. Therefore, as the injected CO_2 is being dissolved into the formation brine, the concentration gradient decreases, resulting in a lower dissolution rate. In other words, since the aqueous phase is fairly-immobile, the CO_2 dissolution, therefore, is limited by the rate at which the molecular diffusion removes the dissolved CO_2 at the dissolution boundary (Pruess, Karsten and Zhang 2008). More information about the model and operation data can be found in Table 3.1.

Table 3.1. Model properties and operation data

Parameter		Value
Number of cells (NX×NY×NZ)		81×1×100
Cell size (m) (DX×DY×DZ)	Section 2.1.1.	175×8000×1
	Rest of chapter	250×8000×1
Water diffusion coefficients (m^2/day)	CO_2	0.0001
	H_2O	0.0005
Rock compressibility at 150 bars (1/bars)		5.0E-5
Irreducible water saturation (S_{rw})		0.36
Initial water saturation		1.0

Absolute permeability (mD)	500
Porosity	0.2
Pressure at the 1500 m depth (bar)	150
Simulation period (years)	1030
Injection rate (sm^3 per day)	1,368,603
Perforated layers	50 to 100
Reservoir Temperature at 1500 m (^oC)	45
Duration of injection	30 years
Equation of state	Peng-Robinson

Figure 3.1 shows the relative permeability and capillary pressure curves used in this study. They were measured at Heriot-Watt University using an SSG sample as part of the CASSEM project (Smith *et al.* 2012). The relative permeability to brine and CO_2 and the capillary pressure are denoted by K_{rw}, K_{rg} and P_c, respectively. The irreducible water saturation is 0.36, resulting in a possible maximum gas saturation of 0.64. A critical feature of the relative permeability curves carried out on the SSG is the low CO_2 end-point relative permeability (around 0.05). Therefore, the effective permeability of the rock saturated with CO_2 is about 20 times lower than when it was saturated with brine.
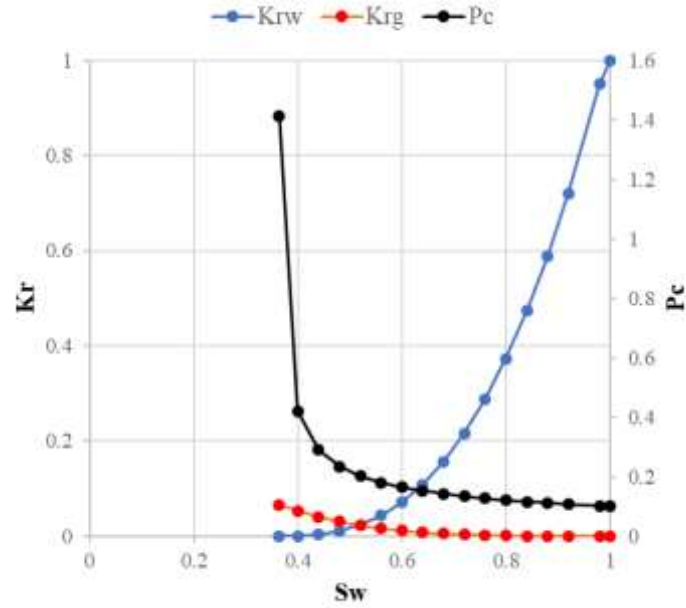
Figure 3.1. Relative permeability and capillary pressure curves using SSG samples (Smith et al. 2012).

3.2.1.1. Reservoir boundary

As mentioned above, one method to decrease the computational cost is to focus on a selected section of the main site and apply porosity multipliers at the edges of the sub-model to account for the deactivated sections. In the first part of the study, the impact of boundary conditions on the CO_2 plume migration and dissolution in horizontal and tilted (0.5°, clockwise direction) planar (no rugosity) models are investigated (Figure 3.2). The multipliers (M in Figure 3.2) represent extra pore volume and are located on the left, right and both sides of the 2D models (x-axis), respectively. In order to maintain a constant pore volume, the same for all the models, in the cases where the multipliers are on both sides, their values are divided by two (M/2 in case e and f). No-flow boundary condition is considered along the y-axis.
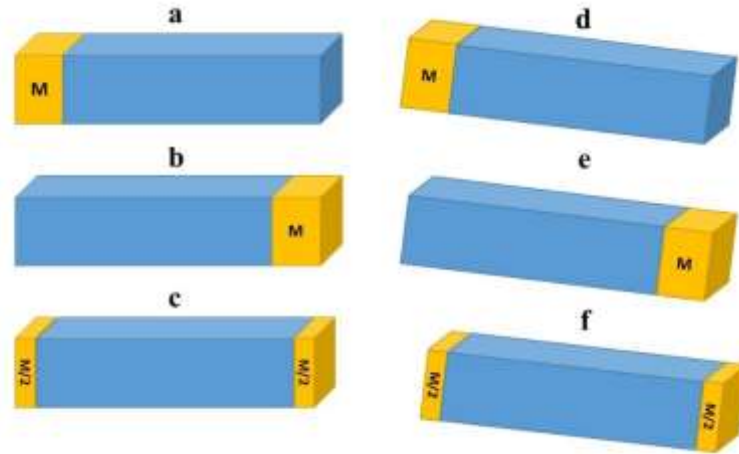
Figure 3.2. Schematic of the multiplier position used for flat (2a-2b-2c) and 0.5° tilted (2d, 2e, 2f) models.

The main model is large, and the pressure response at the boundaries is negligible. Therefore, for this part of the study in order to observe the effect of boundary conditions more precisely, all the cell sizes in the x-direction were reduced from 250 m to 175 m (30% reduction), while other properties were kept the same as in the section (3.2.1).

The injector is perforated between layers 50 to 100. The simulation results indicated that the pressure change in the mid-perforated layer (75th) is more significant than for other layers. Therefore, the pressure response is monitored at cells (1,1,75) and (81,1,75) or both if the multiplier is located at the left (x=3), right (x=79) or both sides of the aquifer, respectively. The pressure is monitored at two columns after the multiplier to ensure that the pressure wave does not reach the boundary and the infinite acting condition is valid. Figure 3.3 shows the schematic of the model used to study the impact of boundary conditions. The multipliers are applied to all the layers located in x=3 (cases a and b) or x=79 (cases b and e) or both (cases c and f). The main goal of this section is to find a proper multiplier to apply to the synthetic models in the next section, so they meet the infinite acting condition.
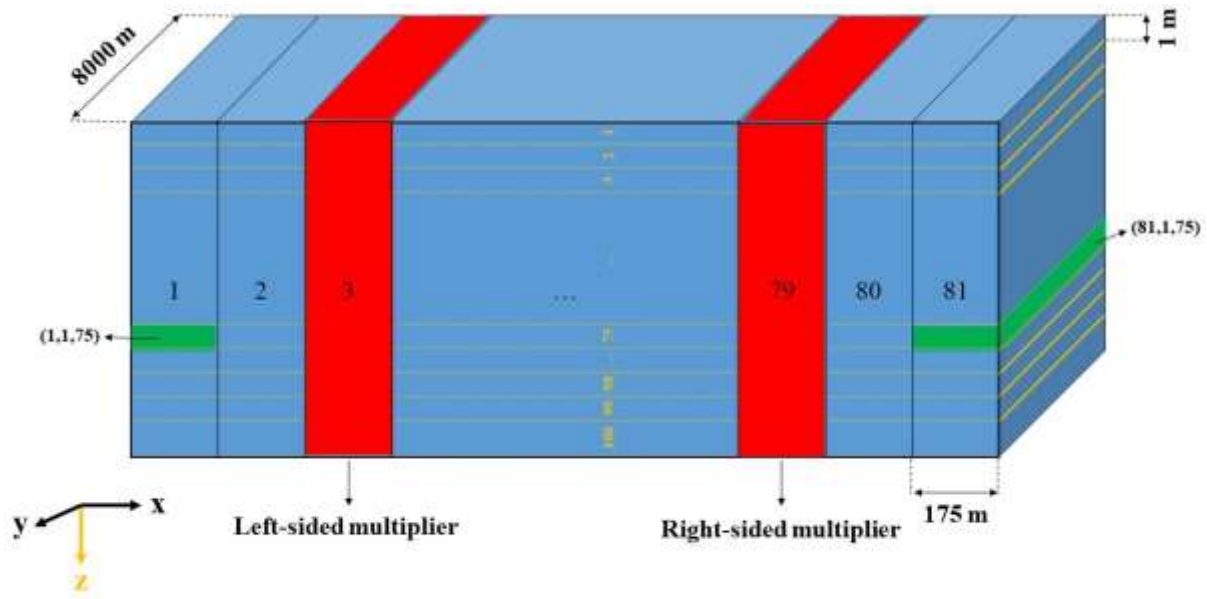
Figure 3.3. Model schematic.

3.2.2. Caprock morphology analysis

The second part of the work presented here is focused on the impact of the caprock shape on the CO_2 dissolution and plume migration in geological storage formations. In order to make the synthetic model more realistic, the structural properties of several real sites were studied carefully (Table 2.2). This was undertaken to find the common range of structural reliefs available at their top surface. Therefore, the models are categorised based on their structural reliefs in small (0-20 m), medium (20-50 m) and large-scale (> 50 m) groups.

As observed in Table 2.2, most of these real and recommended storage sites have small to medium scale structural reliefs; considering this fact, ten different equations are employed to synthesise the models (a-j) for this part of the chapter. A combination of sine, arc-tan and tan (tilted models) equations is employed, and ten different caprock surfaces are created. The CO_2 is injected for 30 years, followed by a 1000-year post-injection period. Applying the small-scale topography variations on the models, the impact of rugosity, which is not detected in seismic investigations, is considered in the study. A suitable multiplier found in the first section of the chapter is applied to all the synthetic models to guarantee the infinite acting condition in the models.

The equations representing the morphology of the caprock in the models are functions of amplitude (A), wavelength (W) and the tilt(θ). The morphologies (a-j) used in this chapter can

be generalised into six sets of equations listed in Table 3.2, where Z_0 is the caprock depth, and B is constant.
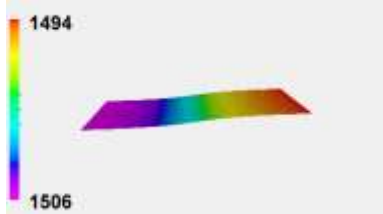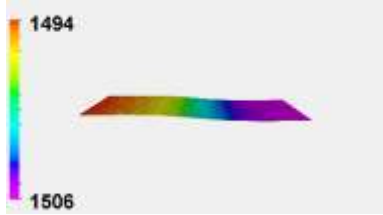
Table 3.2. Generalised equations used in this chapter.
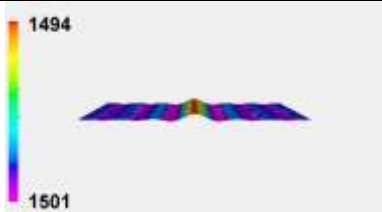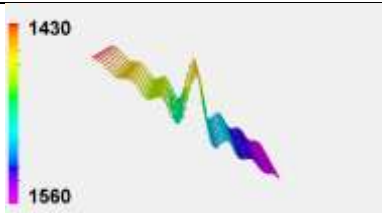
Equation	Condition	Cases
$f_1 = Z_0 + B \, tan^{-1}(\frac{x}{W})$	$B \neq 0$	a, b
$f_2 = Z_0 + B \, tan^{-1}(\frac{x}{W})$ $+ A \, sin(\frac{2\pi x}{W})$	$B \neq 0$ $A \neq 0$	c
$f_3 = Z_0 + A \, sin(\frac{2\pi x}{W})$	$A \neq 0$	e, f
$f_4 = Z_0 + A \, sin(\frac{2\pi x}{W})$ $+ x \, tan(\Theta)$	$A \neq 0$	g, h
$f_5 = Z_0 + B \, \dfrac{sin(\frac{2\pi x}{W})}{x}$	$B \neq 0$	i
$f_6 = Z_0 + B \, \dfrac{sin\left(\frac{2\pi x}{W}\right)}{x}$ $+ x \, tan(\Theta)$	$B \neq 0$	j

Using the derivative (the slope of the tangent line at any point) and integral (represents the signed area of the region bounded) of each of the equations, which provides the area below the

curve, it is, therefore, possible to find the conditions without trapping and structural trapping capacity. It should be noted that the word structural trapping capacity here refers to the amount of CO_2 trapped just beneath the caprock in the structural reliefs controlled by the amplitude and the tilt angle. Table 3.3 illustrates the top surface characteristics of the synthetic models, including their equations, 3D view, structural relief, slope and scale.

Table 3.3. Top surface characteristics of each model.

case	top surface equation	3D view (top surface)	structural relief (m)	slope (º)	scale
a	$1500 - 5\tan^{-1}\dfrac{x}{1500}$		0	0.03	Small
b	$1500 + 5\tan^{-1}\dfrac{x}{1500}$		0	0.03	Small
c	1500 $- 5\tan^{-1}\dfrac{x}{1500}$ $+ 0.5\sin\dfrac{2\pi x}{500}$		1-2	0.34	small
d	1500		0	0	small

e	$1500 + 2\sin\dfrac{2\pi x}{1000}$	1498 1501	2-4	0	Small
f	$1500 + 2\sin\dfrac{2\pi x}{2000}$	1498 1502	2-4	0	Small
g	$1500 + 2\sin\dfrac{2\pi x}{1000} + x\tan\dfrac{2\pi}{180}$	1500 1775	1-2	2	Small
h	$1500 + 2\sin\dfrac{2\pi x}{2000} + x\tan\dfrac{2\pi}{180}$	1500 1775	1-2	2	Small
i	$1500 + 1000\dfrac{sinx}{x}$	1494 1501	1-6	0	Small
j	$1500 + 1000\dfrac{sinx}{x} + xtan\dfrac{\pi}{180}$	1430 1560	20-90	0.37	Medium

3.2.3. Analytical calculation

The CO_2 plume is trapped beneath the formation only if there is a down-dip structure on the top surface to stop its migration. The derivative of the equation representing this specific

feature has an opposite sign to the slope. For instance, Figure 3.4 shows a graph with a positive slope, in which trapping can occur thanks to the down-dip structures with a negative derivative.
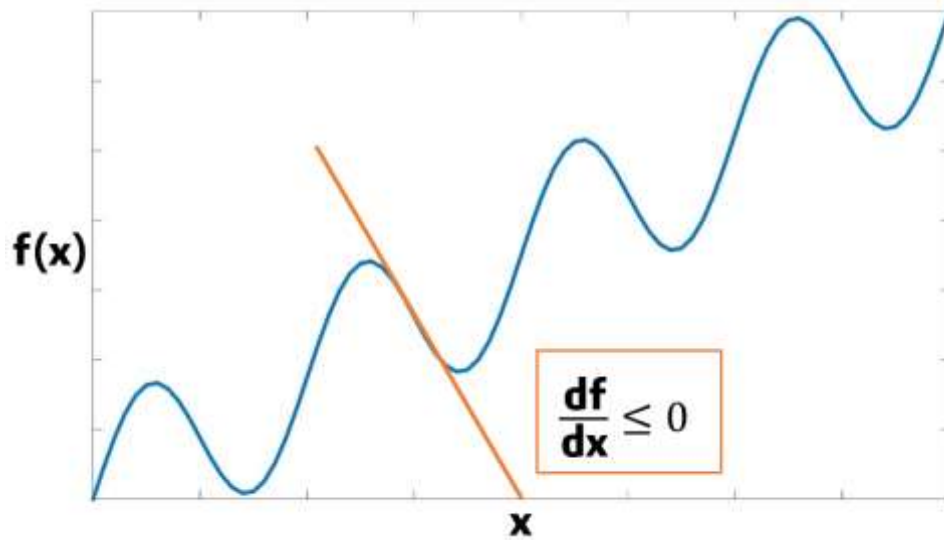
Figure 3.4. A structure with an opposite derivative sign to the slope is required to have structural trapping.

Therefore, in order to secure a non-trapping condition, the derivative of the top surface equation should always have the same sign as the slope, i.e. if the slope is positive then $\frac{df}{dx} \geq 0$ and *vice versa*.

The area under the curves represents the possible amount of trapping. As shown in Figure 3.5, the integral of the top surface equations can evaluate the amount of structural trapping capacity.
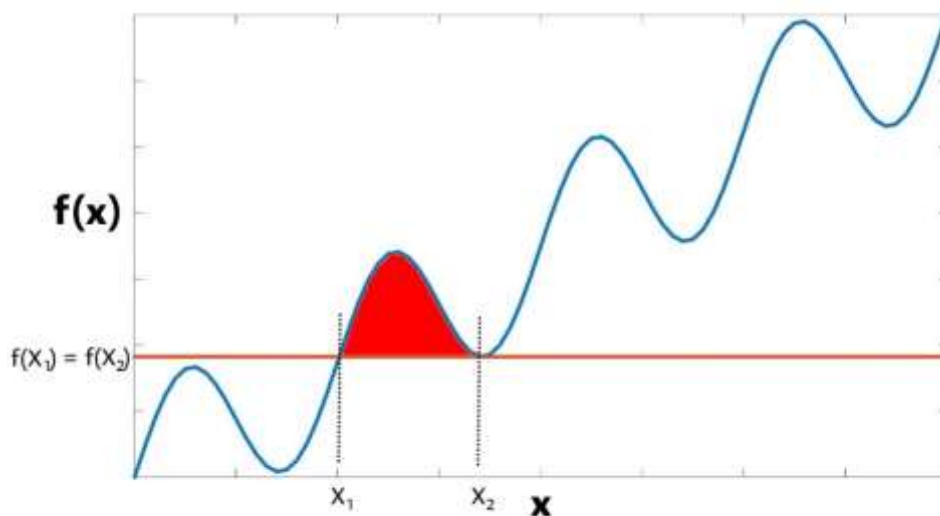
Figure 3.5. The red area represents the possible storage capacity of an anticline.

It is possible to evaluate $(X_2, f(X_2))$ by setting the derivative to zero and $(X_1, f(X_1))$ as the intersect of the horizontal line passing from the spill point (X_2) and the curve. Having X_1 and X_2, the structural trapping capacity can be calculated using the following equation:

Structural trapping capacity $=[\int_{X_1}^{X_2}[f(x) - f(X_1)]dx] \times Y \times \phi \times (1 - S_{rw})$ Equation 3.2,

where Y is the length of the 2D model in the y-direction, ϕ is the porosity and S_{rw} is the irreducible water saturation.

3.3. Results and discussion

3.3.1. Reservoir boundary

In this part of the chapter, a porosity multiplier is used in the model edges to add extra pore volume to the reservoir, and its effect is investigated on the overall CO_2 storage process. Initially, different values for the multiplier (6E+2, 1E+3, 2E+3, 1E+4, 2E+4, 5E+4, 1E+5, 2E+5 and 1E+7) are considered and, while monitoring the pressure at the boundary, the suitable porosity multiplier was selected. The selection criteria are to meet the infinite acting condition, which means the pressure wave should not touch the cells in the boundaries throughout the simulation. Figure 3.6 shows the pressure variation in the cell (81, 1, 75) located in the right end of the model (Figure 3.3), throughout the simulation for different values of multipliers applied to the right side of the horizontal planar aquifer (Case b in Figure 3.2). It is evident in Figure 3.6 that for a multiplier higher than 1E5, the pressure remains relatively constant in the boundaries throughout the injection period and validates the infinite acting assumption. Similar results were observed for other cases presented earlier in Figure 3.2 (a, c, d, e and f) and a multiplier of 1E5 on one side (Cases a, d and e) or 0.5E5 on both sides (Cases c and f) confirmed the infinite acting condition. Therefore, three different values of 1E5, 1E7 and 1E9 (equal and higher than 1E5) are considered when studying the impact of extra pore volume at the boundary on CO_2 plume migration and dissolution.
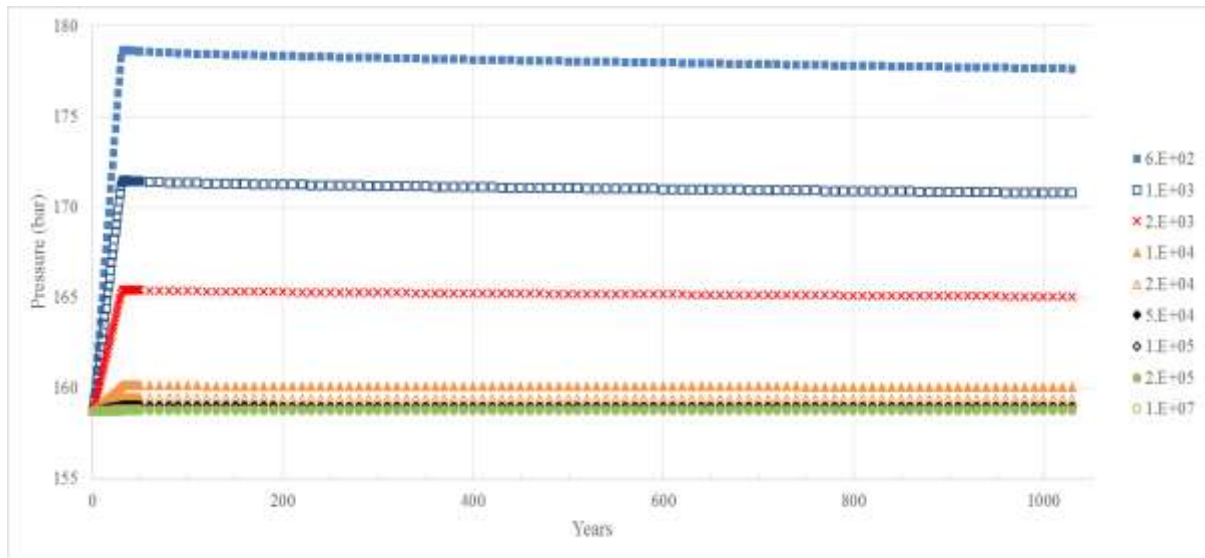
Figure 3.6. The pressure variation at the cell (81,1,75) resulting from different multipliers (Horizontal case).

Using the multipliers results in additional volume in the reservoir, which consequently changes the model's pressure propagation. Figure 3.7 shows the pressure distribution two years after the start of injection (the cases relate to the cases in Figure 3.2), in which a total multiplier of 1E7 is applied at the left (7a, 7d), right (7b, 7e) and both sides (7c, 7f) of the horizontal (7a, 7b and 7c) and 0.5° tilted (7d, 7e and 7f) planar models. There are 100 layers in the model of which the lower half is perforated. The pressure is lower in the vicinity of the multipliers (edges). Considering all the parameters being constant, the fluid tends to migrate from a higher pressure zone to the lower pressure one (Schlumberger 2017). The pressure distribution near the injection point (middle) is relatively similar in all the cases regardless of the multiplier position and value. Therefore, a lower pressure zone near the boundaries (as a result of extra pore volume) results in a higher pressure difference and consequently a higher driving force. Consequently, the injected plume tends to move towards the area with higher multipliers.
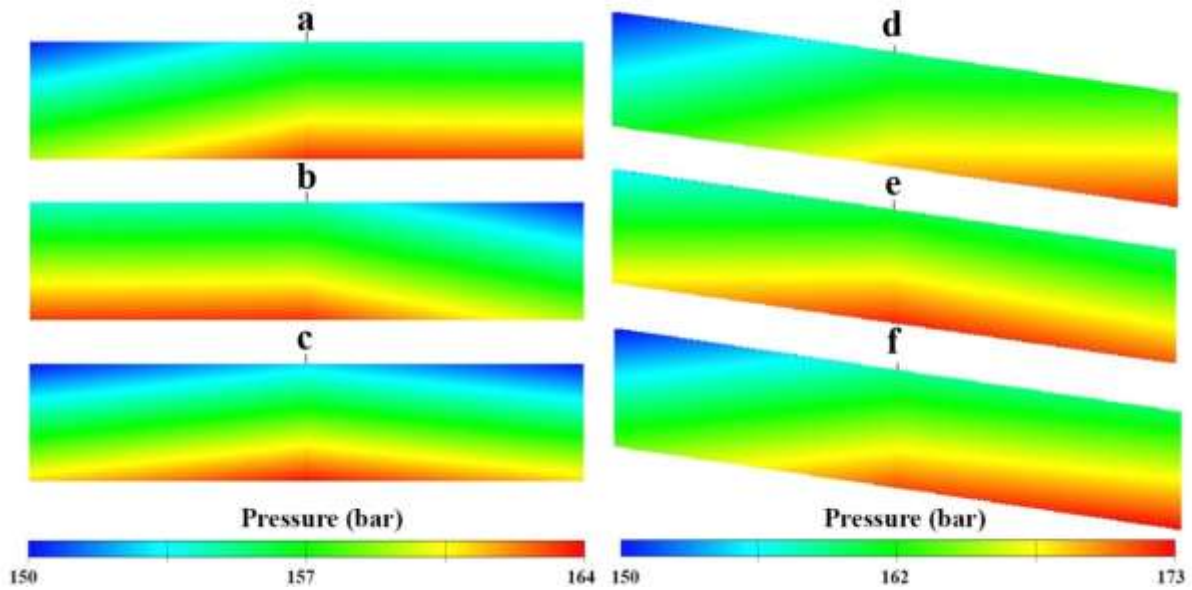
Figure 3.7. The pressure distribution in the reservoir two years after the start of injection, for the horizontal (a, b and c) and 0.5° tilted (d, e and f) planar models with a total multiplier of 1E7 in left (a and d), right (b and e) and both (c and f) sides of the aquifer. All figures are exaggerated with a factor of 25 in the z-direction. Here the cases (a-f) relate to cases in Figure 3.2.

The percentage of dissolved CO_2 at the end of the injection and post-injection periods for both the tilted and planar case is shown in Figure 3.8. Figure 3.8a and Figure 3.8b illustrate the percentage of dissolved CO_2 at the end of the injection (30 yrs.) and post-injection (1030 yrs.) periods, respectively, for the planar model. The CO_2 plume does not reach the cells with the volume multipliers in any of the cases. Since the model is symmetric, regardless of the multiplier being on the right or left side, the dissolution becomes almost the same in the planar cases. There is a minor difference (0.1% error) in Figure 3.8b, which is likely due to numerical errors and is negligible. The results also indicate that CO_2 dissolution in the brine, when the reservoir is open from one side, is higher than when it is open from both sides. The large one-sided extra pore volume results in a more significant pressure difference between the two boundaries (the one with multiplier has lower pressure). This consequently helps the plume to move further to the open side, and hence the CO_2 comes into contact with more formation water. It is also evident in the pressure distribution in Figure 3.7, that if the reservoir is open from only one side, the pressure difference between the centre, where the injector is located,

and that boundary is higher. This higher pressure difference results in an increased driving force and further migration of the plume to the open side.

Figure 3.8c and Figure 3.8d show the results for the tilted models. Since the model is tilted in a clockwise direction, the buoyancy force and elevation difference deviate the plume to the left-hand side, and as a result, the primary dissolution occurs on the left side while leaving the brine on the right side intact. Having the multiplier on the right side leads to a portion of the plume dispersing into the formation water to the zone full of low-saturated brine, consequently increasing dissolution. Moreover, the overall dissolution of the tilted model is greater than the planar case.

While the of position the porosity multiplier changes the amount of dissolution, the impact of its value on the results is not that significant, and the amount of dissolution is relatively close for all the three values of e multipliers in both the tilted and horizontal models. The only exception is in Figure 3.8d for the tilted model with the multipliers located on both sides, in which a higher multiplier results in more dissolution. The reason for this could be that while the up-dip migration of the plume towards the left side of the model is mainly dominated by the buoyancy force (and not the multiplier on the left side), increasing the multipliers on both sides results in a stronger buoyancy force on the right side of the model and leads the plume towards the unsaturated formation brine. In order to have the infinite acting condition, a total multiplier of 1E7 is considered on both sides (half each) of the models in the next section of the chapter (similar to the cases e and f in Figure 3.2).
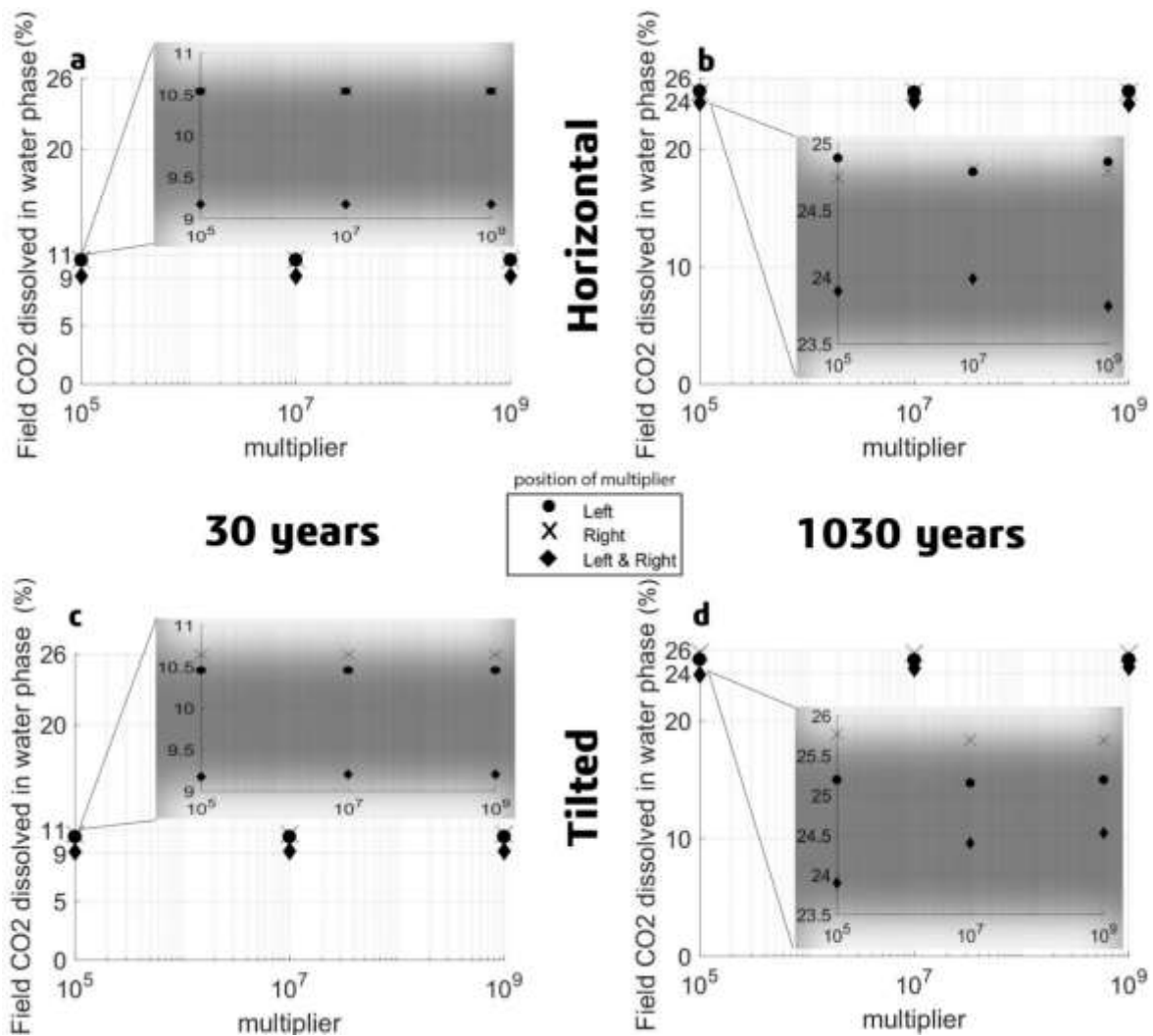
Figure 3.8. (a), Percentage of dissolved CO_2 at the end of injection (horizontal model), (b), Percentage of dissolved CO_2 at the end of the simulation (horizontal model). (c), Percentage of dissolved CO_2 at the end of injection (tilted model). (d), Percentage of dissolved CO_2 at the end of the simulation (tilted model). The multiplier is on the left, right and both sides of the models.

3.3.2. Caprock morphology

Once the plume reaches the caprock, it migrates in the horizontal direction, while its dissolution in the formation water beneath the plume occurs vertically. Due to its lower density, the plume migrates up-dip in the tilted aquifer. Similar to the theory of differential entrapment of hydrocarbons proposed by (Gussow, William C. 1968; Gussow, William Carruthers 1954), once the first sand ridge is filled to its spill point, the free CO_2 moves up-dip beneath the caprock and to the next available ridge (Figure 3.9). The plume migration is inhibited if its

thickness is on the same scale as the relief amplitude. Since it takes a while for the plume to migrate upward, the effect of rugosity is negligible during the injection phase. Therefore, the focus on the long-term CO_2 migration and the desired time-period is one thousand years after the cessation of injection.
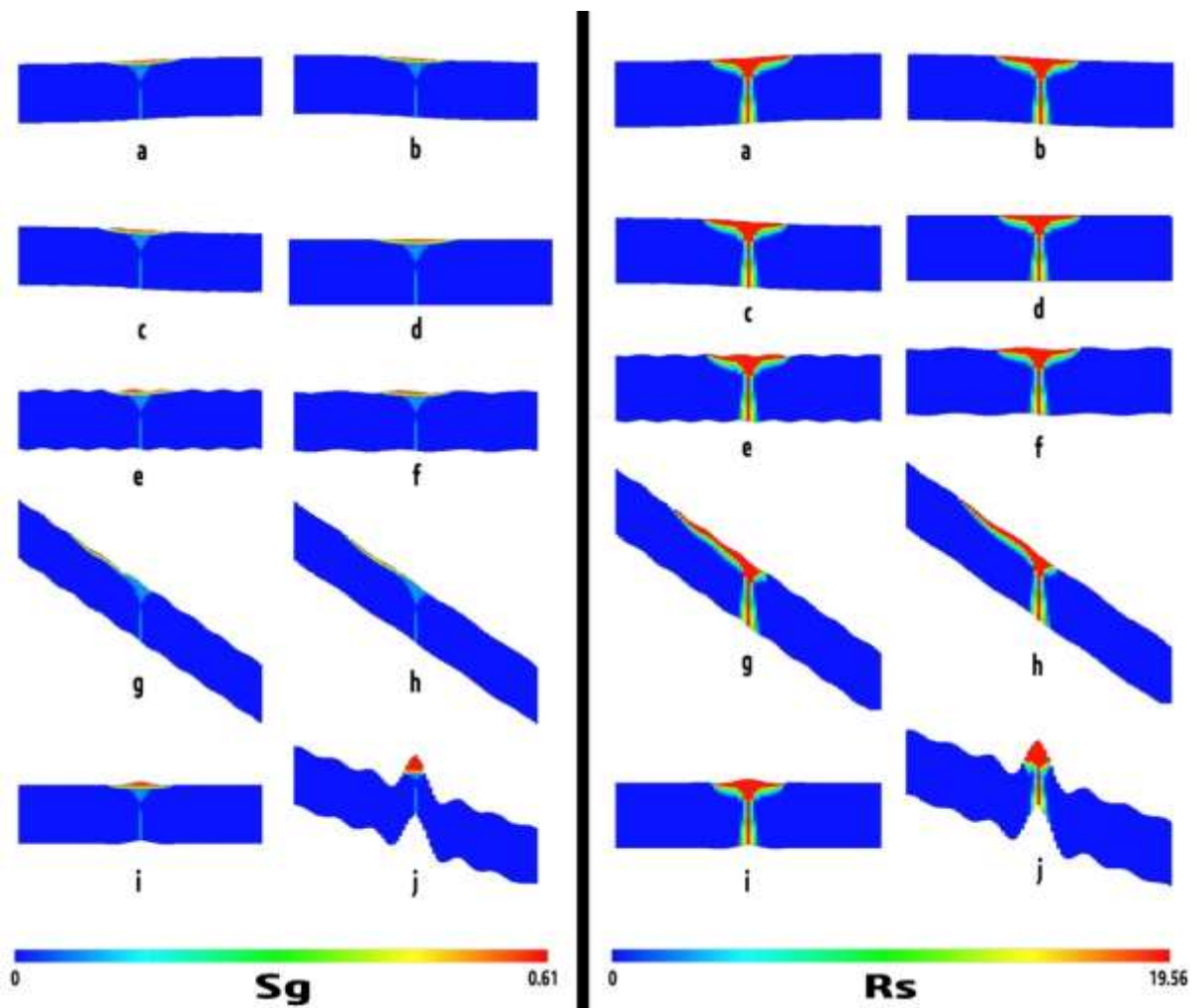
Figure 3.9. Gas saturation (left) and gas water ratio (right) 1000 years after the end of CO_2 injection in all models. Here the cases (a-j) relate to cases in Table 3.2.

Figure 3.10a illustrates the percentages of the total injected CO_2 dissolved in the brine for all the cases (a to j). Similar to the previous studies (Gasda, S. E., Nilsen and Dahle 2013; Kumar et al. 2005; Shariatipour, S. M., Pickup and Mackay 2016), in the tilted reservoirs (Cases g and h), where the CO_2 plume extent is the greatest, and it interacts with more formation water, the

dissolution reaches a maximum. The lowest dissolution occurs where the plume extent is inhibited by the structural relief, resulting in a thicker plume with less area of extent. (Case j). The results show the negligible impact of the rugosity on the plume dissolution while the dissolution decreases in the models with large-scale structures (Cases i and j). Based on Equation 2.1, the diffusion rate of the CO_2 across a unit of area is a linear function of the concentration gradient. In other words, as the injected CO_2 accumulates near the wellbore and dissolves into the brine, its diffusion rate at this location decreases as the brine is already saturated. The results for dissolved CO_2 in the aquifer show that immediately after the commencement of injection, when there is only unsaturated brine, a noticeable portion of the injected CO_2 will dissolve rapidly. Figure 3.10a clearly shows that the curves have a higher slope during the injection phase. As the local cells become saturated due to the lower gradient in the concentration, however, the dissolution rate drops. The remaining free gas migrates towards the lower concentrated regions where low saturated formation water is available. Since the portion of the injected CO_2 is much higher than the dissolved one, the slope has a downward trend throughout the injection period (30 years). After the shut-in, since no more CO_2 is being added, the percentage of the dissolved CO_2 rises with a smaller slope. (Wang *et al.* 2016) suggested that the dip angle does not have a significant influence on the plume migration and dissolution during the injection phase, which was confirmed in the study. This is evidenced by the dissolution (Figure 3.10a) and migration (Figure 3.10b) curves that are the same for all the models in the first 30 years of simulation.
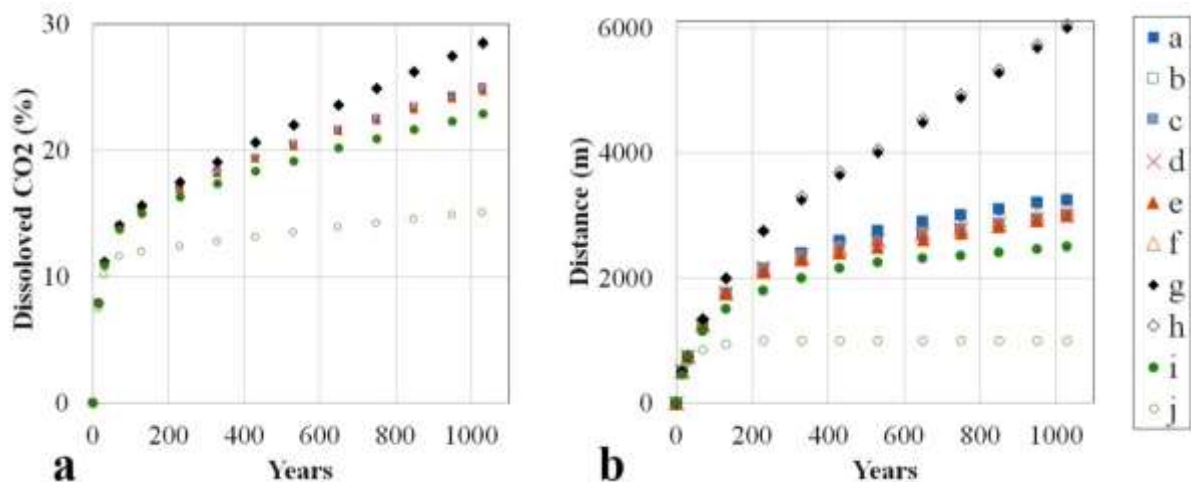
Figure 3.10. (a) Percentage of the dissolved CO_2 for all the models. (b) The migration distance of the plume front over time. Here Cases (a-j) relate to cases in Table 3.2.

The advancement of the plume front for all the cases is presented in Figure 3.10b. Similar to the results presented in previous work (Pruess, K. and Nordbotten 2011; Shariatipour, S. M., Pickup and Mackay 2016; Wang *et al.* 2016), there is a linear trend in the graph a short period after the end of injection, indicating a constant frontal speed. The nonlinearity during the injection phase is due to the vertical migration of the plume toward the caprock once injection commences. The impact of wavelength on the plume migration is negligible, and the frontal advancement in the horizontal (e and f) and the tilted (g and h) models with various wavelengths is about 3000 and 6000 metres, respectively. Similar results were achieved by (Han and Kim 2018b). The results also show a higher migration distance in the tilted models due to the reduction of the CO_2 density in these cases as it migrates upwards toward the slope (Shariatipour, S. M., Pickup and Mackay 2016). The CO_2 source in the study is an injection well. Therefore, the plume shape during the injection phase in dominated by the injection-induced pressure (Wang *et al.* 2016). The resulting advancement graphs, however, are similar to the work in which the CO_2 was released by assigning a uniform saturation (Han and Kim 2018b; Pruess, K. and Nordbotten 2011).

3.3.3. Analytical calculation

The structural trapping criteria for each of the cases are evaluated using the first derivatives of the equations representing the caprock in Table 3.3. The results are presented in Table 3.4.

Table 3.4. The structural trapping criteria for each of the cases.

Cases	Derivative	Condition	Condition
a, b	$\dfrac{B}{W(\frac{x^2}{W^2}+1)}$	$B<0$ (slope >0)	trapping on the right-side of the injection point
		$B>0$ (slope <0)	trapping on the left-side
c	$\dfrac{B}{W(\frac{x^2}{W^2}+1)}+\dfrac{2A\pi cos\left(\frac{2x\pi}{W}\right)}{W}$	$B<0$ (slope >0)	trapping on the right-side
		$B>0$ (slope <0)	trapping on the left-side
e, f	$\dfrac{2A\pi cos\left(\frac{2x\pi}{W}\right)}{W}$	-	Always trapping
g, h	$\dfrac{2A\pi cos\left(\frac{2x\pi}{W}\right)}{W}+tan(\Theta)$	$tan(\Theta)\geq\frac{2A\pi}{W}$ ($\Theta\geq tan^{-1}(\frac{2A\pi}{W})$)	No trapping
i	$B\left(\dfrac{2\pi cos\left(\frac{2x\pi}{W}\right)}{Wx}-\dfrac{sin\left(\frac{2x\pi}{W}\right)}{x^2}\right)$	-	Always trapping
j	$B\left(\dfrac{2\pi cos\left(\frac{2x\pi}{W}\right)}{Wx}-\dfrac{sin\left(\frac{2x\pi}{W}\right)}{x^2}\right)+tan(\Theta)$	$\Theta\geq tan^{-1}(-B\left(\dfrac{2\pi cos\left(\frac{2x\pi}{W}\right)}{Wx}-\dfrac{sin\left(\frac{2x\pi}{W}\right)}{x^2}\right))$	No trapping

As can be seen, except in the tilted models in which the possibility of trapping depends on the tilt degree, the structural trapping is guaranteed in all other cases. The caprock morphology has a significant impact on the CO_2 structural trapping and retardation of the plume migration. As

shown earlier in the simulation results, the plume's spread is inhibited if its height is on the same scale as the amplitude of the relief. Therefore, for thin plumes (resulting from low injection rates or longer migration distances associated with dipping aquifers lacking structural traps), the small structural reliefs retard their migration and result in a more secure CO_2 sequestration, while for thicker plumes, their effect is negligible.

3.3.3.1. Case study

In this part of the chapter, the equation which represents Case (j) is used. The goal is to compare the amount of trapping predicted by the analytical estimate with the numerical simulation results. The results are then validated through numerical simulations. The model dimensions for the numerical simulations are the same as in section (3.2.1). For $\lambda = 1000$ m, $Z_0 = 1500$ m $and\ B = 10000$, the equation representing the caprock morphology becomes:

$$Z = 1500 + 10000\ \frac{sin\left(\frac{2\pi x}{1000}\right)}{x} + x\ tan(\Theta) \qquad\qquad \text{Equation 3.3}$$

The synthesised aquifer model used in this section is illustrated in Figure 3.11.

Figure 3.11. Aquifer model used for numerical simulation and analytical calculation. All figures are exaggerated by a factor of 25 in the z-direction.

The analytical method indicated that for the model studied, the structural trapping capacity for 4° tilted (and above) becomes zero. Moreover, using the same approach, the amount of structural trapping capacity for the models with 0, 1, 2, 3 and 4 degrees tilt angles, respectively, was calculated and the results are listed in the second column of Table 3.5.

Table 3.5. Structural trapping capacity estimated using the analytical method and numerical simulations.

Tilt angle	Analytical calculation (million cubic metres)	Numerical simulation (million cubic metres)
0	25.26	22.14
1	14.06	14.94
2	7.18	9.42
3	2.9	2.76
4	0	1.44

To compare the results, numerical simulations are undertaken for the same models. Figure 3.12 illustrates the simulation results for free CO_2 trapped beneath the caprock structures for various tilt angles. To compare the simulation results with the analytical method, the plume must have enough time to migrate. For this purpose, and keeping all other factors constant, the post-injection period was extended to 5000 years. The plume is not immobilized, however, and would extend further for a longer simulation duration, which introduces some error in comparing the results with the analytical approach.
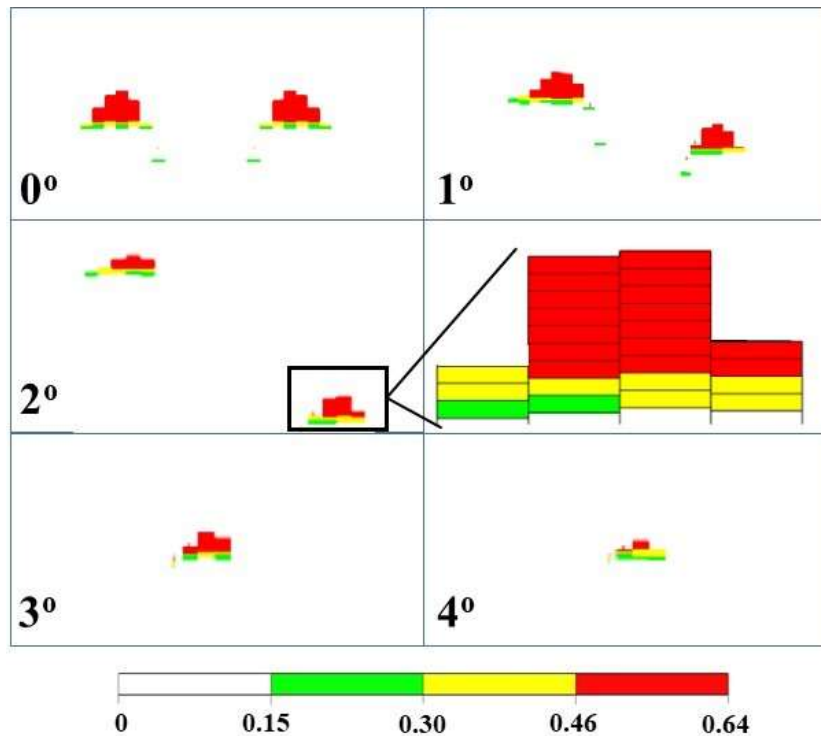
Figure 3.12. Cross-section view of the free CO_2 structurally trapped beneath the caprock. All figures are exaggerated by a factor of 50 in the z-direction.

As shown in Figure 3.12, increasing the tilt angle significantly decreases the amount of structural trapping. Results showed that for the 5° tilted (and above) models, the structural trapping capacity is zero, which is the same for the analytical approach. Moreover, by knowing the cell dimensions, saturation and porosity, it is possible to calculate the volume of the CO_2 for each of the models (Figure 3.12, 2° tilted model). The results are listed in the third column of Table 3.5. Possible sources of error could be the factor of time (as mentioned above) and grid geometry. While the analytical approach considers the curvy edges of the model, the geological model used in the numerical simulation consists of cuboids. Therefore, the volume considered in numerical simulations could be smaller and introduce some error, depending on the grid resolution.

Moreover, the results presented here are site-specific and valid for the studied model. The goal here, however, is to check the performance of the analytical approach for rapid estimation of structural trapping capacity. This could be useful in site screening before performing any numerical simulations to decrease the computational costs.

3.4. Concluding remarks

The impact of top surface morphology and reservoir boundary on the plume advancement, along with structural and dissolution trapping mechanisms were investigated, using numerical simulations and analytical calculations. To make the synthetic model more realistic, the structural properties of several real sites were studied carefully, and their structural relief classified into three scales (small, medium and large).

The CO_2 dissolution in brine in an aquifer closed on one side (closed faults, salt walls etc.) is seen to be more significant than one that is open from both sides. The dissolution is strongly dependent on the formation dip, whereby increasing the tilt results in the injected CO_2 having more space to migrate upwards and interact with more formation water. The least dissolution occurs where the major portion of the injected CO_2 is trapped in a sand ridge or an anticline. The impact of the dip angle on the plume migration and dissolution during the injection phase was found to be negligible (Figure 3.10). Due to higher buoyancy forces, the results showed a higher migration distance in the tilted models.

The possibility of structural trapping was estimated through analytical calculations. The results showed that, except for the tilted reservoir models where the degree of tilt plays a significant role in the plume migrations, some structural trapping is guaranteed. The comparison between the numerical simulation and analytical calculations for structural trapping capacity estimation in a synthetic model was reasonably acceptable. Therefore, it is suggested that an analytical approach is used for initial site screening and selection before full reservoir simulations.

It is worth mentioning that while two-dimensional idealized sinusoidal patterns are assumed in the study, three -dimensional ones, in reality, are more complicated. Moreover, the patterns are not preserved well in real cases due to various geological events, such as erosion (Mountney, Posamentier and Walker 2006). It would be valuable to see the results from this chapter on a more complex 3D model with various types of rugosity and sinusoidal pattern on a different caprock region.

Chapter 4 [‡]

Accuracy of VE models to study caprock morphology

4.1. Introduction

Numerical simulators are essential tools for studying problems related to the safe storage of CO_2 in saline aquifers. They have become popular when investigating safety, feasibility and economic concerns related to a CCS proposal. Therefore, we must have confidence in the results provided by numerical simulators and understand how sensitive their responses are with respect to storage site parameters.

One of the key sensitivity issues when modelling CO_2 storage is caprock geometry, both at the large and smaller scale (Ahmadinia, M., Shariatipour and Sadri 2019; Onoja and Shariatipour 2018). The caprock geometry of sedimentary rocks is usually deformed over geological time, which results in structures such as tilted beds and folds. As mentioned previously in Chapter 2, sinusoidal structures formed through deformation and deposition processes are common in sedimentary rocks. They are observed at various scales of which folds and bedforms are the main types (Han and Kim 2018a). Folds resulting from non-isostatic pressure (stress) are the most significant type of sinusoidal features and have three broad classes: anticlines, synclines and monoclines. As discussed, the occurrence of dipping strata and sine-wave structures is widespread in geological settings. The current chapter assumes that such heterogeneous features (rugosity and dipping strata) preserved in the targeted storage site could have an impact on the CO_2 plume storage and trapping process.

The model data representing the formation characteristics will always be uncertain in a 3D simulation of CO_2 storage. Regardless of the predominant driving force in the model, heterogeneity may considerably alter the plume migration path. Most of the aquifers, in reality, have complex geology, such as the Sleipner in the North Sea, which has a complex, layered structure. The detailed modelling of the aquifer is not always available due to the limited number of exploration wells and scarce seismic data. Although the caprock morphology governs the plume migration path in the long-term, oversimplified top surfaces are sometimes considered in simulation studies (Shariatipour, Seyed M., Pickup and Mackay 2016).

Current approaches cannot fully resolve the problems related to physical modelling, upscaling, and numerical modelling in the practical simulation of CO_2 in geological formations. Therefore, the problem needs to be simplified to be computationally feasible. A benchmark study was performed (Nordbotten, J. M. *et al.* 2012) using three distinct approaches: reduced physics, upscaling and a non-converged discretisation to simplify the problem. The CO_2 storage in a simplified aquifer was simulated using different simulation approaches to answer relevant storage questions. The results for the various simulation methods and assumptions diverged, suggesting that, even with highly idealised problems, the numerical simulation tools do not always provide convincing results.

In this chapter, the CO2lab module in MRST (Bao *et al.* 2017) is employed, and the results have then been compared with three numerical solutions provided by the ECLIPSE software, namely E300, E100 and EVE. It is worth noting that E300 is a compositional simulator, and thus differs significantly from the other three, all based on the black-oil formulation. The Computational Geoscience Group has developed the Matlab Reservoir Simulation Toolkit (MRST) within the Department of Mathematics and Cybernetics in the division of SINTEF Digital in Norway. The CO2lab module is based on the vertical equilibrium assumption, which facilitates the modelling of large-scale CO_2 migration. The vertical equilibrium method supports modelling of the most relevant physical effects involved in long-term migration, and its applicability on realistic models has been the topic of past multiple studies (Bandilla, Karl and Celia 2019; Gasda, Sarah E., Nordbotten and Celia 2009; Nilsen, Lie and Andersen 2016b). For the long-term storage of CO_2, plume migration is controlled by gravity and capillary forces (Bjørnarå et al. 2014). Since the gravity segregation is often over a reasonably short timescale (due to the difference between the fluid densities), the plume can often be assumed to form a thin layer beneath the caprock after the injection phase has ended (Ahmadinia, M. et al.). Thus,

the vertical fluid segregation is prompt, compared with the up-dip migration, and one can assume that the fluids are fully segregated and are in vertical equilibrium.

It is possible to formulate the VE model in a black oil simulation framework as it has the same structure for multiphase flows as standard equations. The VE model in the MRST (MVE) is based on fully implicit solvers and is adaptable to industry standards (Nilsen, Lie and Andersen 2016a). As mentioned above, the VE assumption is valid for the long-term storage of CO_2 where the timescale is larger than the vertical segregation time. It should be noted that the VE model avoids errors caused by vertical discretisation, but is built on the assumption of vertical equilibrium, and will, therefore, introduce modelling errors of its own if this assumption is not justified. When using a VE approach, vertical heterogeneity in the permeability is ignored, which is a source of error if there are substantial vertical variations in permeability. Some recent studies (Møyner and Nilsen 2017; Møyner, Andersen and Nilsen 2018), however, have applied VE in a multilayer setting with strong permeability contrast, combined with full 3D discretisation locally where needed. The errors introduced by a VE assumption are in many cases smaller than the errors induced by low lateral resolution grids to make the 3D simulations computationally feasible (Nilsen, Lie and Andersen 2016b).

In a VE formulation, the problem dimension is reduced to 2D. The considerable reduction in the number of unknowns of the 2D system compared to the 3D system significantly reduces the computational cost of the problem. Therefore, it allows the modeller to increase the lateral grid resolution, beyond what would be otherwise impractical for 3D simulations. Using the up-scaled 2D variables from the VE formulations, it is possible to reconstruct the 3D solution through analytical calculations. Many researchers (Coats *et al.* 1967; Coats, Dempsey and Henderson 1971; Martin 1958; Martin 1968) used similar models several decades ago in the petroleum industry.

The performance of a number of 3D numerical methods has been investigated (Class *et al.* 2009) on specific problems related to the CO_2 storage in geological models. The results showed a reasonable degree of agreement. The major sources of error were believed to be due to gridding, wrong inputs and different interpretations of the problem (such as boundary conditions). An early comparison of full 3D simulations and VE calculations on a real model was undertaken on the Utsira formation (Nilsen et al. 2011a). A simplified model that did not include capillary pressure and dissolution was considered in their work. The results showed that the VE model was significantly faster than the 3D simulation for the case studied.

Moreover, when segregation is achieved, the solutions provided by the VE models were more accurate than their 3D counterparts. The spatial distribution of reservoir permeability was modified to match the observed and calculated plume extension data for the Sleipner model. The authors (Cowton *et al.* 2018) developed a vertically integrated fluid flow simulator, and their results were nearly identical to those of E100. Several (10 in total) mathematical and numerical models were applied (Class *et al.* 2009) to three different benchmark studies, including leakage of injected CO_2 into overlying formations through a leaky well; enhanced gas recovery (EGR) by injection of CO_2 and; CO_2 plume spreading and dissolution and storage mechanisms in a large-scale heterogeneous reservoir. According to their study, realistic heterogeneities and uncertainties, due to different ways of incorporating heterogeneity within the applied spatial discretisation, have a noticeable impact on the results. A simplified CO_2 storage study was designed (Nordbotten, J. M. *et al.* 2012) in order to understand the extent of variability in model predictions due to applying different modelling approaches to the same problem. Six research groups participated using the 3D simulator (four groups), MVE and analytical approaches. Despite considering a relatively simple, idealised problem, the resulting model predictions varied significantly. The error sources were mainly due to a difference in physical processes (such as dissolution and capillary pressure), numerical modelling approaches, upscaling, and problem definition interpretation.

The work presented below is one of the first benchmark studies on the impact of caprock morphology on CO_2 storage migration using several modelling approaches (E100, E300, EVE and MVE). In particular, the impact of small-scale, sinusoidal undulations in the caprock (referred to as 'rugosity') are investigated on CO_2 plume migration and dissolution trapping. For this purpose, fifteen sets of 3D geological models are constructed with a wide range of rugosity and slopes in Matlab; and systemically analysed the performance of four simulation approaches in a CO_2 storage study. The objective is to show the benefits of using the VE approach for CO_2 migration and dissolution in a geological model while focusing on a realistic caprock morphology.

4.2. Mathematical formulation

In this section, the governing equations for the flow dynamics in the VE and 3D models are compared. Equation 4.1 describes the mass conservation in the 3D simulations on the fine-scale,

$$\frac{\partial(\varphi \rho_\alpha s_\alpha)}{\partial t} + \nabla \cdot \rho_\alpha u_\alpha = \rho_\alpha q_\alpha \qquad \text{Equation 4.1}$$

where,

α: fluid phase (w or g),

φ: porosity,

ρ_α: fluid density,

s_α: phase saturation,

q_α: phase volumetric flux,

u_α: is the fluid velocity, given by the multi-phase extension of Darcy's equation

$$u_\alpha = -k\lambda_\alpha(\nabla P_\alpha - \rho_\alpha g) \qquad \text{Equation 4.2}$$

where,

k: rock absolute permeability,

λ_α: fluid mobility,

$\lambda_\alpha = \lambda_\alpha(s_w) = \frac{k_{r\alpha}(s_w)}{\mu_\alpha}$, $k_{r\alpha}$ and μ_α denote for relative permeability and fluid viscosity respectively

P_α: phase pressure,

g: gravitational acceleration,

Replacing the parameters in   Equation 4.1 with their vertically integrated counterparts, it is possible to derive the governing equation for the vertical equilibrium approach. For simplicity, a sharp interface between the fluids is assumed. A detailed derivation can be found in (Bandilla, Karl W., Celia and Leister 2014; Nilsen, Lie and Andersen 2016a; Nilsen et al. 2011b). Here the final mass conservation relation in the VE model is presented. Plume thickness below the caprock is used as a variable to present the equation in fractional form (Nilsen et al. 2017).

$$\varphi \frac{\partial h}{\partial t} + \nabla f(h)\left(U_t - k(\rho_w - \rho_g)\Lambda_g(h)\Lambda_w(H-h)g\nabla(z_t + h)\right) = Q_g \qquad \text{Equation 4.3}$$

where,

h: plume thickness,

H= aquifer thickness,

φ: porosity,

ρ_α: phase density,

z_t: top surface depth,

U_t: total volume flux which is given by s vertically integrated version of the multiphase extension of Darcy's equation,

$$U_t = -k\Lambda_t(h)(\nabla P_i - [\rho_w - (\rho_w - \rho_g)f_g(h)]g\nabla(z_t + h)) \qquad \text{Equation 4.4}$$

where,

P_i: pressure at the interface of gas and water,

f_g: fractional flow function for the gas phase, which is given by,

$$f_g = \Lambda_g(h)/[\Lambda_w(H-h) + \Lambda_g(h)] \qquad \text{Equation 4.5}$$

It is important to note that upscaled mobility (Λ_t in   Equation 4.4) is different from the fine-scale (λ_α in   Equation 4.2) and is defined as (Nordbotten, Jan Martin and Celia 2011):

$$\Lambda_\alpha \equiv \int_{\xi_B}^{\xi_I} \lambda_{\alpha,||}k_{||}dz\, \boldsymbol{K}^{-1} \qquad \text{Equation 4.6}$$

where,

ξ_B= elevation of the bottom of the formation (surface),

ξ_I= elevation at which two fluids are separated (surface),

$\boldsymbol{K}^{-1}$= integrated permeability,

The upscaled parameters in the VE formulation are obtained by integrating the fine-scale ones across the aquifer's thickness with respect to the z-direction. Therefore, despite λ_α which depends on three spatial parameters 'x', 'y' and 'z', Λ_t depends on 'x' and 'y' only (in addition to time). Several models are available to reconstruct fine-scale saturation and mobility based on the upscaled saturation, out of which the sharp interface is employed while performing the VE based simulations. The method is valid when the capillary pressure effect is negligible in the 3D model. More details can be found in (Andersen, Gasda and Nilsen 2015).

Both ECLIPSE and MRST have implemented their equations using finite-volume discretisation that is fully implicit in time.

4.2.1. Dissolution in E300, E100, EVE and MVE

CO_2 dissolves into the brine and saturates at values of a few percent per volume. The CO_2 dissolution algorithm provided by the CO2STORE keyword in E300 allows the carbon dioxide to dissolve in the aqueous phase. The fugacity function for aqueous CO_2 is constructed to match the solubility data, based on which the equilibrium between aqueous CO_2 and brine is defined. E300 in the current study uses the Peng-Robison equation of state to compute the fluid properties at their corresponding temperature and pressure (Schlumberger 2017). The CO_2 solubility in water is a function of temperature, pressure and salinity, calculated from the Chang et al. correlation (Chang, Coats and Nolen 1996).

The fluid properties in E100 are provided from two dimensional (brine and dissolved CO_2) tabular data which are a function of pressure and are interpolated and extrapolated if required, at a constant slope. The tables for E100 can be derived from the E300 fluid inputs, using the PVTi program in ECLIPSE to make sure the input properties are identical. Therefore, E100 and E300 input properties are identical with a high degree of accuracy, and the only difference is in their formulation method, which is black oil and compositional in E100 and E300, respectively.

Vertical Equilibrium in ECLIPSE (EVE) is an option available in E100. Using EVE, apart from the saturation data (used to calculate relative permeability and capillary pressures), other data and the simulation approach are the same as in E100. In E100 the dispersed saturation function is specified (fluids are assumed to be evenly distributed over the grid block). At the same time, EVE enables us to specify either dispersed or segregated saturation functions or a weighted

average of the two (VE assumption, where fluids are in hydrostatic equilibrium). Therefore, dissolution in EVE is handled the same way as it is in E100, i.e. using the PVT tables.

While using MVE, the CO_2 and brine are assumed to be separated by a sharp interface, leading to an up-scaled relative permeability function that is linear (Nilsen, Lie and Andersen 2016b). Viscosity and compressibility are interpolated from a sampled table (identical to the one used in other simulations) within the desired temperature and pressure range. In such a fully segregated system, dissolution occurs only in the interface region. Since CO_2 saturated brine at the interface is denser than the ambient brine, convective mixing may be triggered to significantly enhance dissolution by transporting saturated brine away from the two-phase region and downwards into the vertical column. This process occurs spontaneously in sufficiently resolved 3D simulators, but in MVE dissolution is mainly governed by a constant upscaled "rate" value and a maximum dissolution parameter. The "rate" is constant and depends on both the rock and fluid properties. Before starting the main benchmark study, some simulations are performed using E300 and calculated the gas flow rate for an individual block to set an accurate value for this rate. Using this flow rate, the average downward migration speed of CO_2 during the post-injection period is calculated. In this way, it is possible to estimate the suitable up-scaled rate value for the MVE. After ensuring that the rate is a good representation of the dissolution occurring in the 3D simulations, the benchmark study is performed.

4.3. Numerical simulations

4.3.1. Model set-up

The purpose of this chapter is to investigate the outcomes of different simulation approaches applied to the models with different rugosities and aquifer top-surface slopes. Long-term plume development, the amount of dissolved CO_2, and computational requirements are compared. For this purpose, a homogeneous closed boundary aquifer was defined, to which rugosity and slope were added, depending on the specific test case. The horizontal permeability is 50 mD which is in the range of the In Salah storage site. CO_2 is injected through one centre injector for ten years with a rate of 0.5 Mt/year, comparable to 20% of the emissions of a 500 MW coal-fired power plant (Orr 2009). The injection is then followed by 1000 years of post-injection migration. Details of aquifer parameters are available in Table 4.1.

Table 4.1. Aquifer parameters

Parameter		Value
Number of cells (NX×NY×NZ)		201×201×9
Reservoir size (km) (LX×LY×LZ)		40×40×0.1
	DX×DY	199×199
Cell size (m)		5 (layers 1-4)
	DZ	10 (layers 5-7)
		25 (layers 8-9)
Rock compressibility (1/bars)		4.35E-5
Water density at 1500 m depth (kg/m^3)		1049
CO_2 density at 1500 m depth (kg/m^3)		468
Residual water saturation (S_{rw})		0.27
Residual CO_2 saturation (S_{rc})		0.20
Horizontal Permeability k_h (mD)		50
Vertical to horizontal to Permeability (k_v/k_h)		0.1
Porosity		0.2
Pressure at the 1500 m depth (bar)		147
Simulation period (years)		1010
Number of time steps		200 (100*0.1 years + 100*10 years)
Water viscosity at 150 bar (Centipoise)		0.444
CO_2 viscosity at 150 bar (Centipoise)		0.033
Reservoir Temperature		80ºC

The relative permeability curves are shown in Figure 4.1.
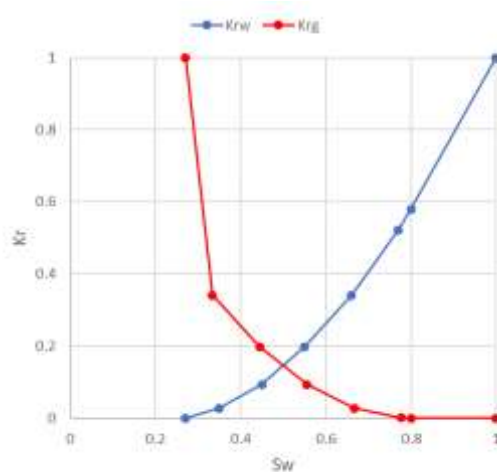
Figure 4.1. Relative permeability curves (Smith *et al.* 2012)

Four parameters, including the aquifer top-surface slope and amplitude of the rugosity in x and y directions, were chosen for the sensitivity analysis. The following formula describes the contact boundary between the caprock and reservoir:

$$z(x,y) = A[sin(\omega_b x) + sin(\omega_b y)] - R_x sin(\omega_c x) - R_y sin(\omega_c y) + x\, tan(S_x) + y\, tan(S_y)$$

Equation 4.7

where $\omega = \frac{2\pi}{W}$ is the angular frequency of the sine wave function and z, x and y are the z, x and y-directional coordinate of the caprock surface, respectively.

The terms A, ω_b and ω_c are constant in Equation 4.7 at the values of 40 (m), 25 (rad/m) and 150 (rad/m), respectively, while R_x, R_y, S_x and S_y are unique for each case. The first two terms (with "A" as a multiplier) represent the main structural traps. The next two negative terms represent rugosity, which has a higher frequency than the main structural traps ($\omega_c > \omega_b$). The next two tangential terms represent the model tilt angles. The amplitude of rugosity, and model dip angles in the x and y directions are represented by R_x, R_y, S_x and S_x , which are the sensitivity analysis parameters in this chapter.

The base case model is flat (not tilted, $S_x = S_y = 0$), without rugosity ($R_x = R_y = 0$) and the caprock is presented local domes only using the first two terms in Equation 4.7 (Figure 4.2). The amplitude of the dome is 40 m, having $R_{x,y} = 20$ adds a sinusoidal structure with an average amplitude of 20 m to the dome.
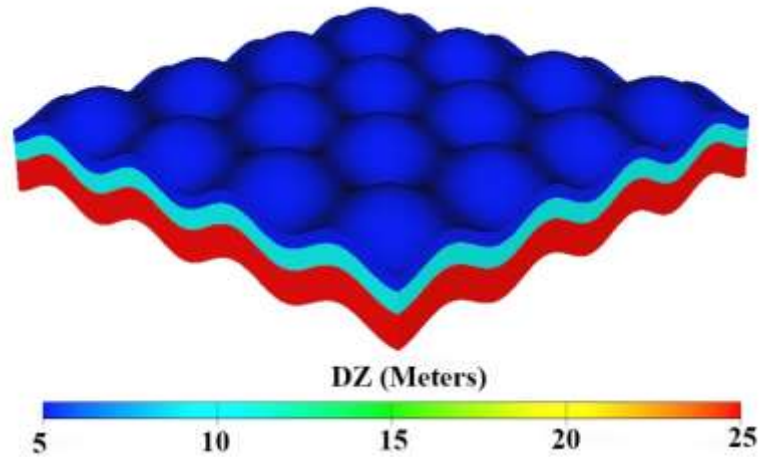
Figure 4.2. The thickness of Base case (Not to scale)

To analyse how dipping and small-scale structures affect the CO_2 storage process, a function was written in Matlab to construct the geological models using different rugosity and slope in x and y directions. The models (Table 4.2) were then automatically imported into MVE, E100, E300 and EVE simulators separately and their corresponding results for CO_2 dissolution and computational time were analysed in Matlab. The list of simulation cases is available in Table 4.2.

Table 4.2. List of simulation cases

Case #	R_x (m)	R_y (m)	S_x (º)	S_y (º)	Case #	R_x (m)	R_y (m)	S_x (º)	S_y (º)
BASE	0	0	0	0	8	20	0	0	0
1	0	0	0	5	9	20	0	0	5
2	0	0	5	0	10	20	0	5	0
3	0	0	5	5	11	20	0	5	5
4	0	20	0	0	12	20	20	0	0
5	0	20	0	5	13	20	20	0	5
6	0	20	5	0	14	20	20	5	0
7	0	20	5	5	15	20	20	5	5

4.3.2. Justification of constant temperature assumption

The shallowest part of the domain corresponds to a 1.5 km depth, and a constant temperature of 80ºC is considered in all the models. The impact of temperature becomes more significant in the tilted models. The highest tilt angle in this chapter is 5º, which results in the following condition (Figure 4.3):

- CO_2 will be injected at a depth of 3.25 km, which is feasible in CO_2 storage studies such as the Rousse site in France (4 km) and Weyburn in Canada (3.8km) (Espinoza and Santamarina 2017).
- The temperature at the top of the model (1.5 km depth) is 80ºC.
- The temperature at the injection point (3.25 km depth, middle) is 115ºC.
- The temperature at the upmost of the plume (2.55 km depth) is 101ºC.
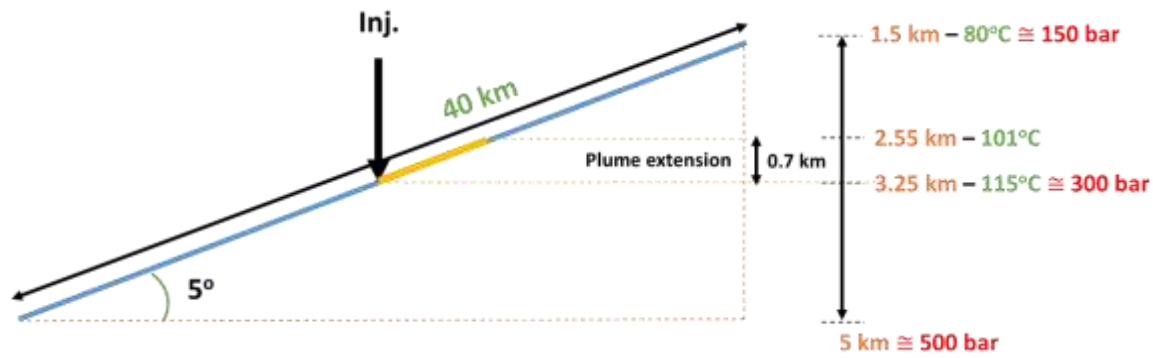
Figure 4.3. Reservoir condition in 5° inclined models. Approximated temperature and pressure values are given at each depth.

If one compares the tilted models (injection point at 3.25 km, 115 °C) with the flat models (injection point at 1.5 km, 80 °C), considering a constant temperature, a 35°C (115 °C-80 °C=35 °C), the change in temperature will be ignored (which is also equivalent to the distance from the injection point to the top of the model in the tilted models). In other words, in this chapter, the temperature is at a constant value of 80°C while the real temperature at the injection point in the models with 5° tilt would be 115°C. According to the CO_2 solubility data in water (Kohl and Nielsen 1997), a change in temperature from 80°C to 115°C at 300 bars (pressure at the injection point in the tilted models, Figure 4.3), results in a 0.2% error in CO_2 solubility. Based on the theoretical data, under high temperature and pressure conditions (such as those used here), CO_2 solubility becomes a weak function of temperature, making the constant temperature assumption (within the aquifer boundaries) reasonable. Three sets of experiments are performed using E300 to support this argument. The surface temperature varies between 0-30°C (Bachu 2003). Setting the surface temperature to 15°C, three sets of the geothermal gradient were including:

- Exp1: A geothermal gradient of 43°C/km until the depth of 1.5km, followed by 20°C/km from 1.5km downward, which is the same condition shown in Figure 4.3. A related point to consider is that there are real cases with abnormal geothermal gradients within the certain depth, such as Soultz-sous-Forêts (Gérard *et al.* 2006), in which at a depth of 1000m the geothermal gradient is 100°C/km and decreases to 50 °C/km at 2000m.

- Exp2: A constant geothermal gradient of 20°C/km.

- Exp3: A constant geothermal gradient of 43.3°C/km.

Details of the geothermal gradients in all the experiments are available in Figure 4.4.
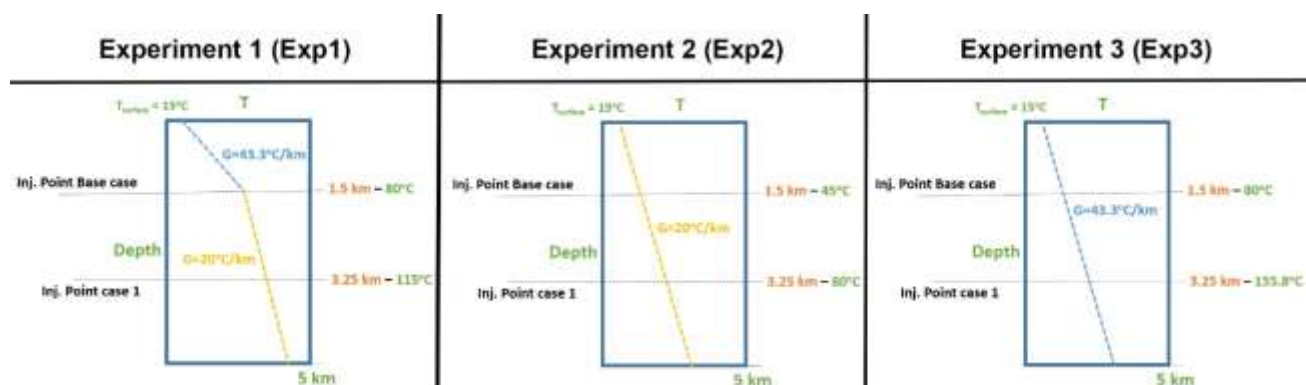
Figure 4.4. Temperature versus depth data in all the experiments.

The simulation is performed using Base Case (0,0,0,0) and Case 1 (0,0,0,5) in E300, considering the temperature versus depth data presented in Figure 4.4. The averaged absolute errors between the results from these experiments (variable temperature in aquifer according to depth) and the ones used in this chapter (constant temperature in the aquifer) are reported in Table 4.3. A constant temperature of 80°C is considered, which means that the CO_2 is injected at this temperature in tilted and flat cases. The corresponding injection temperature for Base Case in Exp1 and Exp3 and Case 1 in Exp2 is also 80°C (Figure 4.4) which explains the minimum averaged absolute errors in these scenarios.

Table 4.3. The averaged absolute error between the results from the experiments and the ones used in this chapter for Base Case and Case 1.

	The averaged absolute error		
	Exp1	Exp2	Exp3
Base Case (0,0,0,0)	0.99%	5.29%	2.01%
Case 1 (0,0,0,5)	4.51%	1.92%	5.36%

These results confirm the observation from the CO_2 solubility data in water (Kohl and Nielsen 1997) and show that regardless of the temperature gradient (Exp1, Exp2 or Exp3), at the

operation conditions (above 150 bars and at 80ºC), the impact of temperature on the overall dissolution is relatively small, although not always completely negligible.

4.3.3. Simulation results

The CO_2 plume saturation in the top cells of the base case was compared with four other cases (4, 5, 11 and 12) at the end of the simulation in Figure 4.5. There is a good agreement between the final plume distribution results from the ECLIPSE (E100, E300 and EVE) and MRST (MVE) models. The plume migrates farther in the tilted models (Case 4 vs 5) while rugosity on the top surface limits the extent of its migration (Bases case vs 12).

The upscaled (VE) saturation is not the true fine-scale (3D) saturation, but the fraction of CO_2 in a total vertical column, which is plume thickness divided by aquifer thickness (when disregarding residual saturation). To present the vertical equilibrium results more effectively, 3D CO_2 saturations are reconstructed from the VE solution for the mobile and residual CO_2 interfaces and then projected onto a 3D image. For this purpose, based on the value of calculated CO_2 thickness, saturation values are allocated to the corresponding cell in the 3D grid. For more information, see (Nilsen, Lie and Andersen 2016a).
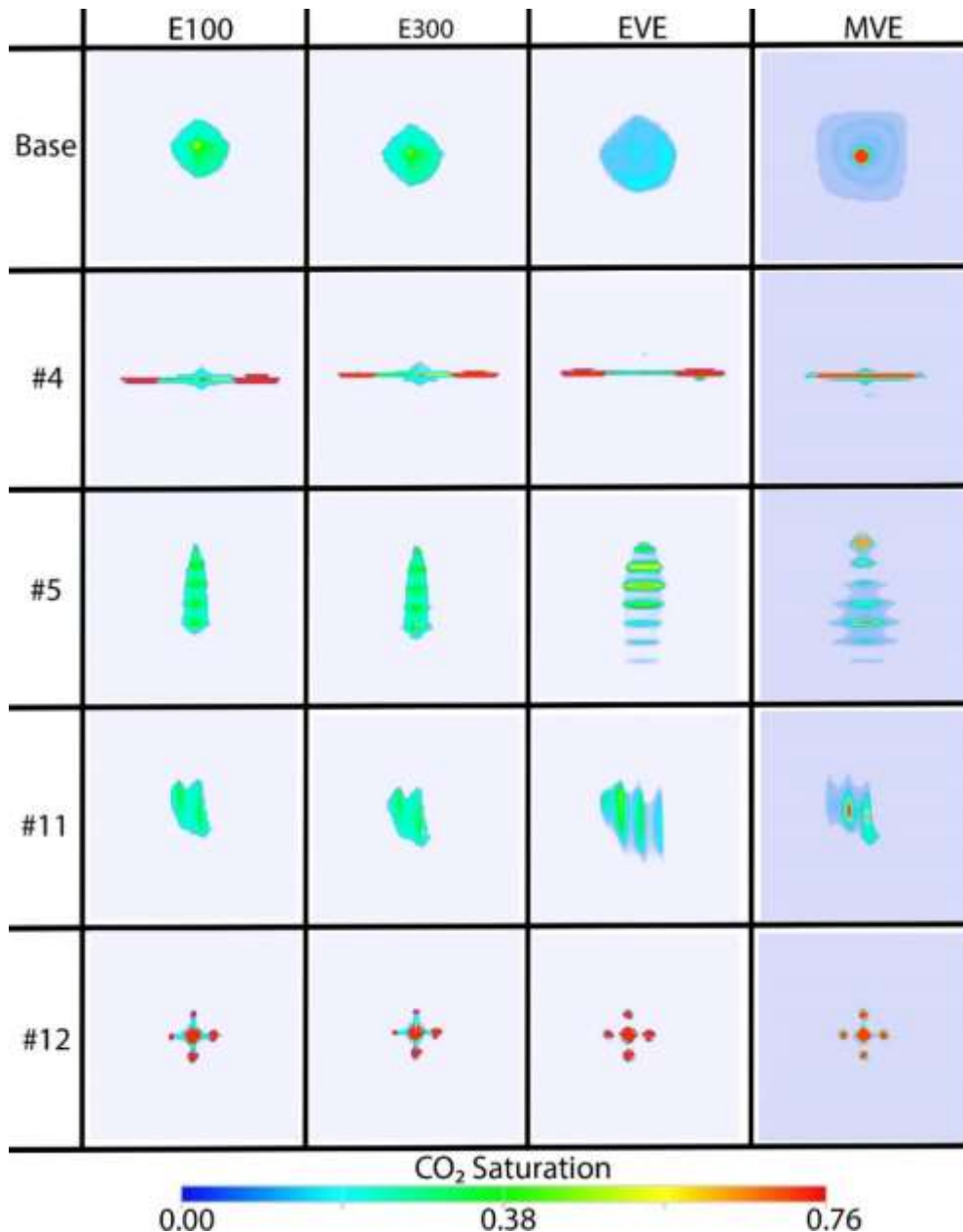
Figure 4.5. CO$_2$ saturation profile at the end of the simulation.

The extent of the plume seen to be is higher in the VE model (EVE and MVE) which could be partially due to the earlier segregation, and partially due to the numerical diffusion caused by limited vertical resolution in the 3D model. Another reason is that since the vertical permeability is 5 mD, the plume spreads much further before reaching the top. Eventually, part of the plume becomes trapped residually while moving upward, seen in the 3D simulations (E100 and E300). In the VE model, however, the plume's upwards migration is instantaneous. Figure 4.6 clearly illustrates this statement. The top and side (middle layer) views of the plume

distribution are illustrated for the E300 and EVE model. The extent of the plume at each end is shown with an arrow. A noticeable portion of the CO_2 becomes trapped residually in the E300 model in the bottom layers, resulting in lower migration distance/speed.
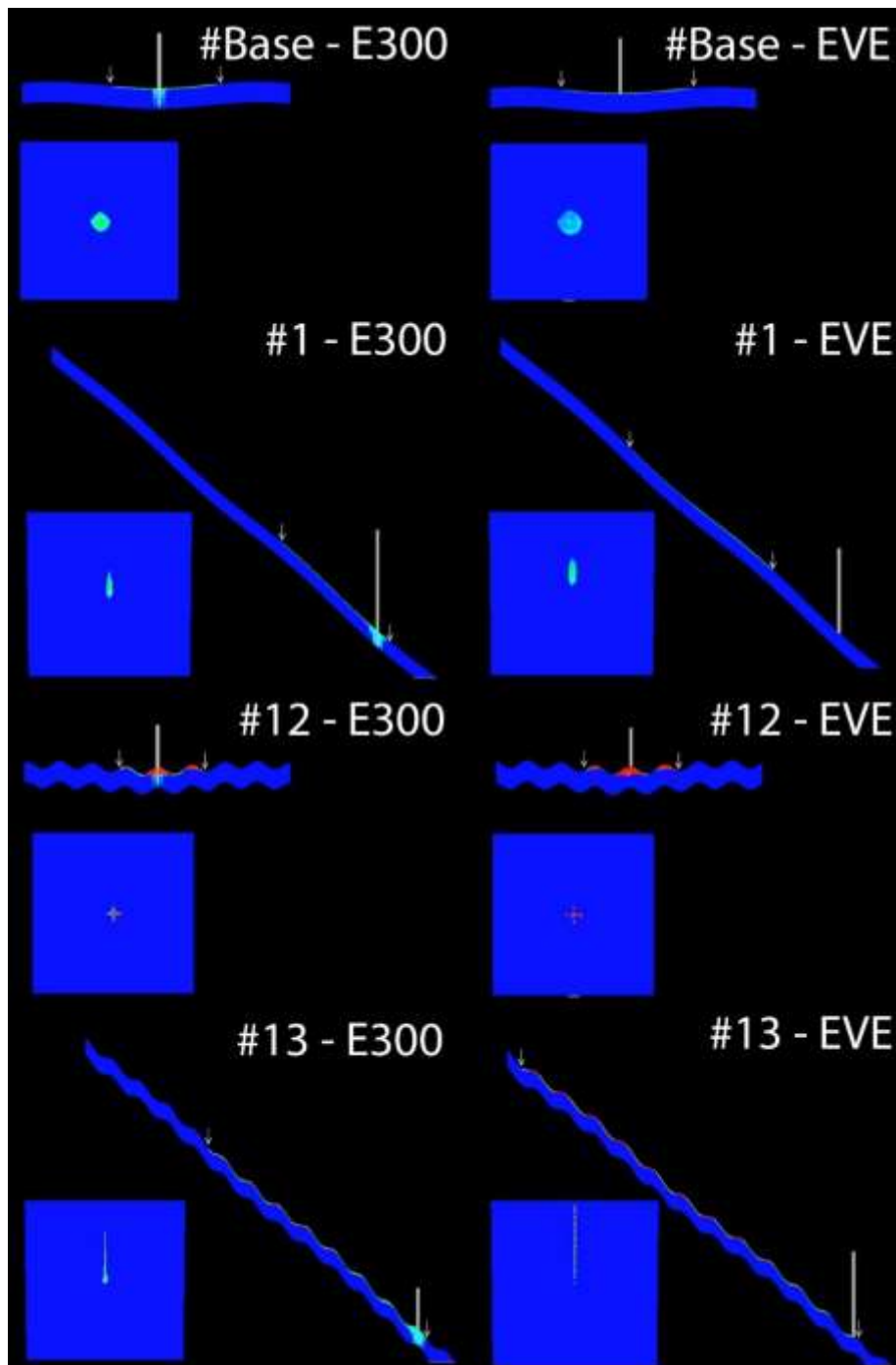
Figure 4.6. The side and top views of plume distribution in E300 and EVE models.

The percentage of CO_2 dissolution for all the cases is presented in Figure 4.7. The amount of dissolved CO_2 at the end of injection, at mid-way and the end of the simulation are investigated. Based on the current simulation parameters, using formula (19) from (Andersen and Nilsen 2018), the segregation time can be shown to be in the order of 20 years for this scenario. The results indicate a discrepancy in the early stages (10 years, which is less than the segregation time), which is likely caused by the assumption that VE is not approximately valid at this point. The dissolution is higher in the VE models (EVE and MVE) than in 3D (E100 and E300). As mentioned above, when using the VE model, the plume migrates to the top of the aquifer instantly, which consequently increased its contact with fresh brine, migrated a farther distance, and exhibited a higher dissolution. This statement is consistent with the two different trends observed for the VE and 3D models as well. For instance, while the dissolution is higher in the Base Case (R_x=0, R_y=0, S_x=0, S_y=0 or 0,0,0,0) than for Case 1 (0,0,0,5) in the 3D models, the trend is opposite for the VE models. This is because by increasing the aquifer slope, the cone-shaped CO_2 plume around the well area extends further upslope, thereby increasing in volume and leading to more residual trapping of the CO_2 (Figure 4.6). In other words, the plume migration distance becomes smaller in the 3D than the VE models, resulting in less contact with *in-situ* brine in distances further away and therefore a lower dissolution. To confirm this argument, for Bases Case (0,0,0,0) and Cases 1 (0,0,0,5), the horizontal and vertical permeabilities were increased to 500mD and 50mD, respectively. The results show an increase in dissolution by increasing the tilt angle in both E100 and E300. The corresponding amount of dissolved CO_2 in brine for both simulators for the Base Case (0,0,0,0) and Case 1 (0,0,0,5) became 39.1% and 41.6%, respectively, while with lower permeability they were 31.1% and 27.2%, respectively.

In the flat cases, the injected CO_2 moves vertically upwards with limited lateral migration at the bottom layers (compared to the tilted models), eventually resulting in lower residual trapping and therefore higher dissolution. Figure 4.6 also shows that the residual trapping in the Base Case and Case 12 (20,20,0,0) is lower than their equivalent tilted models which are Cases 1 (0,0,0,5) and 13 (20,20,0,5), respectively. A similar conclusion was reported in previous studies (Shariatipour, S. M., Pickup and Mackay 2016), where the dissolution was seen to decrease by increasing the tilt in the models with low vertical permeability. Moreover, to assure that the resulted dissolution trend is not due to the error introduced by low vertical resolutions, the Base Case (0,0,0,0) and Case 1 (0,0,0,5) were refined to 90 cells in the vertical direction (i.e. 1m vertical resolution). The results remained relatively unchanged, and as

observed before, the dissolution in the tiled model (Case 1) was less than the flat one (Base case).

Another reason for the different observed behaviours in the dissolution in the 3D and vertical equilibrium models is possibly due to the differences in fluid properties and saturation data. (See section 2.1).

The results for the E100 and E300 are similar throughout the simulation. While both VE approaches show similar overall trends, the MVE shows a higher dissolution due to differences in how dissolution is modelled in the EVE and MVE models, as described earlier. The minimum dissolution occurs in the flat model with rugosity in both the x and y directions (#12), which is because the plume becomes immobilised in small structural traps (Figure 4.6). In this case, even in 3D models, increasing the slope results in a higher dissolution, so as a consequence Cases 13 (20,20,0,5) have a higher dissolution than Case 12 (20,20,0,0), which was not seen for Cases 1 (0,0,0,5) versus the Base case (0,0,0,0). As is clear in Figure 4.6, the plume extent in Case 13 (20,20,0,5) is significantly higher than Case 12 (20,20,0,0) for both E300 and EVE models.
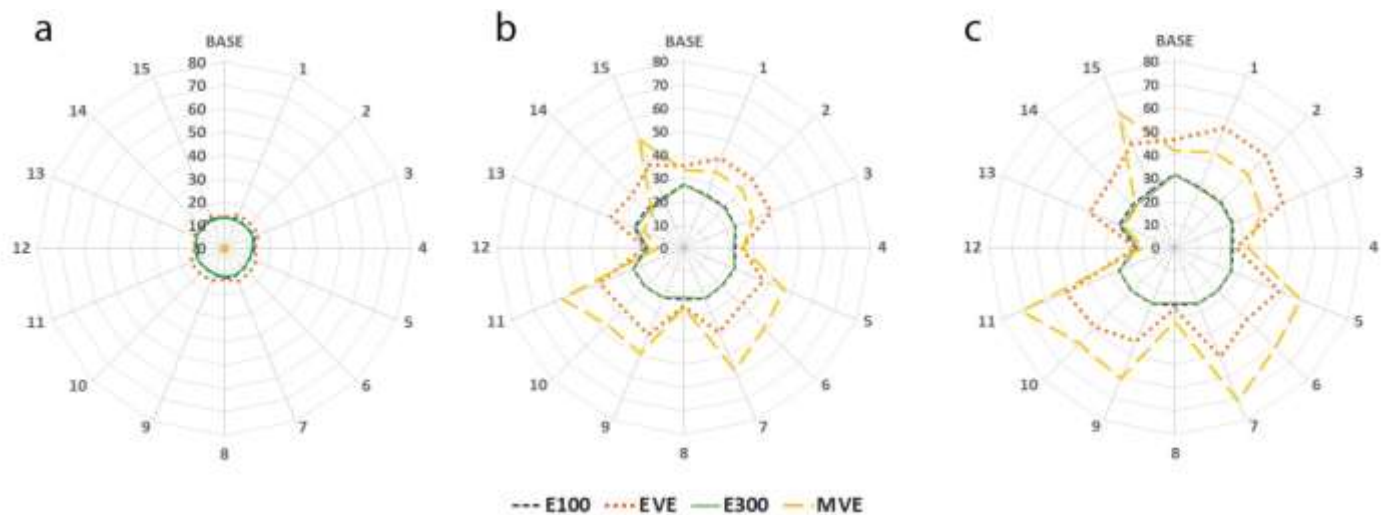
Figure 4.7. CO_2 dissolution in the aquifer (percentage of total injected CO_2), for all the cases after 10 (a), 500 (b) and 1010 (c) years.

Figure 4.8 shows the simulation time for all the models. The computational time is evaluated using the same hardware for all the simulations. As expected, both VE models have significantly lower computational cost than the 3D simulators. Top surface rugosity and tilt do not appear to play any major role in regard to the computational time.
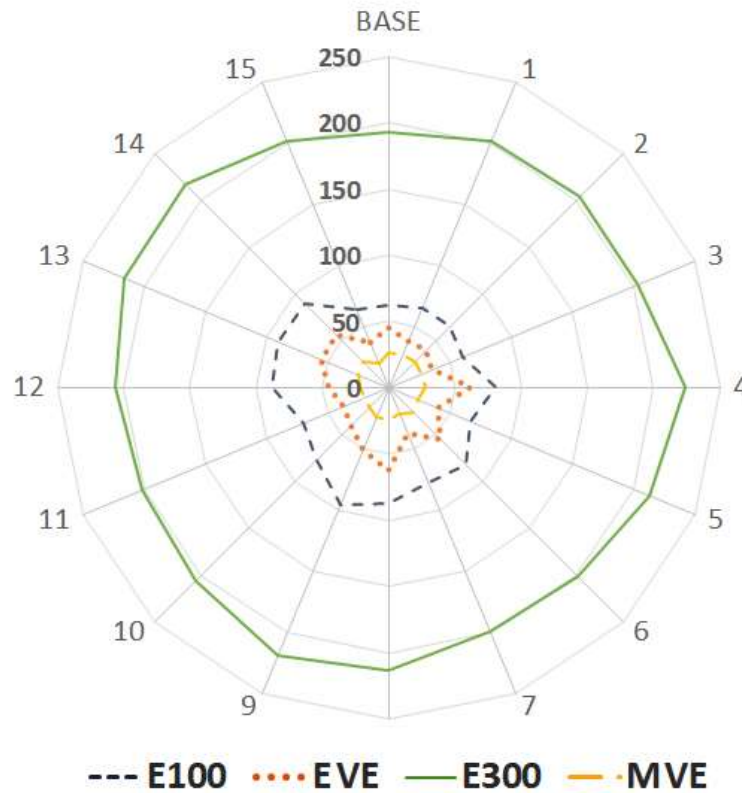
Figure 4.8. Simulation time for all the cases (minutes)

4.4. Conclusion and remarks

In this chapter, four simulation models, including EVE, E100, E300 and MVE, are compared. The simulations were performed on a homogenous model with a relatively low permeability of 50 mD and 5 mD in the horizontal and vertical directions, respectively. The impact of the reservoir slope on dissolution in 3D simulators was different from what was expected in high permeability aquifers. As reported in previous studies, increasing the tilt angle resulted in a farther migration of the CO_2 and more significant contact with the brine, which consequently increases the dissolution (Pruess, K. and Nordbotten 2011; Wang et al. 2016). However, the trend in 3D simulators was opposite, and the dissolution was seen to decrease with increasing the tilt angle, which is thought to be due to residual trapping of the plume in lower layers due

to limited vertical permeability. Therefore, the match between the results from VE and 3D simulators observed in previous studies might not be the case in tight reservoirs. The results showed a good agreement between the plume shapes in all the models. Concerning the computation costs, MVE was seen to outperform the E100, E300 and EVE models significantly.

Chapter 5 [§]

Role of caprock morphology in history matching

5.1. Introduction

While a portion of the CO_2 injected into underground reservoirs as part of a long-term sequestration process will be securely stored through a combination of physical, capillary and dissolution trapping mechanisms, a large part will remain as a free phase in the short to medium term. If there is no proper barrier to impede its progress, such as an anticline, the free phase will move upslope along the caprock. As mentioned in Chapter 2, general seismic surveys can detect large-scale features in the caprock, including domes, traps and spill points. Their detection level and resolution, however, does not cover rugosity, i.e. the topography variation below 10 m (Jackson *et al.* 2010). Therefore, uncertainties in geological models are unavoidable as they are usually developed based on limited data, which consequently introduces errors into the simulation process. A popular method to mitigate the model uncertainty in reservoir engineering problems is history matching using the pressure and production data (Silva *et al.* 2017).

The Sleipner CCS project is the first storage project demonstrated at commercial scale (Ghosh, Sen and Vedanti 2015; Torp and Gale 2003). The CO_2 is captured from the nearby gas processing field and then injected into the reservoir at an approximate rate of one million tonnes per year (Korbøl and Kaddour 1995; Torp and Gale 2003). The reservoir had by 1 January 2019 stored approximately 17.8 Mt of CO_2 from the start of the operation (Furre, A-K *et al.* 2019). The storage site is a saline aquifer located at a depth of 800-1000 m (Arts *et al.* 2004; Head *et al.* 2004). Although no leakage has been reported in the site, constant monitoring of

---

[§] The content of this chapter is taken from the following paper:

Ahmadinia, M. and Shariatipour, M. (2020) Analysing the role of caprock morphology on history matching of Sleipner CO_2 plume using an optimisation method. Greenhouse Gases: Science and Technology 10 (5), 1077-1097.

The candidate planned and developed the methodology, performed all the simulation and analysis, and wrote the manuscript. The co-author supervised the project and provided feedback on the manuscript.

the storage process it crucial in managing the leakage risk throughout the operation (Nooner *et al.* 2007). Moreover, developing an understanding of the plume behaviour in this specific site is essential for decision-making purposes in regard to other global site choices. Several studies (Cavanagh, Haszeldine and Nazarian 2015; Chadwick RA and Noy DJ. 2010; Hodneland et al. 2019; Nilsen et al. 2017) have aimed to gain a better understanding of the plume migration behaviour in the Sleipner and to find a satisfactory history match of the CO_2 plume migration. The caprock model used has been suggested to be a cause of the poor match between the observed and simulated plume outline in the Sleipner (Bandilla, Karl W., Celia and Leister 2014; Nilsen et al. 2017; Zhu et al. 2015).

Typical uncertain parameters considered in history matching problems are porosity, and absolute and relative permeability data (Sadri *et al.* 2019). The focus of the current chapter is on caprock rugosity. Through a parameter estimation approach using an adjoint-based optimization method, the approach was tested by recreating a reference CO_2 plume shape in a synthetic model. The unknown parameter is caprock slope and elevation. Subsequently, the methodology was applied to the Sleipner 2019 benchmark model and improved the plume match by modifying the caprock elevation. Simulations were performed based on the vertical-equilibrium assumption using the CO2lab module in MRST. The simulator is then coupled to an adjoint-based optimisation tool found in MRST to minimise the mismatch between the observed and simulated plume shape.

5.2. Materials and methods

5.2.1. Part I: Synthetic model description

Initially the optimization tool was tested on a problem with a known answer. A plume outline has been created using specific slope and caprock topography variations and is referred to as "observed" plume. Using the optimization tool, the "observed" plume outline was recreated through systematic optimization of uncertain parameters, i.e. aquifer slope and caprock topography. Since the answer is already known, this step helps to validate the approach before applying it to a more complex model such as Sleipner. The contact boundary between the caprock and aquifer of the synthetic models in the first part of the chapter is represented by Equation 5.1. The z-axis is oriented downwards.

$$z(x,y) = B[sin(\omega_1 x) + sin(\omega_1 y)] + A_x \, sin(\omega_2 x) + A_y \, sin(\omega_2 y) + x \, tan(S_x) + y \, tan(S_y) \quad \text{Equation 5.1}$$

Where

$\omega = \dfrac{2\pi}{W}$: Angular frequency of the sine wave function

x, y and z: Directional coordinate of the caprock surface

A and B: Amplitude of the sine wave function

S: Model dip angle

In Equation 5.1, the first two terms (with "B" as a multiplier) represent the main structural traps. The rugosities in the x and y directions are presented by the next two terms, with a higher angular frequency than the main traps ($\omega_2 > \omega_1$). The last two terms represent the model slope.

B, ω_1 and ω_2 are constant in Equation 5.1 at values of 35 (m), 15 (rad/m) and 100 (rad/m), respectively. The model parameters are the rugosity amplitude and model slope in the x and y directions, presented by A_x, A_y, S_x and S_y , respectively, which are subjected to change in order to find the best match.

A single CO_2 injector is considered at the centre of a homogenous model, injecting CO_2 for 12 years (starting from 1999) with a constant flow rate of 0.5 Mt/year, equivalent to 20% of the CO_2 emission of a 500 MW coal-based power plant (Orr 2009). Further information about the model is presented in Table 5.1.

Table 5.1. Synthetic model parameters

Parameter	Value
Reservoir grid resolution (NX×NY×NZ)	101×101×4
Reservoir size (km) (LX×LY×LZ)	15×15×0.1
Rock compressibility (Pa^{-1})	1.00 E-10
Water density (kg/m^3)	1020
CO_2 density (kg/m^3)	760
Residual water saturation (S_{rw})	0.11
Residual CO_2 saturation (S_{rc})	0.21
Permeability (mD)	500
Porosity	0.2
Simulation period (Years)	10
Bribe viscosity (Pa.S)	8.0E-4
CO_2 viscosity (Pa.S)	6E-5
Caprock depth (m)	1500

The numerical simulation of CO_2 injection and migration was initially performed on a synthetic model with a known slope (S_x and S_y) and rugosity (A_x and A_y). The resulting plume outline was recorded and subsequently reinterpreted as "observed" data. New models were synthesized with different inputs for the investigated parameters (slope and rugosity in the x and y directions). Simulations were then performed on individual synthetic models using the nonlinear optimization framework. The investigated parameters were calibrated within predefined limits to match the original "observed" data.

5.2.2. Part II: Sleipner 2019 benchmark model

The Sleipner 2019 Benchmark Model (Santi A., Furre A.K. and Ringrose P. 2020) is a reference dataset from the Sleipner CO_2 storage site. This site, located off the western coast of Norway using part of the more extensive Utsira Formation as a storage site, has been commercially used by Equinor ASA, a Norwegian state-owned multinational energy company, as a CO_2 storage site since 1994, to prevent CO_2 emissions associated with the gas production from the same region. The site has been extensively monitored from its inception, and a series of time-lapse seismic datasets that documents the migration of the injected CO_2 has been established and (along with associated well logs and baseline seismic) has served as an input to the creation of the benchmark model. The 2019 benchmark model is the first complete 3D model of the Sleipner covering eight reservoir zones interbedded with eight continuous shale layers. The geological model used in this part of the chapter consists of the caprock, a sand wedge (L9, highlighted in red in Figure 5.1) and a shale layer on the bottom. Other layers are ignored as the focus is on the behaviour at the top surface. The seismic lateral and vertical resolutions are about 12.5 m (Santi A., Furre A.K. and Ringrose P. 2020) and 8 m (Chadwick, RA et al. 2004) respectively.
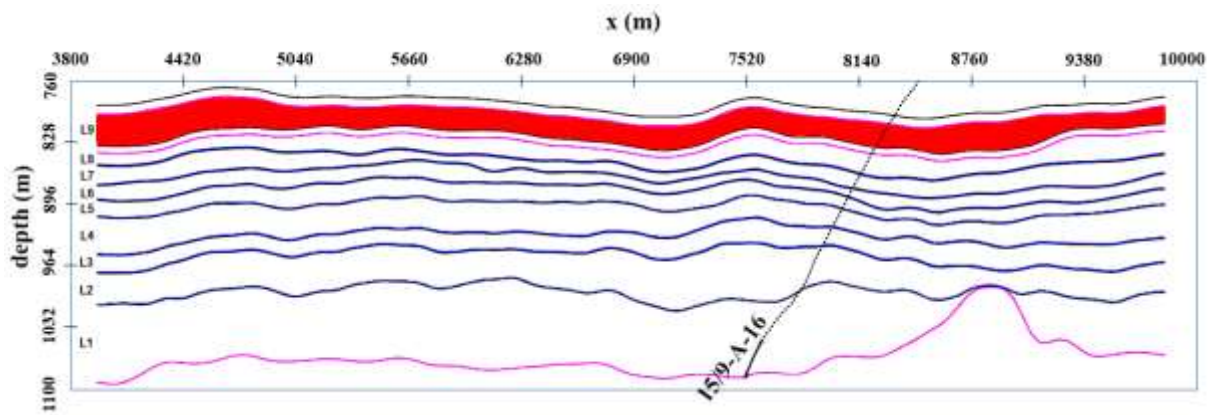
Figure 5.1. Depth data for Sleipner 2019 benchmark original model. Purple line: bottom of the reservoir; blue lines: intra-formational shale layers; red zone: the only sand layer considered in this study (L9); dotted line: injection well in the original model; 15/9-A-16: injection well.

A single CO_2 injector (15/9-A-16) is considered in the model (Santi A., Furre A.K. and Ringrose P. 2020) operating with injection rates as in (Nilsen et al. 2017) for 12 years (1999 to 2010) and are listed in Table 5.2. The rates presented in the table are representative of the CO_2 entry rate into Layer 9.

Table 5.2. CO_2 reservoir volume entry rates taken from (Nilsen et al. 2017)

year	1999	2000	2001	2002	2003	2004	2005	2006	2007	2008	2009	2010
rate (m^3) $\times 10^6$	0.03	0.08	0.14	0.21	0.31	0.44	0.62	0.87	1.18	1.57	2.06	2.65

As the internal layers are not considered, the entire CO_2 plume will reach the top-surface immediately once injected. In contrast, in reality, the plume encounters and passes through eight shale layers, and part of it becomes trapped before reaching the ninth. To avoid an unrealistically large plume, the optimization tool was used to initially calibrate the injection rate. The results showed that using a rate multiplier of 0.7, which is in agreement with the range reported by (Nilsen et al. 2017), would improve the plume match (9% improvement in plume match in 2010 for instance). Therefore, the resulting plume roughly represents the fraction of CO_2 that has reached the upper layer based on the time-lapse seismic data. This rate multiplier is applied to the simulations in the second part of this chapter (Sleipner model).

Dissolution and mineralization trapping mechanisms have been neglected due to the time scale of the study. Relative permeability data have been taken from (Singh VP et al. 2010) with a residual saturation of 0.11 and 0.21 allocated to the brine and CO_2, respectively. The impact of temperature on density (and viscosity) is modelled with sampled tables of density and viscosity as functions of pressure and temperature using the TREND library (Span *et al.* 2015). Further information about the model can be found in Table 5.3.

Table 5.3. Sleipner model information

Parameter	Value	Reference
Porosity	0.27 – 0.4	(Holloway et al. 2000; Lothe and Zweigel 1999)
Permeability (mD)	(1.1 – 5) E3	(Lindeberg et al. 2001)
Number of cells (NX*NY*NZ)	64*118*47	(Santi A., Furre A.K. and Ringrose P. 2020)
Cell dimensions (m) (DX*DY*DZ)	50 * 50 * 2	(Santi A., Furre A.K. and Ringrose P. 2020)
Area (km^2)	18 (6*3)	Seismic depth map
Seafloor temperature (^{o}C)	7	(Nilsen et al. 2017)
Brine viscosity (Pa.s)	8E-4	(Nilsen et al. 2017; Singh VP et al. 2010)
CO_2 viscosity (Pa.s)	6E-5	(Nilsen et al. 2017; Singh VP et al. 2010)
Brine viscosity (Pa.s) at 8.1 MPa	1020	(Bickle et al. 2007)
CO_2 viscosity (Pa.s)) at 8.1 MPa	760	(Alnes, Eiken and Stenvold 2008)
Brine compressibility (Pa^{-1}) at 8.1 MPa	4.37 E-10	(Nilsen et al. 2017)
CO_2 compressibility (Pa^{-1}) at 8.1 MPa	4.37 E-9	(Nilsen et al. 2017)
Rock compressibility (Pa^{-1}) at 8.1 MPa	1.00 E-10	(Nilsen et al. 2017)
Thermal gradient (^{o}C/km)	35.6	(Nilsen et al. 2017)

5.2.3. Numerical simulation

The numerical simulations are performed using the CO2lab module in MRST (Bao *et al.* 2017), which uses a simplified version of flow equations based on a vertical equilibrium (VE)

assumption. VE modelling is based on two main assumptions. The first is that brine and CO_2 are assumed to be in hydrostatic equilibrium throughout the simulation. In the second, vertical flow migration is considered negligible compared to lateral migration (Nordbotten, Jan Martin and Celia 2011). Due to the significant difference between the CO_2 and brine densities, segregation is considered to occur instantly, and the fluids form two separate layers. For typical operation conditions and formation thickness in geological CO_2 storage projects, the VE assumption is likely to be valid for horizontal permeabilities above 100 mD (Court et al. 2012). Note that the permeability in Sleipner's layer nine is between $1100 - 5000$ mD.

Moreover, because of the difference in the densities of CO_2 (~760 kg/m^3) and brine (~1020 kg/m^3), the ninth layer of the Sleipner is characterized by gravity segregation (Nilsen et al. 2017). Using the VE method, it is possible to model the most relevant physical aspects of long-term CO_2 storage. Its feasibility in the context of CO_2 storage has been investigated in previous studies (Ahmadinia, Masoud et al. 2019; Bandilla, Karl and Celia 2019; Gasda, Sarah E., Nordbotten and Celia 2009; Nilsen, Lie and Andersen 2016b) and was also employed to model the Sleipner benchmark (Bandilla, Karl W., Celia and Leister 2014; Nilsen et al. 2011a; Nilsen et al. 2017; Singh VP et al. 2010). Singh et al. showed that strong segregation occurs in Sleipner, and the plume migration is strongly affected by the caprock morphology (Singh VP et al. 2010). The VE modelling was compared with a full 3D black-oil simulator, and the results showed that the VE model could capture the flow physics of the Sleipner benchmark (Nilsen et al. 2011a). The CO_2 plume behaviour in Sleipner observed in the VE model was observed to be the same as a full 3D simulation model (Bandilla, Karl W., Celia and Leister 2014). In the VE model, the problem dimension is reduced from 3D to 2D. This significant reduction in the number of unknowns also significantly reduces the computational cost and allows the modeller to consider a higher lateral grid resolution beyond what would be practical in full 3D simulations. It is then possible to reconstruct the full 3D model from the 2D one as a post-processing step, using analytical calculations (Nilsen, Lie and Andersen 2016b). More details can be found in Section 4.2.

5.2.4. Optimization framework

The optimization tool employed in this chapter is implemented in the MRST. It can be used for solving optimal control problems with forward and adjoint solvers and implements a quasi-

Newton optimization routine using Broyden–Fletcher–Goldfarb–Shanno (BFGS) updated Hessians (Lie 2019).

In the first part of the chapter (synthetic model), model parameters are A_x, A_y, S_x and S_y which are scalar values representing the rugosity amplitude and aquifer slope in the x and y directions, respectively (Equation 5.1). In the second part of the chapter, however, the model parameter is dz, the absolute local elevation changes in caprock depth and has a size equal to the number of cells in the top row of Sleipner layer 9 ($64 \times 118 = 7552$).

Note that only the plume thickness (h) was matched, and the objective function in this chapter exclusively depends on plume saturation. The optimization framework aims to find a set of model parameters and minimize the misfit function in the form of $J = \sum J_m$ where

$$J_m(h_m) = \sum_{cells} V(h^m - h_{obs}^m)^2 + \sum_{cells} \beta dz^2 V \qquad \text{Equation 5.2}$$

where

m = Time-instance of the set of observed CO_2 plume thickness (h_{obs}). Four sets of observed data (2001, 2004, 2006 and 2010) are used in both parts of this chapter.

h = Simulated plume thickness given the model parameters.

V = Aquifer volume found below each cell in the 2D top surface grid.

β = Regularization term (equals to 0.1).

While adjusting dz in the work in the second part of the chapter, the degree of freedom is very large in the optimization problem (equivalent to the z-value of all caprock cells in Sleipner model). The regulation term (α) prevents possible overfitting of the data. In other words, this term restricts the drastic modification of the top surface elevation, which could occur by assigning a maximally shallow z-value to all grid cells within the observed plume and a maximally deep z-value to the ones outside. See sections 2.3 to 2.6 in (Nilsen et al. 2017) for more information about the implemented adjoint-based optimization framework in the MRST and (Jansen 2011) for more details about solving adjoint equations.

5.2.5. Sørensen–Dice coefficient

Several approaches are available to quantify the similarity of the plume migration resulting from two different geological models. One method used in previous studies (Han et al. 2011;

Manceau and Rohmer 2014; Manceau and Rohmer 2016) compares the plume centre of mass with a reference point, such as the injection point. Here the Sørensen–Dice coefficient (SDC), a statistic used to quantify the similarity of two discrete samples was used (Dice 1945; Sørensen 1948). The approach showed promising results when applied to the Ketzin (Lüth, Ivanova and Kempka 2015) and Sleipner (Allen, R. et al. 2018; Hodneland et al. 2019) CO_2 storage sites to compare the similarity of the simulated and observed CO_2 footprint. SDC ranges between 0 and 1, where an SDC equals one corresponds to identical samples. The SDC coefficient is defined as:

$$SDC = \frac{2|X \cap Y|}{|X|+|Y|}$$ \hfill Equation 5.3

where,

X: The plume outline from the simulation at the desired time

Y: The observed footprint generated from the seismic data at the same time as X.

Note that the SDC coefficient is not implemented into the optimization framework and, as mentioned in section 5.2.4, the objective function in this chapter is solely a function of plume thickness (i.e. saturation). Once the model parameters are optimised, the SDC coefficient is calculated after running a forward simulation using the optimised parameters.

5.3. Results and discussion

5.3.1. Part I: The Synthetic model

The approach was initially tested on a synthetic model with the aim being to optimise the model parameters. The adjoint-based optimization tool is employed to effectively minimise the mismatch between the observed and simulated plume outline by changing the rugosity amplitude (A_x and A_y in Equation 5.1) and aquifer slope (S_x and S_y in Equation 5.1). Two sets of limits to optimize the variables are considered: scenarios "a" and "b" in which the optimised value could be any value within $(0-10)$ and $(0-20)$, respectively. The observed plume outline is achieved with the following set of inputs: $A_x= 7$ m, $A_y=3$ m, $S_x= 4^o$ and $S_y= 2^o$. Six sets of initial guesses are considered which are listed in Table 5.4. Moreover, the number of iterations for each optimisation run is also reported in Table 5.4. Results clearly show that optimisation requires a higher number of iterations in scenarios "b" than "a". Therefore, the narrower range

can decrease the computational cost, although this could introduce the risk of missing the optimum points.

Table 5.4. Initial guesses and search range for each of the model parameters.

Scenario	Model parameter limit			
	A_x (m)	A_y (m)	S_x (º)	S_y (º)
a	0-10	0-10	0-10	0-10
b	0-20	0-20	0-20	0-20
Observed	7	3	4	2

Case		Number of iterations	Initial model parameters			
			A_x (m)	A_y (m)	S_x (º)	S_y (º)
1	a	11	0	0	0	0
	b	15				
2	a	10	10	10	10	10
	b	12				
3	a	10	10	10	0	0
	b	11				
4	a	8	0	0	10	10
	b	12				
5	a	11	0	10	0	10
	b	13				
6	a	9	10	0	10	0
	b	10				

Assigning the initial guess values to the model parameters results in different plume outlines in 2001, 2004, 2006 and 2010, shown in Figure 5.2.
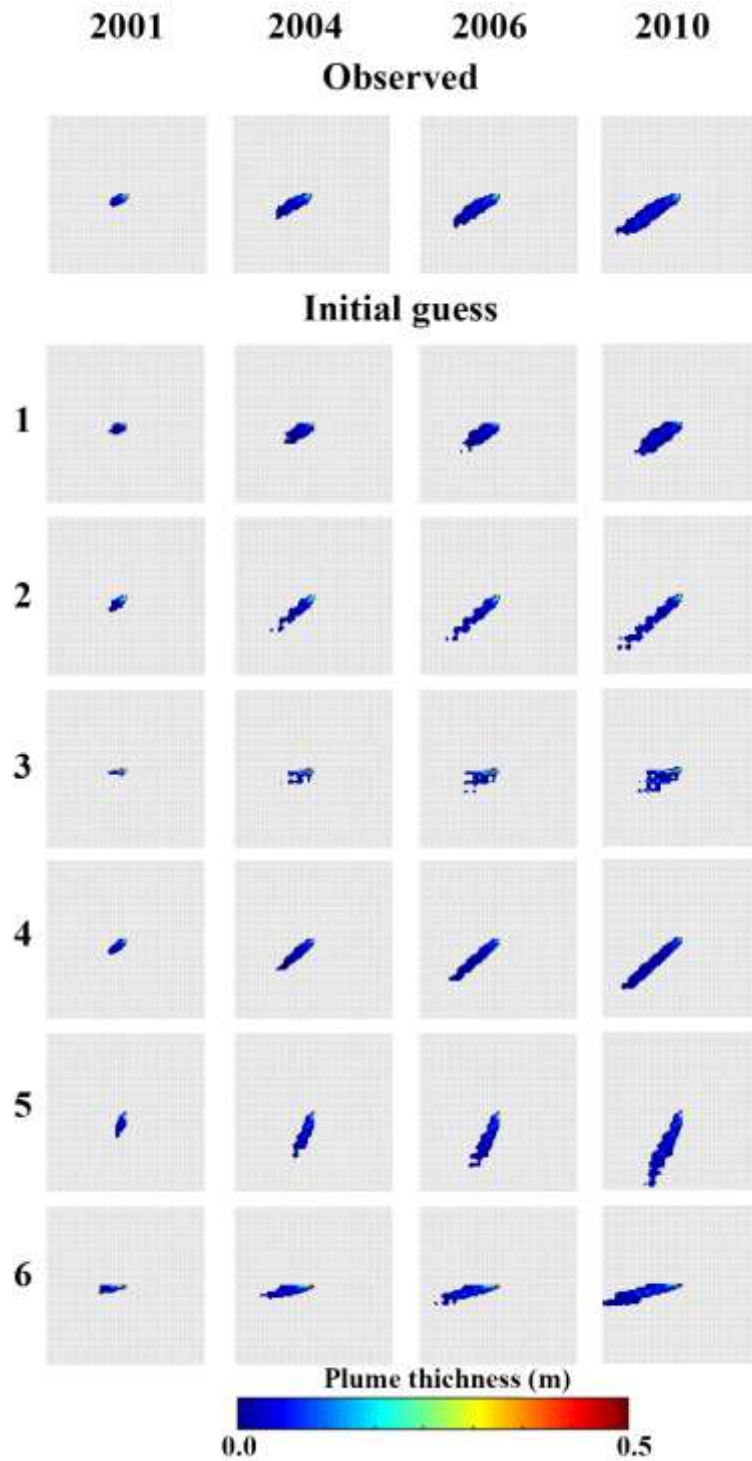
Figure 5.2. Initial CO_2 Plume saturation profile for the synthetic models in 2001, 2004, 2006 and 2010.

The corresponding SDC for plume outlines using initial model parameters is listed in Table 5.5.

Table 5.5. Dice coefficient of the initial guess models.

| Case | Dice coefficient | | | |
	2001	2004	2006	2010
1	0.81	0.74	0.74	0.75
2	0.69	0.66	0.68	0.71
3	0.71	0.62	0.62	0.61
4	0.68	0.65	0.68	0.71
5	0.36	0.31	0.29	0.29
6	0.55	0.55	0.58	0.59

The calibrated models for all the cases resulted in an SDC of ~1, i.e. the observed and simulated plume outline completely matched throughout the simulation. The calibrated CO_2 plume thickness profile for the synthetic models (scenario "a") are presented in Figure 5.3. The results indicate that a satisfactory plume match is achieved regardless of the starting point (Cases 1 to 6) and ranges (scenarios "a" or "b") used in this chapter.
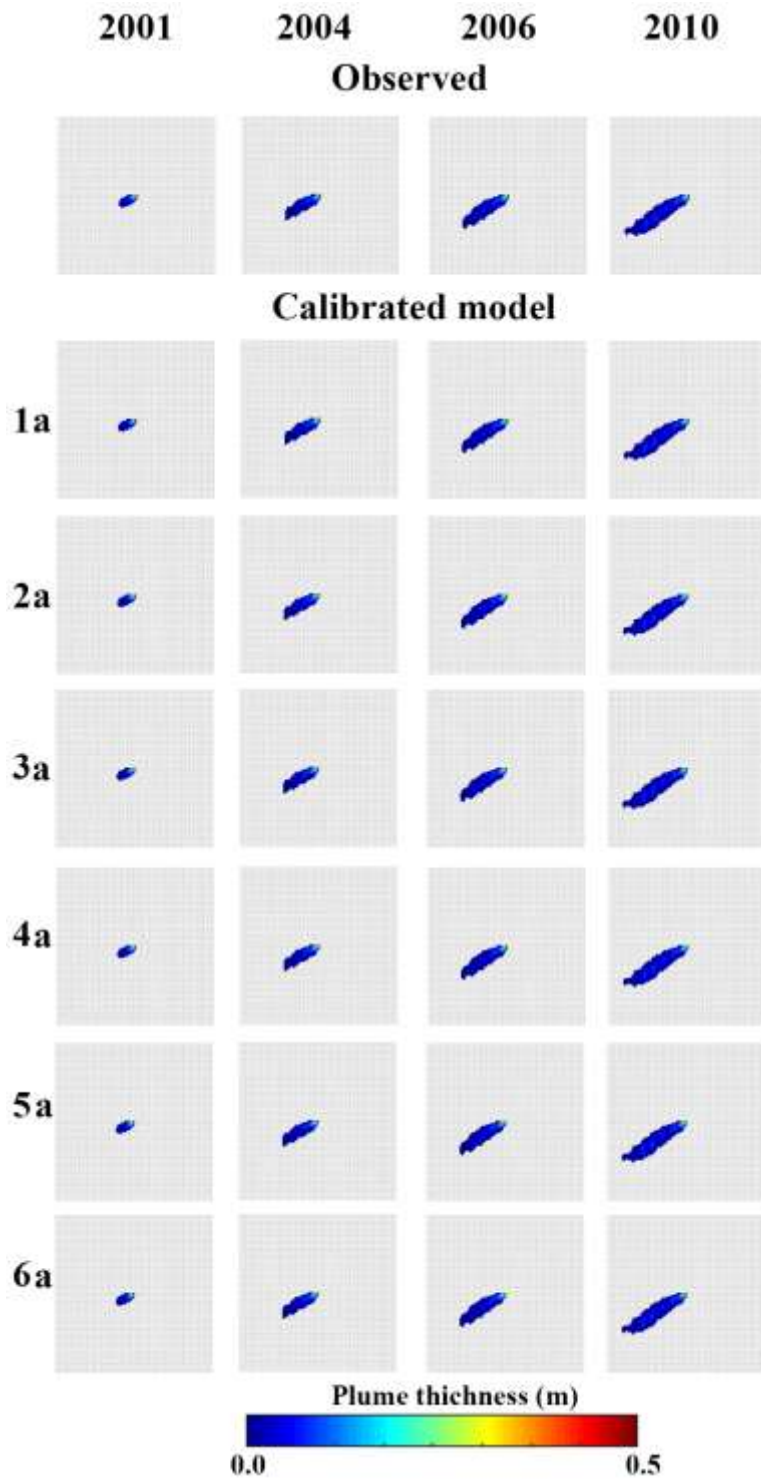
Figure 5.3. Calibrated CO_2 plume thickness profile for the synthetic models (Scenario "a") in 2001, 2004, 2006 and 2010.

Here the results are compared based on the calibrated values for the model parameters. Figure 5.4 shows the optimised values for all the cases. As mentioned earlier, the observed plume

outline is achieved when setting $A_x= 7$ m, $A_y=3$ m, $S_x= 4°$ and $S_y= 2°$ in Equation 5.1. For this study, no significant dependence on the initial guess is observed for the final solution obtained; except for Case 3 ($A_x= 10$ m, $A_y=10$ m, $S_x= 0°$ and $S_y= 0°$) where optimization results for both scenarios "a" and "b" were less accurate than other cases. Note that in more complex optimization settings, the choice of the start point would be important and here the problem is simplified.
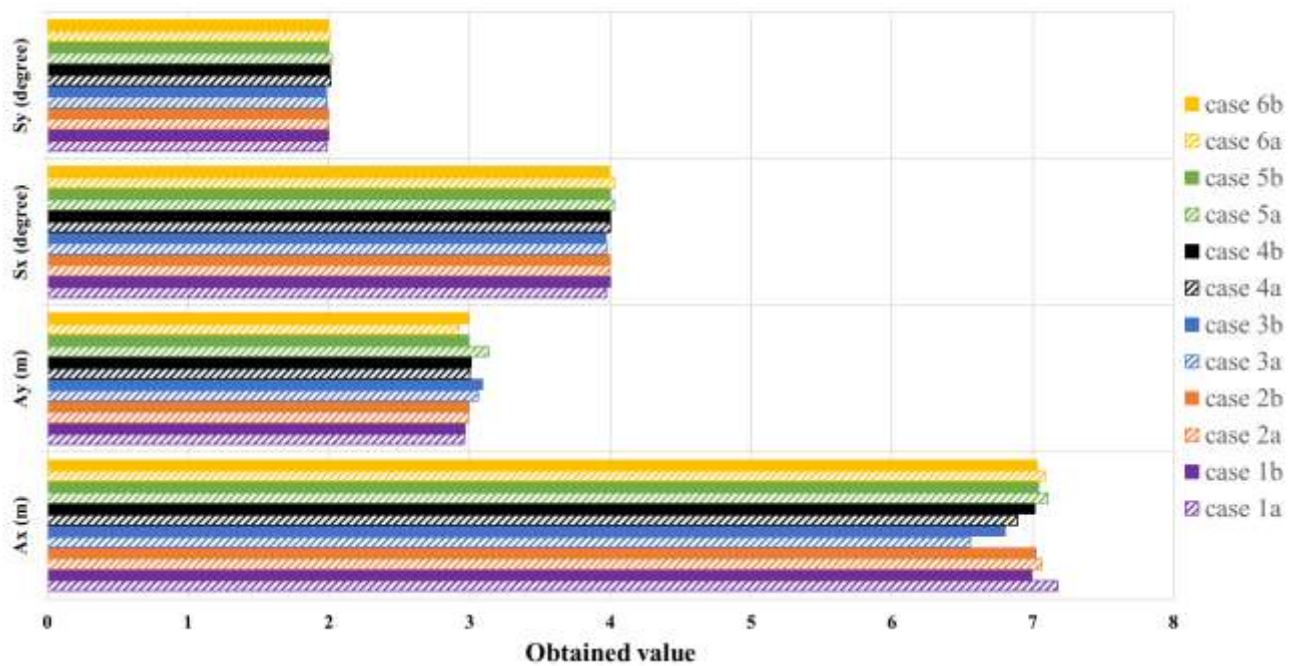
Figure 5.4. Optimized values for all the cases.

The averaged error in the match between the observed and calibrated model parameters for each of the cases is presented in Figure 5.5. Setting tighter bounds (scenarios "a") for the parameter ranges did not result in a better match, which can be explained by the presence of local optima.
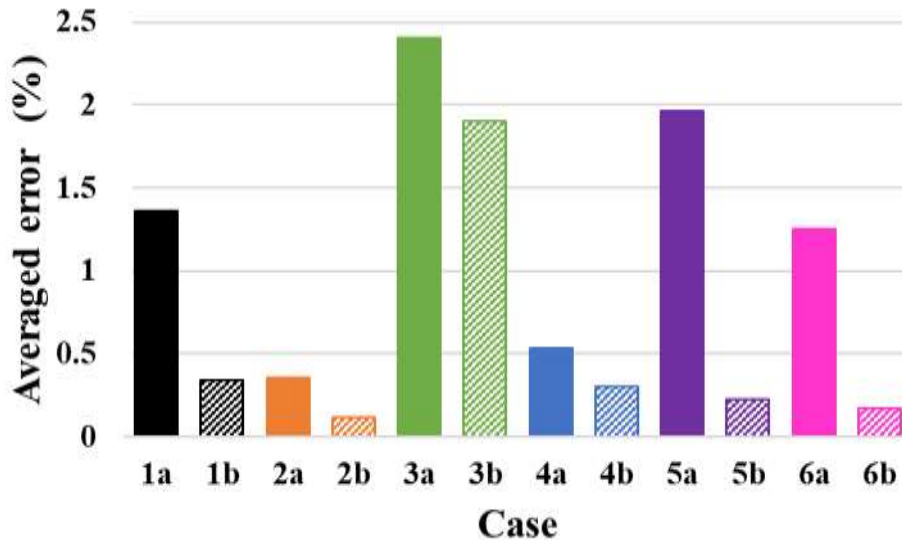
Figure 5.5. The averaged percentage error in the match between the calibrated and observed models.

While there is a small 'wiggle room' in calibrated parameter values, the results clearly show that the optimization tool employed in the work in this chapter can identify precisely a single set of model parameters to match the plume extension at different time steps. In the next section, the results from applying the tool to the recent Sleipner model are discussed. The aim is to calibrate its caprock morphology to improve the match between the observed and simulated plume outline.

5.3.2. Part II: The Sleipner model

The plume outline resulting from the original Sleipner model is compared with seismic data in 2001, 2004, 2006 and 2010 (Figure 5.6). The plume shows a better match in the early years (~70%) than in 2010 (~60%).
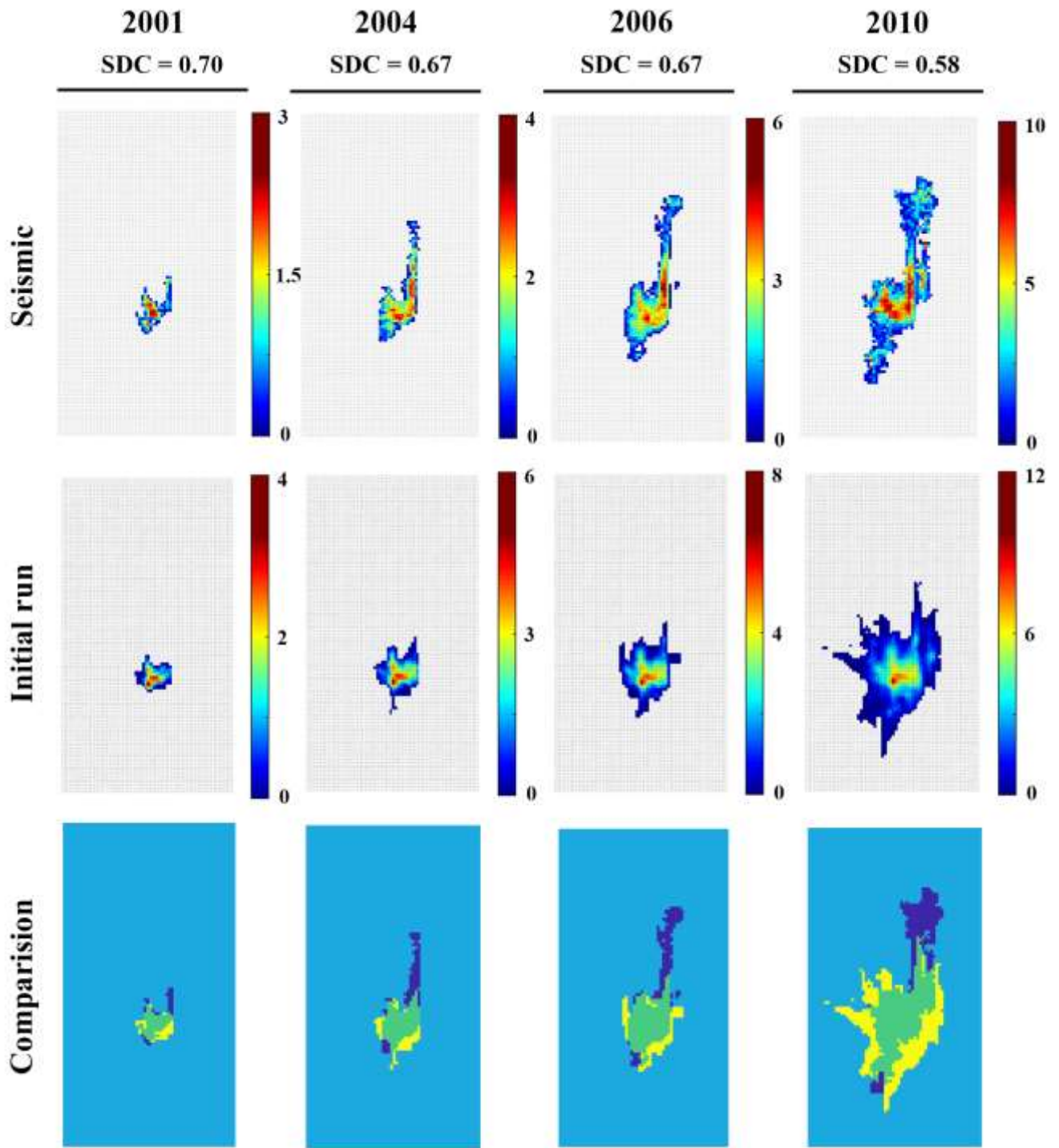
Figure 5.6. Plume outline from seismic (1st row), results from the original model (2nd row), comparison of the plume outlines (3rd row; dark blue: seismic, yellow: simulated, green: overlapped) in 2001, 2004, 2006 and 2010. The legend shows the plume thickness (m).

While several sources of uncertainty have been reported in the Sleipner model, the focus of the work in the presented in the current chapter is to improve the plume match merely by changing the caprock elevation within the seismic detection range (~10 m). Each grid cell in the 2D grid can be freely moved up and down along the z-direction. The resulting plume outline from the calibrated model is compared with the seismic data in Figure 5.7. The result shows an increase in the average SDC in the four studied time steps from 65% (Original model) to 73% (Calibrated model), which is significant. Note that a perfect match is not expected to be found as other parameters affect the Sleipner plume match. Various researchers addressed the different source of uncertainties, such as temperature (Cavanagh and Haszeldine 2014; Hermanrud, C. et al. 2012; Hodneland et al. 2019), CO_2 plume impurities (Hodneland *et al.* 2019), CO_2 density (Alnes, Eiken and Stenvold 2008; Alnes et al. 2011; Cavanagh and Haszeldine 2014; Zhu et al. 2015), the injection rate (Nilsen et al. 2017; Zhu et al. 2015), porosity and permeability (Nilsen et al. 2017) affecting the plume match in the Sleipner model. Calibrating the caprock morphology seems to improve the match in the middle of the plume, where CO_2 has the highest saturation and forms a reverse "L" shape. SDC cannot observe this improvement as the plume thickness is not considered in the similarity measurement, which is a limitation of this approach. Moreover, SDC considers the difference in the uncommon area, which is another limitation. In other words, if circle X and Y have an area equivalent to 75% and 125% of circle Z, respectively, then $SDC_{X \& Z} = SDC_{Y \& Z} = 0.75$. Note, as mentioned in Section 5.2.5, the SDC coefficient is not implemented into the optimization framework and is calculated for the model once the parameters are optimised.
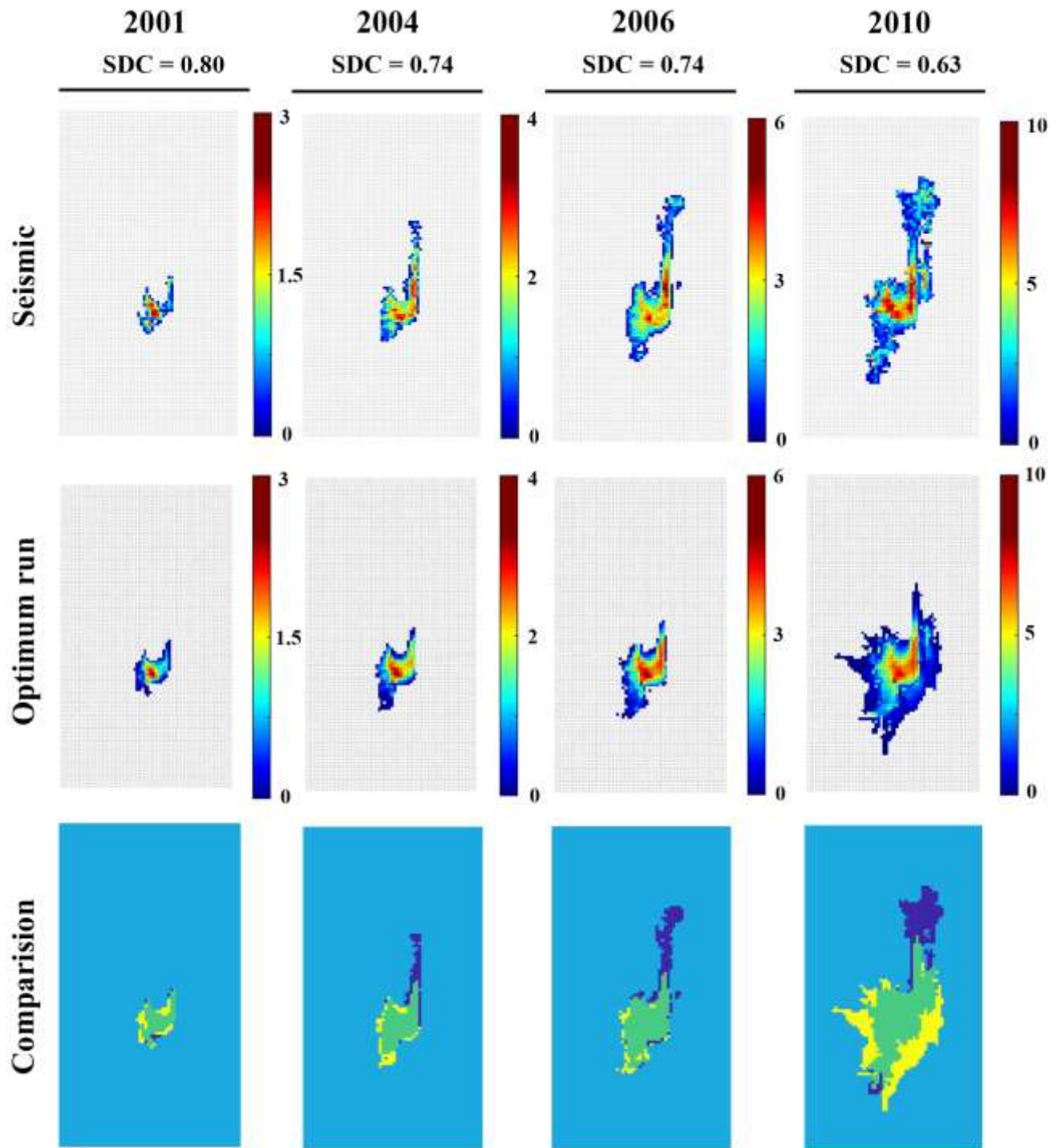
Figure 5.7. Plume outline from seismic (1st row), results from the calibrated model (2nd row), comparison of the plume outlines (3rd row; dark blue: seismic, yellow: simulated, green: overlapped) in 2001, 2004, 2006 and 2010. The legend shows the plume thickness (m).

While the optimization tool could modify the caprock morphology within the Sleipner seismic vertical resolution (~ 8m), the results presented earlier are achieved by a change of ± 10 m. Figure 5.8 shows the elevation change applied to the original geological model. The algorithm seems to decrease the elevation in the region outside the observed plume outline, which might result in a lower structural trapping capacity.
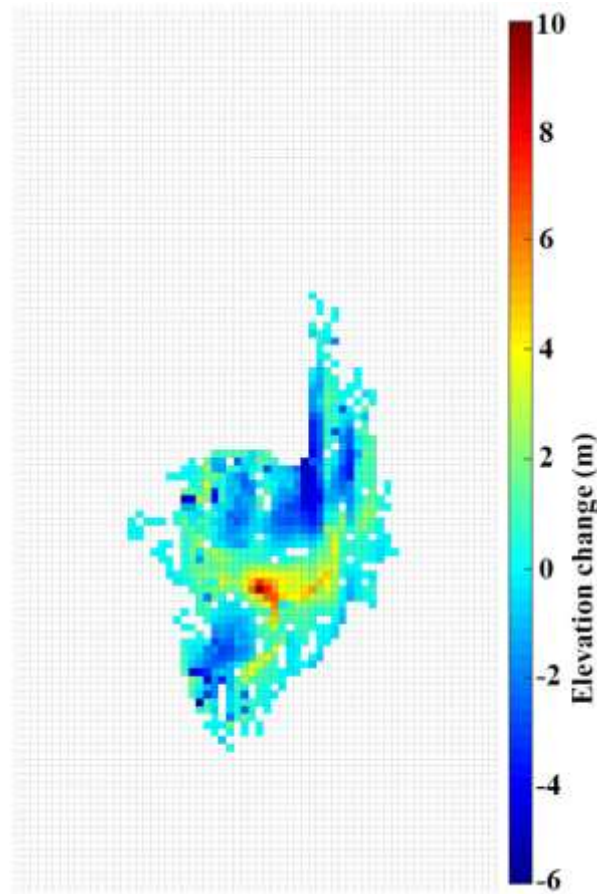
Figure 5.8. Caprock elevation change

5.4. Conclusion

The exercises in this chapter focused on the impact of caprock morphology on CO_2 plume migration and footprint. An optimization code was developed to systematically change the model parameters to minimize the error match between the observed and simulated plume outlines. First, the method was used to predict the CO_2 plume shape in a synthetic model. A set of parameters representing the slope and rugosity in the x and y directions was found using the non-linear simulation-based optimisation tool. The observed plume footprint was successfully reproduced. The method was robust, and the results were satisfactory using different initial

starting points and calibration limits for each parameter. The optimisation tool was employed to improve the plume match in the Sleipner 2019 benchmark model by modifying the caprock morphology within a range smaller than the seismic detection limit. The results showed an average improvement of about 8% in the plume match. A wide range of parameters has been reported in the literature affecting the plume match in Sleipner. The goal here is not to find a perfect match as here the caprock morphology is the only HM parameter. Therefore, the results of the optimization method would be considered a good match.

Moreover, the algorithm significantly improved the match in the middle of the plume, where the CO_2 has the highest saturation and forms a reverse "L" shape. The reported match improvement in percentages, however, did not take this into account as the plume thickness is not considered in the similarity measurement in SDC calculation, which is a limitation of this approach. Given that the objective function used in this chapter is a function of plume thickness only (and not SDC), this limitation, however, does not affect the optimization process but only the resulting presentation.

Chapter 6 [**]

Quantifying the importance of caprock morphology through data analysis

6.1. Introduction

As mentioned in Chapter 5, the Sleipner CCS project, the first storage project on a commercial scale (Ghosh, Sen and Vedanti 2015). The gravity-driven flow was an essential factor in CO_2 plume migration in the Sleipner storage site (Cavanagh, Haszeldine and Nazarian 2015). The researchers (Cavanagh, Haszeldine and Nazarian 2015) applied a capillary flow model to the Sleipner model to solve the over-prediction of viscous effects in gravity segregated systems. While a better match was achieved in the northern part of the plume, the upslope plume migration was overestimated, this being explained as being due to neglecting viscous effects acting against the gravity drive. Therefore, the work in this chapter highlights the importance of gravity-driven flow and suggests using models with enough vertical grid resolution or reduced-orders models, such as vertical equilibrium. To improve the match, higher permeabilities (6 and 10 Darcy) for the Utsira formation have also been considered (Chadwick RA and Noy DJ. 2010; Chadwick, RA et al. 2009). These authors also studied cases with anisotropic permeabilities and increased the temperature to 36°C.

Nilsen et al. (Nilsen et al. 2017) tried to match historical data to the Sleipner storage site. Their results suggested that the plume outline is governed by the caprock, its permeability and the influence of plume density, while the CO_2-brine contact shape and porosity and injection rate affect the plume volume. The impact of uncertainties in temperature and fluid impurities on CO_2 migration in the Sleipner was investigated (Hodneland et al. 2019). While the impact of

---

CO_2 impurity on plume migration was negligible, the authors found that raising the average storage site temperature to 46°C improves the history matching results.

Most of the previous studies undertaken on the Sleipner model took a one factor at a time (OFAT) approach (Allen, R. et al. 2018) in which the response to one parameter is investigated, and the rest are kept at their initial value. Some other works also considered a limited number of parameters in their sensitivity analyses (Hodneland et al. 2019). To fully span the uncertainty space, to the best of our knowledge, this is the first time the focus will be on the cross-correlation of six important parameters, to show their impact on the overall CO_2 migration and trapping in Sleipner. Several sources are considered including uncertainties in the geological model (porosity, permeability and caprock morphology), fluid (CO_2 density), aquifer property (temperature) and operational condition (injection rate). One million samples of the six uncertain parameters are generated within their reported ranges in the literature for the Sleipner model Layer 9 and ran a simulation for each input parameter set. The study was performed on the most recent Sleipner Benchmark simulation grid, 2019 (Santi A., Furre A.K. and Ringrose P. 2020). Considering the computational cost, the forward simulations are performed using the VE modelling approach implemented in MRST-CO2lab (Nilsen, Lie and Andersen 2016a; Nilsen, Lie and Andersen 2016b). CO2lab is an add-on module providing a family of computational tools specially developed to study the long-term CO_2 storage in large-scale aquifer systems. The MRST-CO2lab performance was compared with full 3-D simulations in previous studies (Ahmadinia, Masoud et al. 2019; Nilsen et al. 2011a), and showed promising performance. Each forward simulation of CO_2 injection in Layer 9 for 12 years, took about 30 seconds using the VE approach; while using the same computational power configuration the simulation could take up to 10 and 14 hours in black-oil and compositional simulation tools, respectively. In order the make this study feasible in terms of computational time, a cluster system is used to run 80 parallel simulations at a time. Random forest (RF) and decision tree (DTree) (Dumont et al. 2009; Tin Kam Ho 1995) models available in Scikit-learn machine learning library in the Python programming language are employed to find the importance of each parameter in the plume shape. The input is a matrix of 1M by six (temperature, rate, porosity, heterogeneity in permeability and porosity, density and caprock elevation) and the output is a matrix of 1M by four (The dice coefficient for four time steps).

6.2. Material and method

6.2.1. Geomodel

As stated previously, the Sleipner model (Santi A., Furre A.K. and Ringrose P. 2020) is for a CO_2 storage site located off the western coast of Norway and is part of the Utsira formation. The model was briefly described in Section 5.2.2. Here, as in Chapter 5, the geological model used for simulation contains the caprock layer, L9 sand wedge (L9, highlighted in red in Figure 5.1) and a continuous shale layer on the bottom. The model is initially fully saturated with brine, at hydrostatic balance. The water density is considered a fixed value of 1020 kg/m^3 (Bickle *et al.* 2007). However, the value of 760 kg/m3 (Alnes, Eiken and Stenvold 2008) for the CO_2 density is subjected to change throughout the simulation (based on different multipliers). The residual saturation of 0.11 and 0.21 was assigned to the brine and CO_2, respectively (Singh VP et al. 2010). The CO_2 is injected for 12 years (1999 to 2010) with the rate similar to (Nilsen et al. 2017), and due to the time scale of the study, the dissolution and mineralization trappings have been neglected. Please refer to Table 5.3 for more information about the model.

6.2.2. Model uncertainty

In the following, further details about the uncertain parameters are provided:

6.2.2.1. Temperature

Temperature uncertainty in the Sleipner model has always been a topic of discussion in the literature (Hodneland et al. 2019). Problems encountered include an unknown subsurface temperature at the time prior to injection, and there being no reliable data is available on the extent of the heat exchange between the injected plume and the aquifer. In addition, the injected CO_2 temperature varies between 43-52°C (downhole temperature) when entering the formation at the injection point and consequently has a complex and time-dependent temperature profile (Hodneland et al. 2019).

Changing the temperature would largely affect the CO_2 density and viscosity, and therefore its buoyancy and mobility. Cavanagh and Haszeldine (Cavanagh and Haszeldine 2014) considered a temperature of 31°C and 37°C at 800 metres depth for the Sleipner layer 9 and Hermanrud et al. (Hermanrud, C. et al. 2012) proposed a temperate range between 34-40°C. In the current study, however, similar to some of the previous studies (Allen, R. et al. 2018;

Hodneland et al. 2019), the following relationship represents the temperature change throughout the model:

$$T(x, y) = T_s + DT + GT \times (Z_s - Z(x, y))$$ **Eq. 1**

where T_s and Z_s denotes the seafloor temperature and depth respectively, GT is the thermal gradient in the vertical direction (°C/km) and $Z(x, y)$ represents the cell depth and DT is the terms considered in this study to modify the aquifer temperature. One million random values of DT between -6 to +6 are considered. Using Equation 1, the temperature at the average reservoir depth (–812m) becomes between 29.9 to 41.9 °C. The plume temperature in this study is considered to be in equilibrium with the geothermal gradient, and the fluid properties (viscosity and density), are a function of pressure and temperature. Similar to the works undertaken by (Singh VP et al. 2010), assigned values for T_s, Z_s and GT are 7 °C, 100 m and 35.6 °C/km, respectively. Nilsen et al. (2017) manually calculated the thermal gradient for Layer 9, and their results were very similar to the benchmark's proposed value of 35.6 °C/km; therefore the same value is used. Temperature ranges used in previous studies on the Sleipner are listed in Table 6.1.

Table 6.1. Temperature range considered for the Sleipner model in previous studies.

Study	Temperature (°C)	Reference depth
(Hodneland *et al.* 2019)	28.6 to 40.6	-818m
(Chadwick RA and Noy DJ. 2010)	29	Top surface
(Alnes *et al.* 2011)	32.2	-768m
(Bickle *et al.* 2007)	35	Average
(Singh VP et al. 2010)	35	Top surface
(Allen, R. *et al.* 2018)	35	Top surface
(Cavanagh, Haszeldine and Nazarian 2015)	35	Average
(Cavanagh and Haszeldine 2014)	31 & 37	-800m
(Baklid, Korbol and Owren 1996)	37	Average

(Hermanrud, C. *et al.* 2012)	34 to 40	Average
Current study	29.9 to 41.9	Average

6.2.2.2. Injection rate

The original Sleipner model is made up of nine layers each separated with a thin shale layer (Figure 1) and the plume is injected at a depth of 1010.5 metres (L1) below sea level (Singh VP et al. 2010). In this study, only Layer 9 (L9) is modelled, and the coordinate of the entry point in L9 is considered to be the same as for L1. In the real storage process, once injected, the plume encounters and passes through eight intra-formational shale layers (which are neglected in the current study) before reaching L9. The shale layers would result in 10-20 m thick CO_2 layers (beneath each shale layer), vertically stacked and extended by hundreds of metres laterally (Gregersen and Johannessen 2001; Zweigel et al. 2004). Despite the accurately mapped areal distribution of the CO_2 plume, its flow behaviour is still subject to uncertainties (Cavanagh and Haszeldine 2014).

The mechanisms of vertical migration (diffusion, migration points or both) and the number and location of vertical migration points, however, are uncertain (Nilsen et al. 2017; Zhu et al. 2015). Vertical migration here refers to the flow from intra-formational thin shale layers to the above sand layer. The injection rates used in this study are similar to (Nilsen et al. 2017) and represent an anticipation of the amount of CO_2 entering Layer 9 and is subjected to uncertainty because we are not sure how much of the injected CO_2 in L1 reaches L9 in reality. One million random rate multipliers (RM) between 0.7 to 1.3 are applied to the benchmark's volumetric rate to include the uncertainty of the entry rate into Layer 9.

6.2.2.3. Density

Another source of model uncertainty addressed in previous studies is CO_2 density (Alnes, Eiken and Stenvold 2008; Alnes et al. 2011; Cavanagh and Haszeldine 2014; Zhu et al. 2015). It is recognised that fluid density depends on temperature; however, changing temperature results in a change in viscosity (and therefore, mobility). Here, especially while undertaking the one factor at a time analysis, one goal is to analyse the impact of density itself on the storage process. Other sources of uncertainty in CO_2 density in the Sleipner model are uncertainty in aquifer pressure (Allen, R. et al. 2018) and the unaccounted impurities in the injected CO_2 (Hodneland et al. 2019), the latter affecting the storage process especially within the temperature range of 32-38 $^{\circ}$C (Hodneland et al. 2019). Therefore, the impact of uncertainty in CO_2 density is studied separately. The simulations are performed using the blackoil formulation

and the impact of the temperature on density (and viscosity) is modelled with sampled tables of density and viscosity as functions of pressure and temperature using the TREND library (Span et al. 2015). An average CO_2 density of 675 ± 20 kg/m^3 was suggested by (Alnes et al. 2011), based on the microgravity surveys which correspond to a plume temperature of around 31ºC. Cavanagh (Cavanagh and Haszeldine 2014) and Zhu et al. (Zhu et al. 2015), however, considered a CO_2 density of 355 kg/m^3 and 479 kg/m^3, respectively. The initial CO_2 density is considered to be 760 kg/m^3 (Alnes, Eiken and Stenvold 2008), and it is then modified using a random density multipliers (DM) between 0.4 to 1.2.

6.2.2.4. Porosity, permeability and caprock elevation

The reported ranges for porosity and permeability data of Sleipner Layer 9 are 0.27-0.4 (Holloway et al. 2000; Lothe and Zweigel 1999) and 1100-5000 mD (Lindeberg et al. 2001), respectively. One million permeability realizations are generated using a lognormal distribution approach within the reported range in this study. Porosity realizations are then generated from permeability data using the Kozeny-Carman correlation (Carman 1937). The typical seismic resolution is around 10 m and topography variations below this resolution are referred to as rugosity (Jones et al. 2009; Pringle et al. 2010) as introduced in a previous chapter. The reported seismic vertical resolution for the Sleipner model is 8 m (Chadwick, RA et al. 2004). In order to investigate the importance of the topography variations below the seismic detection range, one million realizations of top surface elevations within the range of ±5 m are considered using Gaussian random fields.

Figure 2 shows an illustrative (not representative of actual uncertainty ranges) of data for porosity, permeability and caprock elevation perturbations within the mentioned ranges. Note that since the VE model is used, porosity and permeability here refers to their column-wise averaged values. Therefore, the impact of their variation on plume migration might be underestimated in comparison to a full 3D model.
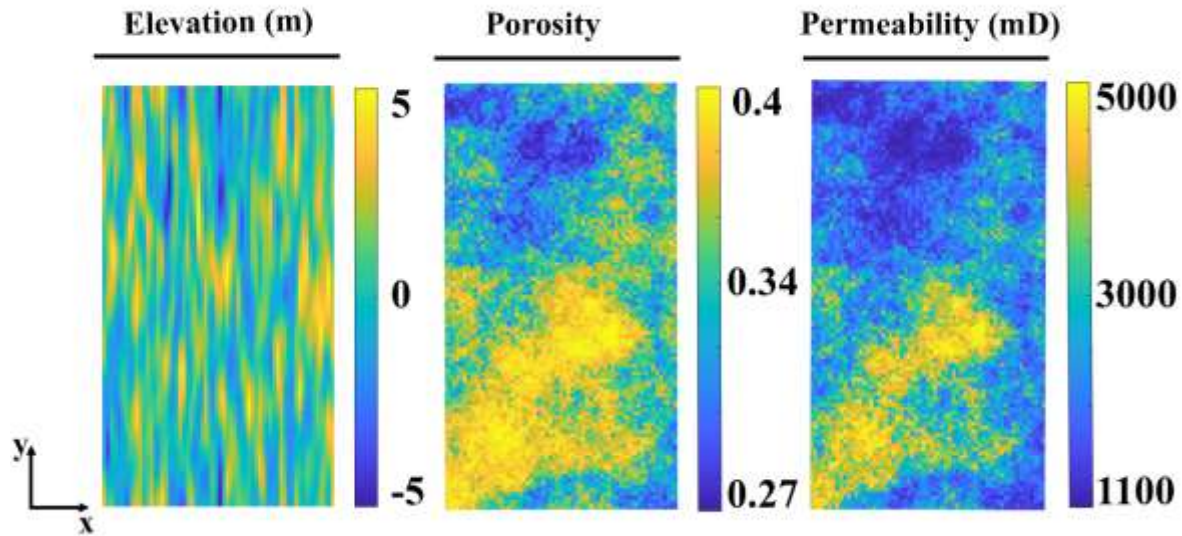
Figure 6.1. Samples of realizations representing the elevation (m), porosity and permeability (mD) distribution in the model. Figures show the top view of the grid (x and y-direction).

6.2.3. Simulation approach

In this study, a set of one Million simulations was undertaken using the co2lab module in MRST (Nilsen, Lie and Andersen 2016a) based on the vertical equilibrium simulation. The impact of uncertainty in caprock topography, CO_2 density, reservoir temperature, porosity and permeability heterogeneity and injection rate are studied on plume migration and structural trapping. In order to treat the parameters equally, in each of the one million simulation runs, the six parameters are randomly selected within their allocated range at once, to provide the inputs of the simulations.

Simulations are performed for two phases, namely CO_2 and formation brine. While a full 3-D simulation of the new Sleipner benchmark model could take up to 17 hrs (five processor system), simulations based on the VE approach could be performed within a minute. A similar VE setup results were promising compared with full 3D simulations models in previous studies using synthetic (Ahmadinia, Masoud et al. 2019) and Sleipner (Cowton et al. 2018; Nilsen et al. 2011a) models. Therefore, the VE method is used in this study to decrease the computational cost. Two base assumptions of VE modelling are the following: The hydrostatic equilibrium between brine and CO_2 is pre-assumed throughout the simulation. Due to the difference between the fluid densities, the gravity segregation process occurs significantly rapidly, and

fluids form two separate layers compared to the lateral plume migration. For injection rates and formation thicknesses typical of geological carbon storage sites, the VE model is likely to be valid for formation permeabilities higher than about 100 mD to have fast vertical segregation of fluids (Court et al. 2012).

It has been observed that injected plume may migrate several kilometres in the horizontal direction with very limited vertical movement (Shariatipour, Seyed M., Pickup and Mackay 2016). This makes the second assumption namely that the vertical flow migration can be considered negligible compared with the horizontal one is valid (Nordbotten, Jan Martin and Celia 2011). In a VE simulation model, the problem is reduced to 2-D, allowing the modeller to allocate the computational cost to increase the lateral resolution beyond what would be otherwise feasible in 3-D simulations. The MRST implementation of a VE model is written based on black-oil based formulations with upscaled models for capillary pressure and mobility.

Note that vertical heterogeneity in permeability is averaged out in VE models. Consequently, in this study, intra-layer flow in the simulation here was not included and by permeability the reference is the horizontal permeability only. In the works undertaken previously (Møyner and Nilsen 2017; Møyner, Andersen and Nilsen 2018), the authors presented a multi-layer VE approach with full 3-D simulations locally where needed. The errors introduced by VE modelling can in many cases be lower than the errors resulting from low lateral resolution to make the 3-D simulations computationally feasible (Nilsen, Lie and Andersen 2016b). Readers are referred to Nordbotten et al. (Nordbotten, Jan Martin and Celia 2011) for a detailed vertical equilibrium model description.

Hodneland et al. (Hodneland et al. 2019) showed that for a certain set of assumptions (thin plumes moving upwards under a sloping caprock), CO_2 migration velocity is given by:

$$V \cong \frac{k(\rho_w - \rho_g)g \sin\theta}{\mu_g \phi}$$

Equation 6.1

where V represents the fluid velocity, θ is the caprock tilt angle and μ_g is CO_2 viscosity. According to Eq. 2, an increase and drop in permeability and CO_2 density values, respectively, results in higher migration speed. Higher permeability means less resistance to flow. Moreover, reducing the CO_2 density results in a higher driving force for the fluid migration, and the fluids

tend to migrate from a zone with higher density to one with a lower value. Within the temperature range used in this study and an average pressure of 83 bar in layer 9 (Hodneland *et al.* 2019), and based on the data provided by (Bachu 2003), increasing the temperature results in lower viscosity and density, thus increasing migration velocity.

6.2.4. Plume similarity

Several methods have been previously utilized to quantify the similarity of the plume migration of two different geological models. Some researchers (Han et al. 2011; Manceau and Rohmer 2014; Manceau and Rohmer 2016) have compared the location of the plume's centre of mass with a reference point, such as injection point or plume centre of mass of the base model. Another method is the Sørensen–Dice coefficient (SDC), a statistic used to quantify the similarity of two discrete samples (Dice 1945; Sørensen 1948),

$$SDC = \frac{2|X \cap Y|}{|X| + |Y|}$$
Equation 6.2

This method has been recently used to compare the similarity of the simulated and observed CO_2 footprint at the Ketzin (Lüth, Ivanova and Kempka 2015) and Sleipner (Allen, R. et al. 2018; Hodneland et al. 2019) storage sites. In this chapter, X represents the plume outline from the simulation at the desired time, and Y is the observed footprint generated from the seismic data at the same time. Therefore, the SDC is equal to twice the overlapping area, divided by the summation of plume outlines (Equation 6.3). SDC ranges between 0 and 1, where an SDC equal to 1 corresponds to identical samples.

To better understand the underlying relationship between the target variables in SDC and the rest of the uncertain variables, it is necessary to employ a reliable data analysis technique that unveils linear/non-linear dependence in data. This provides a later quantification of the importance of each uncertain variable (i.e. input variables of the data-driven model) based on their contribution to the predicted target values. The model inputs are caprock elevation, temperature, density, porosity and permeability heterogeneity and injection rate, while the output (or target) variables are SDC values in different years. Knowing which model is appropriate for a given scenario is not always clear and requires more than one data-driven method to be trained on any supplied dataset. Therefore, a baseline Linear Regression (LR) model was initially fitted to a training set, subsequently predicted an unseen test set (25% of the entire data set), and then the predicted target values against the observed data were

compared. The baseline LR model reached an R-squared of about 0.2, which is very poor. The following models are then used to improve the baseline model prediction:

K-nearest neighbours (KNN): a neighbours-based regression model that performs the learning process based on the proximity of K closest training examples of each query point, where K is a user-defined constant (Goldberger et al. 2004).

Decision Trees (DTree): a tree-based model that sets up decision rules inferred from the observed data. Decision-tree learners can generate over-complex trees that fail to reliably generalise to unseen data (Dumont et al. 2009).

Random Forests (RF): an ensemble method to link the predictions of several decision trees to improve the predictive capability of each estimator while minimising the risk of overfitting (Tin Kam Ho 1995).

The training/testing set used for the baseline (LR) model is used to compare the predictive power of KNN, DTree and RF models, and the results are listed in Table 6.2.

Table 6.2. Comparison of the employed data analysis models.

Model	Mean absolute error	Mean squared error	R-squared
LR	5.3387E-02	3.2598E-03	1.9582E-01
KNN	1.9868E-02	1.0330E-03	8.3654E-01
RF	2.3100E-04	1.0885E-06	9.9938E-01
DTree	9.5000E-05	1.1006E-06	9.9944E-01

Table 6.2 clearly shows that DTree and RF models outperform the LR and KNN models by a large margin, with the RF model having an R-squared of 0.9993. Therefore, the DTree and RF models are kept solely for evaluating variable importance. As to variable importance, simple models strongly represent themselves and are highly interpretable as they are based on simple rules. Complex statistical models, however, such as ensemble methods, are not easy to explain. Instead, an interpretable approximation of the original statistical model can be used to represent an explanation model. To address this problem, a unified structure was used for interpreting

predictions, namely the SHAP (SHapley Additive exPlanations) method introduced by Lundberg and Lee (Lundberg and Lee 2017) in 2017. The SHAP framework identifies the class of additive feature importance methods and finds a solution in this class that quantifies variable importance. SHAP relates to the family of models called ''additive feature attribution methods'' where the real variables are replaced by additive variables in that the explanation model for variable importance is formulated as a linear function of additive binary features. The exact solution to SHAP values is computationally expensive. They can, however, be approximated by combining different additive feature attribution methods. SHAP also provides each feature with an importance value for a particular prediction. Lundberg and Lee (Lundberg and Lee 2017) demonstrated that SHAP is better adjusted using human intuition and more robustly distinguish between model output classes than several existing methods.

6.2.5. Structural trapping estimation

Structural traps (ST), the most immediately available trapping mechanism, corresponding to the local maxima of the top surface play a key role in CO_2 storage. In this trapping mechanism, the CO_2 plume is prevented from migrating further upwards after reaching the caprock (Shariatipour, S. M., Pickup and Mackay 2016). MRST-CO2lab implements several algorithms to identify the ST in the sealing caprock without any flow simulation. Due to its very low computational cost, this method can be used in large models. The "spill path" refers to the path the CO_2 follows beneath the caprock, assuming infinitesimal flow. Once injected, the CO_2 plume tends to move upwards and fill the traps/ridges below the caprock. When a trap has been filled to its spill point, any additional CO_2 will flow to the neighbour trap (Nilsen, Lie and Andersen 2015). Individual traps are connected by spill paths, like lakes being connected by rivers in surface hydrology. The static ST capacity in terms of CO_2 mass is estimated using Equation *6.4* (Nilsen et al. 2015).

$$ST\ capacity = \int_\Omega \rho V \varphi (1 - S_{rw}) \hspace{3cm} \text{Equation 6.4}$$

where ρ denotes for CO_2 density at aquifer condition (kg/m^3), V is trap volume (m^3), ϕ is porosity, S_{rw} is residual water saturation and the integrate is over the boundary of $\Omega \subset R^n$. Note that for traps with the same pore volume ($V\varphi$) but located at a different depth, ST capacity differs due to CO_2 density variation. Readers are advised to refer to (Nilsen et al. 2015) for

more details about ST capacity and spill-point analysis. Other important trapping mechanisms for CO_2 storage are residual, dissolution and mineral trapping mechanisms. Due to the short timescale of the study (12 years) for the Sleipner project, their impacts are neglected.

6.3. Results and discussion

In this section, two simulations are analysed with the best and worst average (in four time steps) plume match, together with the minimum and maximum ST capacity. The importance of each of the uncertain parameters on plume outline is investigated using both the cross-correlation effect of all parameters and a one factor at a time (OFAT) approach. Figure 3 shows the case with the best match between the plume outline from seismic (1st row) and simulation (2nd row) results. The figure also visualises the overlapped area of the plume outlines (3rd row). Note that the presented results are generated from one set of uncertain parameters with the highest average SDC in 2001, 2004, 2006 and 2010. The average SDC of the four time steps for each of the one million simulations are calculated, and the results are ranked from best (highest average SDC) to worst (lowest average SDC) match. The plume outline at the end of each of the studied timestep is reported. The reason to focus on these four outputs is that the plume outline data for Sleipner model is available for limited timesteps, of which 2001, 2004, 2006 and 2010 are used in this study. The primary source of mismatch was the tail-like plume outline which seems to be due to the path governed by the caprock elevation variations that plume follows.

Note that although the vertical seismic resolution is about 8 m, it is possible to calculate the thickness of topmost CO_2 below the seismic detection range using methods such as structural analysis of the reservoir top (Chadwick RA and Noy DJ. 2010; Chadwick, R. A. et al. 2009; White, James C. et al. 2018) and spectral decomposition technique (Huang et al. 2015; White, James C. et al. 2015; White, James C., Williams and Chadwick 2013; Williams and Chadwick 2012).

6.3.1. Best and worst matches

Figure 6.2. Plume outline from seismic (1st row), the simulation results with the best average match (2nd row), comparison of the plume outlines (3rd row; dark blue: seismic, yellow: simulated, green: overlapped) in 2001, 2004, 2006 and 2010. The legend shows the plume thickness (m).

At different time steps, the plume shape shows a good match between the plume lateral extension outline from seismic and simulation studies. However, the presented results are the best averaged outcome from one million simulations and not necessarily the best possible match for the model. The uncertain input parameters for the simulation are listed in Table 6.3.

Table 6.3. Simulation parameters for the case with the highest average SDC.

Parameter	Value
Average SDC of the studied time steps	0.81
Density multiplier (DM)	0.41
Rate multiplier (RM)	0.83
DT (°C)	5.72
ϕ_{avg}	0.30
K_{avg} (D)	2.94
Average elevation change (m)	0.32
Average absolute elevation change (m)	2.36

According to Table 6.3, a lower DM (0.41), and a positive DT (5.72 °C) results in a better match. Analysis of the results showed that the best overall match for the plume outline mainly has a density multiplier of between 0.40 and 0.50, resulting in a CO_2 density of 304 kg/m^3 and 380 kg/m, respectively. These values are similar to those used in the work undertaken by (Cavanagh and Haszeldine 2014) in which the authors suggested a CO_2 density of 355 kg/m^3. A density of 391 kg/m^3 was also suggested by (Nilsen et al. 2017) in one of their calibrated set of parameters for Layer 9. The Sleipner condition is close to the critical point, and CO_2 has a gas-like behaviour under supercritical conditions (Hodneland et al. 2019). Therefore, increasing the temperature results in a significantly lower density and consequently, a higher buoyancy force. A higher temperature at pressures close to the average pressure of 83 bar in Layer 9 (Hodneland et al. 2019), results in a lower viscosity (Bachu 2003) and consequently, higher mobility. In this condition (higher temperature) the CO_2 plume conforms more accurately the caprock morphology. Increasing the temperature was previously (Hodneland et al. 2019) suggested improving the match between simulation and seismic surveys results. As it is shown in

Table 6.3, an RM of 0.83 results in the best average plume match. Note that the results presented here are just one of the many possible "acceptable" results. Since the parameters are

not completely independent, a different set of input parameters might potentially lead to the same if not better results.

Table 6.3 shows that realizations with average porosity and permeability values of 0.3 and 2.94 D, respectively, result in the best match. An average absolute elevation change of around 2.36 m is observed in the case with the highest averaged SDC.

Similar to the previous case, Figure 6.3 shows the results for the case with the lowest averaged SDC over the studied time steps. The uncertain input parameters for the simulation are listed in Table 6.4.
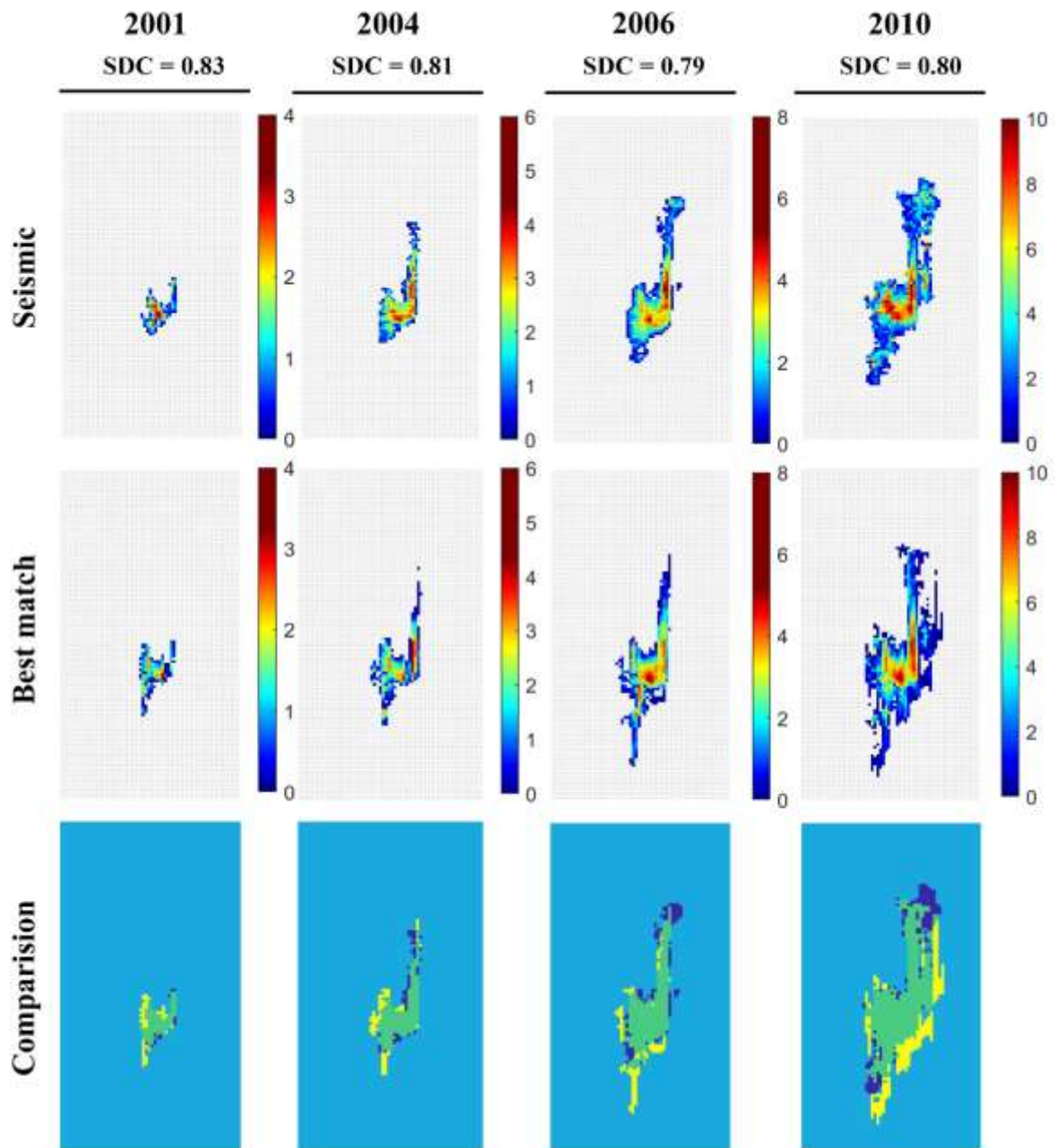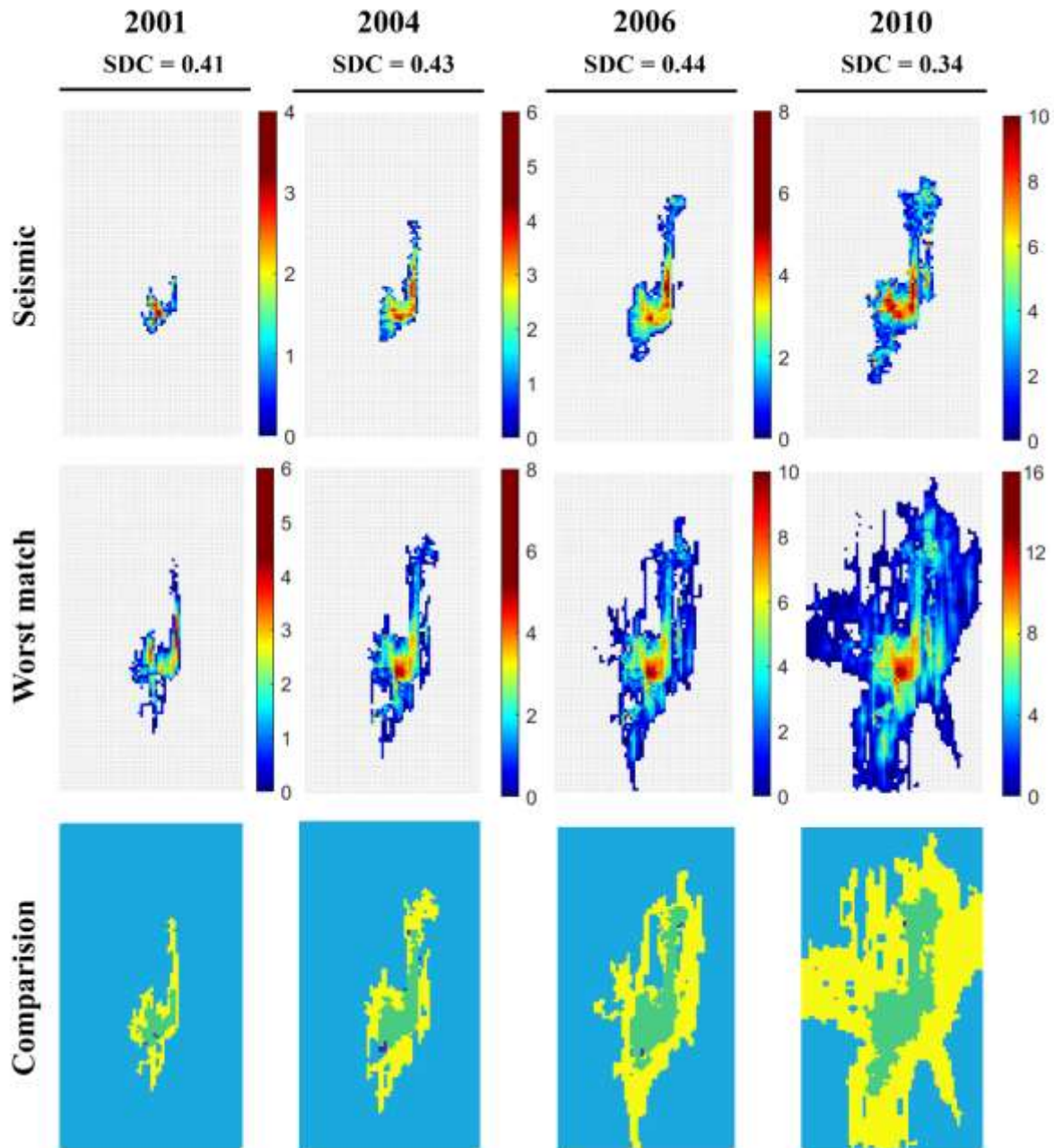
Figure 6.3. Plume outline from seismic (1st row), the simulation results with the worst average match (2nd row), comparison of the plume outlines (3rd row; dark blue: seismic, yellow: simulated, green: overlapped) in 2001, 2004, 2006 and 2010. The legend shows the plume thickness (m).

According to Figure 6.3 (3rd row), all the plume outlines from the simulation results, are larger than those from the seismic studies. This can be justified by the DM and RM values which are almost at their maximum possible range (Table 6.4). The mass flow rate depends on the allocated plume density and a higher density results in a higher mass flow rate of CO_2 (Nilsen et al. 2017). An interesting point about the DT is that a higher reservoir temperature which

113

resulted in a better match in previous cases (Table 6.3), does not necessarily guarantee a better answer as the case with minimum average SDC in 2001, 2004 and 2006 has a DT of 5.95 °C. Therefore, the impact of the parameters on the plume match is affected by the presence of other uncertain parameters, highlighting the limitation of the OFAT approach. The impact of uncertain parameters on plume migration changes throughout the simulation time and the results presented here shows the average impact on plume match. The problem we are dealing with in the Sleipner is complex; therefore, a different set of parameters might account for the best match in each time step. A data-driven modelling approach is used in Section 6.3.3. to find the contribution of each parameter in CO_2 plume migration more precisely.

Table 6.4. Simulation parameters for the case with the lowest average SDC.

Parameter	Value
Average SDC of the studied time steps	0.40
Density multiplier (DM)	1.18
Rate multiplier (RM)	1.29
DT (°C)	5.95
ϕ_{avg}	0.32
K_{avg} (D)	2.87
Average elevation change (m)	0.48
Average absolute elevation change (m)	3.54

6.3.2. OFAT approach

As mentioned earlier the following set of values are assigned to the uncertain parameters in this study:

- DT: -6 to 6 °C.
- DM: 0.4 to 1.2.
- RM: 0.7 to 1.3.

- Porosity: 0.27 to 0.4.

- Permeability: 1.1 D to 5 D.

- Caprock elevation: -5 to +5 m.

In this section, the well-known OFAT approach is used, by analysing the model's response to a change in individual uncertain parameters, while keeping the rest of inputs at their initial state. One hundred values (and realizations for the cases of porosity, permeability and elevation) are considered within the allocated range. The results are presented in Figure 6.4, with the initial values of the model highlighted in purple. It is clear that the initial input data used in this study creates a better representative of the flow behaviour in 2001 (blue line).

It is hard to find a similar trend between the results of the same parameters in various time steps. For example, looking at the overall trend for density, while in 2001 an increase in the DM (higher than 0.4) increases the matching accuracy, the same phenomenon in 2010 results in a lower SDC. A similar trend was observed in the results for RM. A lower RM and DM both result in a lower mass flow rate. As CO_2 is not being injected at a constant rate, the reason behind these trends might be that the rate used in this study in 2010, is higher than the actual flow entering Layer 9.

As claimed in work undertaken by (Nilsen et al. 2017), caprock elevation seems to have a noticeable impact on the plume match. There is no visible relationship between the employed realization for caprock elevation and the calculated SDC in different time steps. The results in 2001, 2004 and 2006, however, show more resemblance than 2010. The elevation is changing within -5 to 5 metres in the current study, with an average absolute elevation change of less than 1.9 (m). As Figure 6.4 shows, even this small variation, which is about a quarter of the vertical resolution, can significantly impact the CO_2 plume migration behaviour.
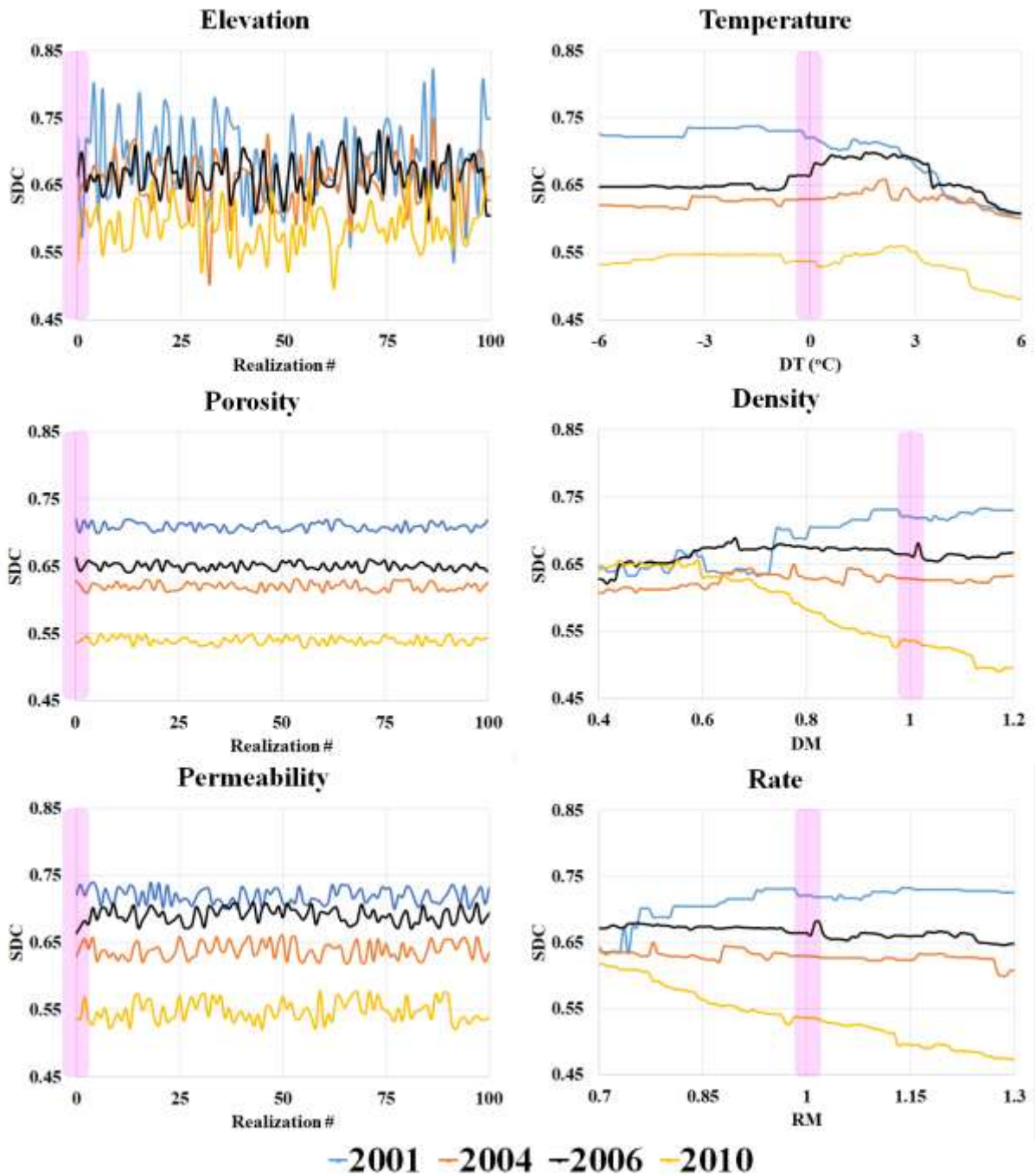
Figure 6.4. Calculated SDC for each of the input parameters using an OFAT approach. Initial values of the model are highlighted in purple. Blue, orange, black and yellow lines represent the results for the years 2001, 2004, 2006 and 2010, respectively.

Note that the overall constant trend of SDC for DT (between -6 to 0) or RM (between 0.7 to 1.3) in 2004 and 2006 does not mean that the plume outline has remained constant while these parameters are changing as it is possible to have two different outlines with the same SDC. This can be observed in Figure 6.5, showing the plume outline in an example case for various

values of DT while keeping other parameters constant. The figure clearly shows that not only plume extensions are not identical, but also the CO_2 plume seems to become thicker by increasing the DT. This could attributed to one of the Dice method's limitations as it considers the difference in the unique elements. In other words, if circle A and B have an area equivalent to 90% and 110% of circle C, respectively, therefore $SDC_{A \& C} = SDC_{B \& C} = 0.90$. Moreover, the plume thickness is not considered in the similarity measure, which is a limitation of this approach.
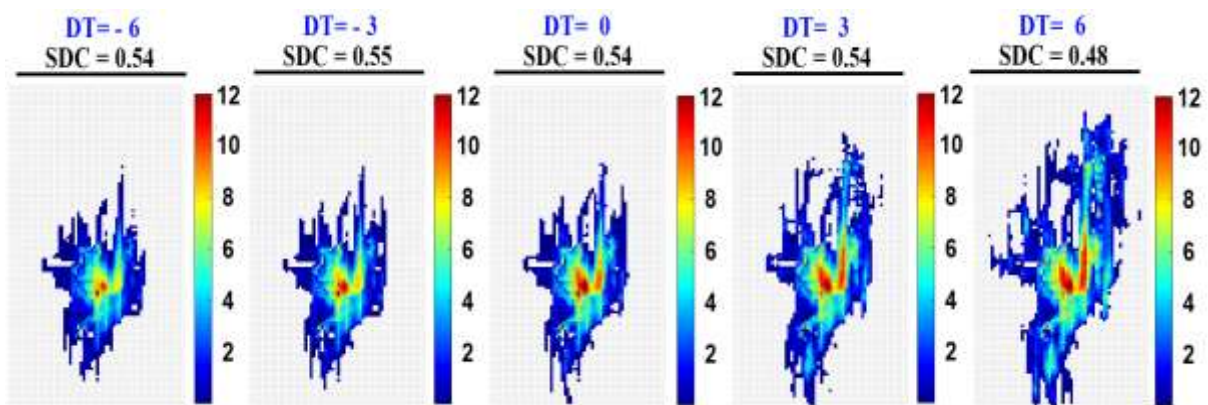
Figure 6.5. Plume outline for various values of DT in 2010. The legend shows the plume thickness (m).

Figure 6.4 shows that the plume match is affected by permeability distribution in the model which is in agreement with the results of the work undertaken by Nilsen et al. (Nilsen et al. 2017). They used adjoint-based sensitivities, adjusting parameters in a way to minimize the mismatch between the observation and simulation. The optimised permeability data set in their work, however, had an average one-order magnitude higher than the original value reported for Layer 9. While the reported range of permeability for Layer 9 is between 1.1 and 5 Darcy, the authors proposed an average permeability of 21.7 Darcy to improve the plume match. In the current study, the range of reported permeability (and porosity) data are not changed; therefore the impact of permeability on overall plume match might be less significant than their work. Uncertainties in porosity show a smaller impact on plume dynamics than uncertainties in permeability and caprock elevation. While the level of perturbations applied to these parameters affects their degree of impact, however, similar results were observed in work performed by (Allen, R. et al. 2018) where even an increase of ±50% of the original average porosity had minimal impact on the match in the Utsira model.

Increasing the DT resulted in a slight improvement in the match for values up to 3°C, followed by a relatively sharp drop for DT between 3 to 6°C. The worst and best average match analysis also showed that a higher temperature does not necessarily improve the match. A recent study on the Sleipner model, however, showed that raising storage temperature would significantly improve the match (Hodneland et al. 2019). Hodneland et al. (Hodneland et al. 2019) used the previous Sleipner model; therefore, the base case of their model has a different caprock elevation than the one used in this study. Moreover, the distribution of porosity and permeability data was also different. Here, the impact of uncertainty in porosity, permeability and caprock elevation in calculated SDC for temperature, density and rate, are examined using the OFAT approach. For this regard, the simulations illustrated in Figure 6.4 are repeated, using new realizations of porosity, permeability and caprock elevation (within the allocated range and using the same distribution approach as in Section 2.2). Subsequently, the model's response to the change in temperature, density, and the rate is analysed (one parameter at a time). Results are shown in Figure 6.6, where the graphs in the Group A (highlighted in yellow) are the same as the ones in Figure 6.4, and the ones in Group B (highlighted in purple) have the new set of data for porosity, permeability and caprock elevation. Results show a mismatch in the trend of SDC between Groups A and B. For instance, despite Group A, increasing the temperature in Group B shows an overall improvement in the match. For density, in Group A, an increase in DM has a negative impact on the overall match in 2010, for Group B however, it increases the SDC. Therefore, it is difficult to make a general statement on the impact of a parameter on the overall match. The lack of agreement in the results shows the limitation of the OFAT approach being due to the complexity of the problem, and the presence of other sources of uncertainty affecting the results. In the next section, a data-driven approach is introduced to investigate the contribution of individual parameters, in the presence of other sources of uncertainty, more precisely.
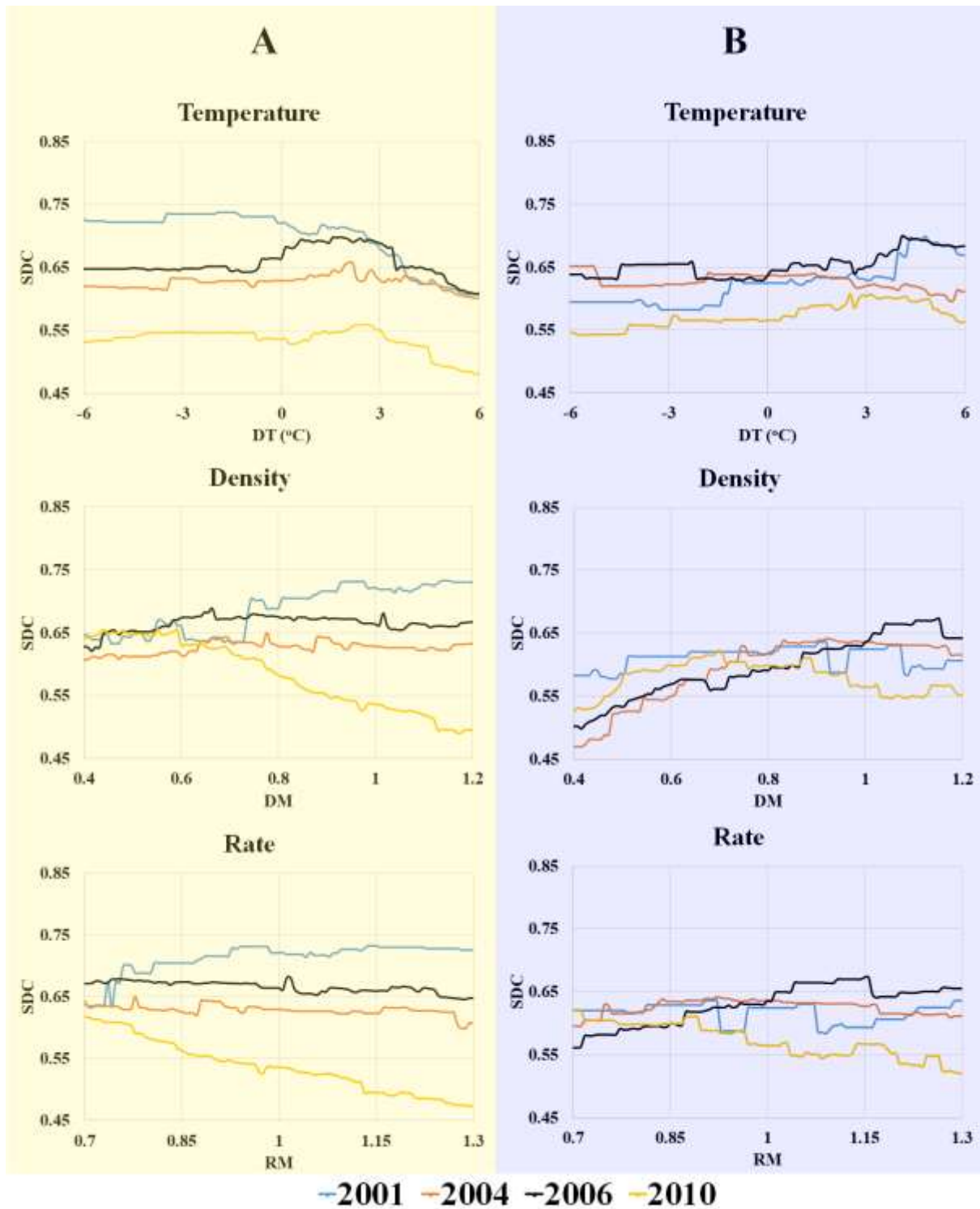
Figure 6.6. Impact of uncertainty in porosity, permeability and caprock elevation in calculated SDC for temperature, density and rate and using an OFAT approach. A group (yellow highlight): same as the ones in Figure 5. Group B (purple highlight): resulted by new sets of data for porosity, permeability and caprock elevation.

6.3.3. Cross-correlation effect of parameters through data analysis

The percentage overall variable importance plots for both RF and DTree models approximated by SHAP are presented in Figure 6.8. All SHAP values are obtained by averaging over five trials with the different starting point (multiple restarts) to ensure the reliability and reproducibility of estimations. Both the RF and DTree models consistently identify density, elevation, temperature, injection rate and heterogeneity in permeability as the most important parameters when averaged over the four years under study. Heterogeneity in porosity is the lowest-impact variable for both RF and DTree models. Percentage variable importance is also computed for every variable each year (see the number in the boxes). A higher percentage shows the dominant impact of the parameter on the SDC or in other words a better match between the simulated and observed plume outlines. For instance, the variable "elevation" has the highest impact on model prediction in 2001 and 2004. Here the trends observed in the RF model is discussed (which are consistent with the DTree model as well).

Results clearly show that the impact of each parameter might change throughout the simulation. For instance, while the elevation is the dominant factor in 2001 (35.59%), its impact becomes less significant later in 2010 (8.37%, RF). Meanwhile, the importance of injection rate and density seems to increase with time and their percentage predictor importance changes from 12.38% and 14.32% in 2001 to 26.55% and 36.40% in 2010, respectively. One justification is that the impact of other uncertain parameters is being overshadowed by the density and injection rate in the later years. This happens because the injection rate used in this study is not constant and increases with time. Density and injection rate are the only two parameters that have a direct impact on the mass flow rate in the aquifer. Since multipliers for these two parameters are being used, a constant amount is not applied throughout the simulation, and as the injection rate in the model increases, the impact of these two multipliers becomes more significant as well. In the case of temperature and caprock elevation, the weight of adjustment in these parameters is constant during the simulation while adding/subtracting a value within the same range over the simulation.

The results also show clearly the importance of caprock elevation in controlling the plume outline. Note that the average absolute change on caprock elevation in this study is about 1.7m with a maximum and minimum of 5m and -5m, respectively. Although there have been several sources of uncertainties reported in the literature for determining the best plume match, the impact of caprock morphology, however, seems to be underestimated as it has average importance of about 21%. An elevation change in a range of about half of the reported seismic

resolution in the Sleipner is used and the impact is yet significant. Permeability and porosity contribute to changing the shape of the plume outline with overall percentage importance of around 10% and 6% respectively.
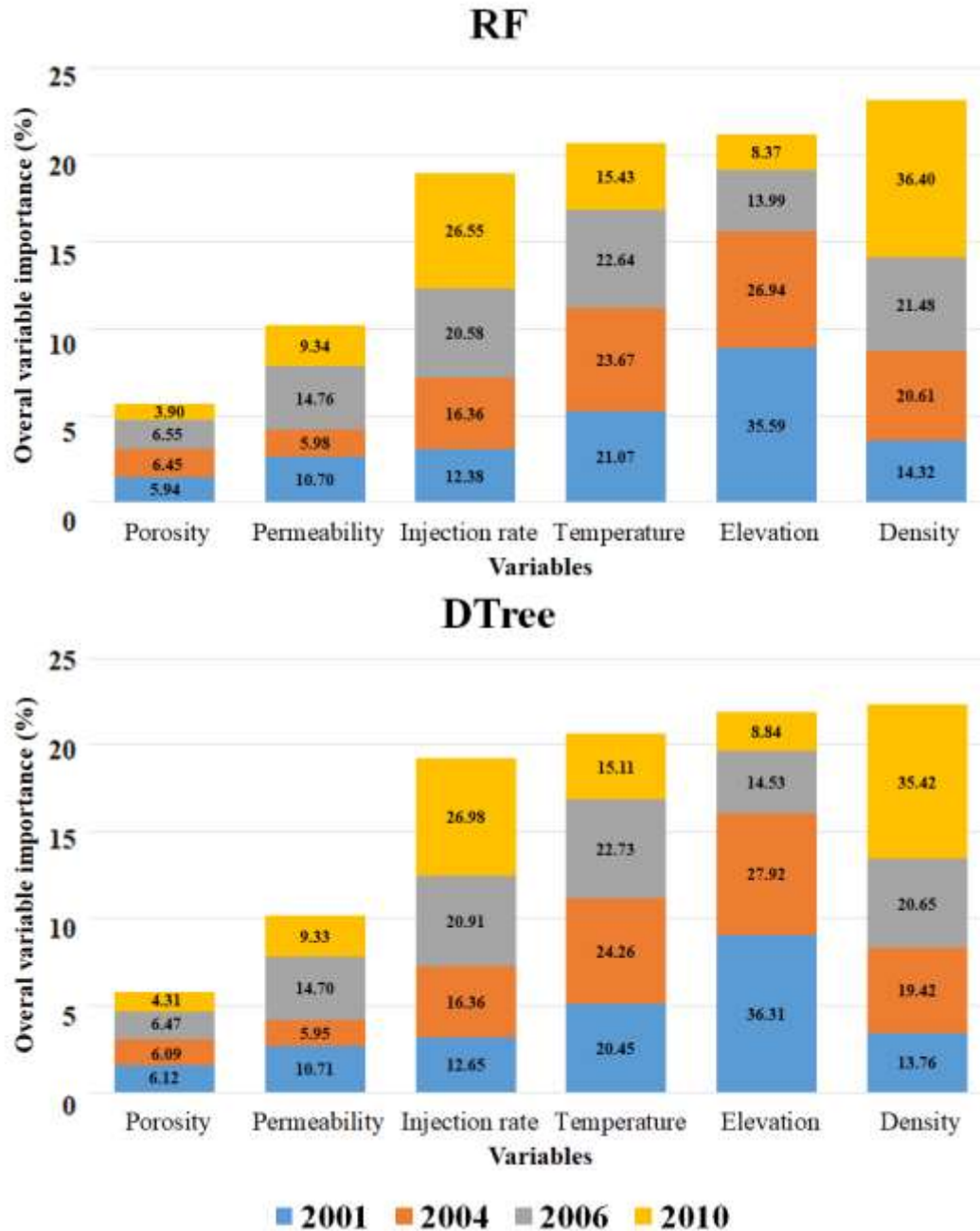
Figure 6.7. Percentage overall variable importance plots for DTree and RF models approximated by SHAP

6.3.4. ST capacity estimation

The parameters in the cases with the highest and lowest ST capacity are listed in Table 6.5. As the CO_2 density increases the structural traps contain more CO_2 (mass = density $\times$ volume (constant)). Therefore, the DMs of 0.4 and 1.2 resulted in minimum and maximum ST capacity, respectively. As mentioned earlier, using a lower temperature in the Sleipner aquifer condition would result in a higher density and consequently higher ST capacity. The findings in this chapter agree with previous works (Allen, R. *et al.* 2018; Bachu 2003) and the minimum and maximum ST capacity corresponds to the DT of 6 and -6, respectively. As expected, a higher (and positive) caprock elevation change and porosity increase the structural trapping.

Table 6.5. Simulation parameters for the cases with minimum and maximum ST capacity.

Parameter	ST capacity	
	Min	Max
ST capacity (Mt)	1.76	3.6
SDC (2010)	0.70	0.41
Simulation #	3414	9581
Density multiplier (DM)	0.4	1.2
ΔT (ºC)	6	-6
φ_{avg}	0.30	0.37
Average elevation change (m)	0.28	0.70
Average absolute elevation change (m)	1.44	2.48

6.4. Conclusions

In the work outlined in this chapter, the focus has been on the cross-correlation of uncertain parameters whose impact was believed to influence the overall CO_2 migration and trapping in

the Sleipner 2019 benchmark model. For this purpose, one million forward simulations were performed analysing the importance of porosity and permeability heterogeneity, reservoir temperature, CO_2 density and caprock elevation of plume outline. To make the study computationally feasible, the simulations are performed using the VE approach. In the work internal layers were disregarded, and the whole thickness of the aquifer as one layer as a single VE model was simulated. Upwards migration of CO_2 through internal layers was implicitly modelled through the rate multipliers. A more complex study would involve applying a VE model to each internal layer which could be considered for future work.

The results showed that CO_2 density values of 304 kg/m^3 and 380 kg/m^3, which were lower than the initially assigned values of 760 kg/m^3, improved the plume match significantly. The CO_2 density was shown to be the most important parameter in controlling the plume migration with the overall importance of 23% followed by the caprock elevation (21%), temperature (21%), the injection rate (19%), and heterogeneity in permeability (10%) and porosity (6%). Note that the best combination of parameters reported in this study is one of the many possible answers. As was shown in the OFAT approach results, the effect of a parameter on the plume outline can be changed in the presence of another parameter.

Chapter 7

Summary, conclusions, and future work

7.1. Summary and conclusions

In this work, the impact of caprock morphology on the CO_2 storage process has been studied. Various approaches and mathematical tools, including analytical calculations, numerical simulation, vertical equilibrium modelling, data analysis, and optimization, were employed for this purpose. The effect of caprock morphology on CO_2 plume migration and trapping was first investigated using a wide range of fully 3D synthetic simulation models (**Chapter 3**). A more computationally feasible approach (i.e. VE modelling) for the problem was introduced and its performance compared with full 3D simulation methods (**Chapter 4**). Once the VE modelling results met the expectations, the study using this approach was carried out. Later an optimization tool is used to reduce the mismatch between the observed and simulated plume outline for the Sleipner model (**Chapter 5**). At this stage it was found that caprock morphology is an important parameter which needs to be carefully implemented in the geological models for a geological CO_2 storage problem. Later on the focus of the work was to quantify its importance in a real case model, in the presence of other uncertain parameters using data analysis tools (**Chapter 6**). Here is the summary and conclusion of the chapters:

In **Chapter 3,** using numerical simulation and analytical calculation, the impact of caprock morphology and aquifer boundary has been studied on plume trapping (structural and dissolution) and migration. This chapter presents a preliminary study on the impact of boundary conditions on the CO_2 plume migration and dissolution for horizontal and tilted caprock models. This was performed because most of the case study models employed for geological CO_2 storage studies are part of larger reservoirs. The obtained results were used in the simulation models of the second part of the chapter, to model appropriately an infinite-acting reservoir. Subsequently, the impact of caprock morphology on the CO_2 plume advancement and its structural and dissolution trapping mechanisms are investigated by performing numerical simulations on synthetic models. Dissolution was seen as a strong function of aquifer dip angle as by increasing the tilt, plume migrates further distances upwards and makes more contact with the unsaturated brine. The tilt angle, however, had a negligible impact on CO_2 dissolution during the injection phase. Minimum dissolution was observed in

cases with structural traps with high amplitudes as they trap the plume and limit its contact with the brine. In terms of the impact of boundary conditions on CO_2 storage process, results showed that the dissolution in aquifers with one closed end (due to faults, salt walls, etc.) is higher than an open aquifer. The amount of structural trapping is evaluated using an analytical method, and results are validated using numerical simulation. This methodology is appropriate for site screening prior to performing any numerical simulation. Results for the amount and possibly of structural trapping for a specific case showed a good agreement between analytical calculation and numerical simulation approaches.

When injected in an aquifer, the free phase CO_2 tends to migrate upwards, due to its lower density compared to the *in-situ* brine. This vertical migration is generally limited to tens of metres depending on the reservoir thickness. The plume migration distance in the horizontal direction could be over hundreds of kilometres (depending on the time horizon, reservoir characteristics, trapping mechanisms involved, etc.). In the general cases, the plume ends up as a separate region below a sealing barrier. This large aspect ratio between the plume migration in the horizontal and vertical directions often allows reduced dimensionality such as vertical equilibrium (VE) models for CO_2 storage simulation. Under a VE assumption, the injected CO_2 plume flow in 3D can be approximated in terms of its thickness to obtain a 2D simulation model, consequently decreasing the computational costs.

In **Chapter 4**, the focus is on comparing the performance of several simulation methods, including ECLIPSE-black-oil (E100), ECLIPSE-compositional (E300) and ECLIPSE-VE (EVE) and VE tool in MRST-CO2lab (MVE). A homogenous model with a constant porosity and permeability is considered for simulation studies to simplify the studied case. The impact of tilt angle on dissolution in 3D simulators was opposite to what was observed in the previous chapter, and the dissolution was decreased by increasing the tilt angle. A low permeability in the vertical direction was considered (5mD compared to the 50 mD in the horizontal direction). Consequently, part of the plume was trapped residually in the bottom layers due to the limited vertical permeability. The dissolution increased, however, with increasing tilt angle in the VE models because segregation occurs instantly, and the plume migrates upwards and lies beneath the caprock without being trapped in the bottom layers. The plume outline in all the models was similar, and in terms of computational cost, MVE outperformed the rest significantly.

The uncertainty of input parameters in reservoir simulation models is unavoidable. A popular technique to tackle this problem and achieve a more reliable result is to adjust the input

parameters to match the simulated production data with the actual hydrocarbon production data; an approach commonly referred to as history matching. Typical parameters adjusted in history matching in reservoir engineering are porosity and absolute and relative permeability data. For CO_2 storage in saline aquifers, however, the caprock morphology plays an important role with respect to the plume migration and storage security.

In **Chapter 5,** a non-linear simulation-based optimisation tool was used in MRST to improve the match between observed and simulated plume by changing the caprock morphology only. The study was first performed on a synthetic model to modify caprock slope and rugosity, where the method showed a good performance and the results were satisfactory for different scenarios. One of the ongoing discussions in the Sleipner field of the Utsira formation CO_2 storage project is to find a satisfactory match for plume migration. Later, after testing the optimization tool on the synthetic models, the method was applied to the most recent benchmark model for the Sleipner to minimize the mismatch between the observed plume from seismic survey and simulation e, by changing the caprock elevation within the seismic detection range (~10 m). The results showed an average improvement of 8% in the plume match. A wide range of parameters has been modified in previous studies on Sleipner to improve the plume match. The results clearly show that one of the parameters which should be considered in history matching of the plume is the caprock morphology.

Several studies have been based on the Sleipner reservoir model to better understand the inherent flow physics of the storage site, to find a satisfactory match of the CO_2 plume migration. Various sources of uncertainty in the geological model and the fluid have been investigated. Most of the work undertaken on the Sleipner model employed the one factor at a time (OFAT) method and analysed the impact of uncertain parameters individually on plume match. In previous chapters, the focus was on the importance of caprock morphology on the geological CO_2 storage process in synthetic models and Sleipner.

Chapter 6 focuses on employing a data analysis approach to quantify the importance of uncertainties in caprock morphology in the presence of other reported sources of modelling uncertainties in the Sleipner 2019 benchmark model. One million simulations were performed using the VE model in MRST and focusing on the cross-correlation effect of porosity and permeability heterogeneity, reservoir temperature, CO_2 density and caprock elevation in overall CO_2 migration and trapping. To the best of the author's knowledge, this is the first time a study has focused on the cross-correlation between six uncertain parameters using data

analysis techniques. The work in this chapter raises the scientific understanding of the complexity of the impact of the reservoir uncertainty on CO_2 plume migration in a real field model. Results showed that caprock elevation was the second most important factor with the overall importance of 21% (after density with importance of 23%), followed by temperature (21%), the injection rate (19%), and heterogeneity in permeability (10%) and porosity (6%).

7.2. Summary of key findings

1. The impact of boundary condition on the storage process showed that dissolution in aquifers with one closed end (due to faults, salt walls, etc.) is higher than an open aquifer.

2. The amount of structural trapping evaluated using the analytical method, was in the same range as numerical simulation. This methodology is appropriate for site screening prior to performing any numerical simulation.

3. In models with low vertical permeability, increasing the tilt angle resulted in a lower dissolution (opposite to what was observed in previous studies).

4. The plume outline in VE and 3D models was similar and in terms of computational cost, MRST outperformed the rest significantly.

5. The results showed an improvement of around 8% in the Sleipner plume match resulting from an average absolute elevation change of 3.23 metres.

6. Calibrating the porosity, permeability, CO_2 density and injection rate resulted in a 5% improvement in the match, and once caprock morphology was included in the optimization process, the match improvement increased by 16%.

7. The caprock morphology of the recent Sleipner benchmark (2019) model does not represent the observed plume outline from seismic and is less accurate than the previous benchmark.

8. Caprock elevation was the second most important factor in controlling the plume migration in the Sleipner model (after density), followed by temperature, the injection rate, and heterogeneity in permeability and porosity.

7.3. Future work

Here are some recommendations for future studies:

- A code in MRST was developed to improve the match between the observed and simulated plume outline, by only changing caprock properties of slope and rugosity

elevation. It would be possible to implement the code as a plug-in for Petrel using the Ocean software development framework by Schlumberger to add caprock morphology as one of the HM parameters.

- An SDC was used to compare the similarity between two plume outlines. Although SDC is a straightforward method, it does not consider the plume saturation distribution into account which could be investigated in future studies.

- While working on the recent Sleipner benchmark model, the internal layers were disregarded, and the focus was on Layer 9 only. A more detailed study would involve applying the VE model to each individual layer and using a stacked VE model instead, where modified transmissibility could represent shale layers.

- One million simulations were run on the Sleipner model. A combination of six input parameters resulted in a wide range of plume outlines and trapping conditions (structural, dissolution and residual). A possible opportunity for future work is to employ a machine learning (ML)approach and train a model to predict the plume migration and trapping mechanisms for Sleipner without running any simulations.

References

Abergel, T., Brown, A., Cazzola, P., Dockweiler, S., Dulac, J., Pales, A. F., Gorner, M., Malischek, R., Masanet, E. R., and McCulloch, S. (2017) 'Energy Technology Perspectives 2017: Catalysing Energy Technology Transformations'

Ahmadinia, M., Shariatipour, S. M., and Sadri, M. (eds.) (2019) 81st EAGE Conference and Exhibition 2019 . 'A Comprehensive Sensitivity Analysis on CO_2 Plume Migration and Trapping Under Tilted Sinusoidal Structures. 81st EAGE Conference & Exhibition. 3 - 6 June 2019. London.'

Ahmadinia, M., Shariatipour, S. M., Andersen, O., and Sadri, M. (eds.) Society of Petroleum Engineers. . 'A History Matching Approach to Estimate Caprock Morphology Parameters for CO_2 Storage in Saline Aquifers. SPE Europec Featured at 81st EAGE Conference and Exhibition. Society of Petroleum Engineers, 2019.'. held 3 Jun 2019 - 6 Jun 2019 at London, United Kingdom. Onepetro: Society of Petroleum Engineers

Ahmadinia, M., Shariatipour, S. M., Andersen, O., and Sadri, M. (2019) 'Benchmarking of Vertically Integrated Models for the Study of the Impact of Caprock Morphology on CO_2 Migration'. International Journal of Greenhouse Gas Control [online] 90, 102802

Ajayi, T., Gomes, J. S., and Bera, A. (2019) 'A Review of CO_2 Storage in Geological Formations Emphasizing Modeling, Monitoring and Capacity Estimation Approaches'. Petroleum Science, 1-36

Al-Khdheeawi, E. A., Vialle, S., Barifcani, A., Sarmadivaleh, M., and Iglauer, S. (2017a) 'Effect of Brine Salinity on CO2 Plume Migration and Trapping Capacity in Deep Saline Aquifers'. The APPEA Journal 57 (1), 100-109

Al-Khdheeawi, E. A., Vialle, S., Barifcani, A., Sarmadivaleh, M., and Iglauer, S. (2017b) Impact of Reservoir Wettability and Heterogeneity on CO_2-Plume Migration and Trapping Capacity [online]. available from <http://www.sciencedirect.com/science/article/pii/S1750583616305072>

Allen, D. J. and Brent, G. F. (2010) 'Sequestering CO_2 by Mineral Carbonation: Stability Against Acid Rain Exposure'. Environmental Science & Technology 44 (7), 2735-2739

Allen, R., Nilsen, H. M., Lie, K. A., Møyner, O., and Andersen, O. (2018) 'Using Simplified Methods to Explore the Impact of Parameter Uncertainty on CO_2 Storage Estimates with Application to the Norwegian Continental Shelf'. International Journal of Greenhouse Gas Control 75, 198-213

Alnes, H., Eiken, O., Nooner, S., Sasagawa, G., Stenvold, T., and Zumberge, M. (2011) 'Results from Sleipner Gravity Monitoring: Updated Density and Temperature Distribution of the CO_2 Plume'. Energy Procedia 4, 5504-5511

Alnes, H., Eiken, O., and Stenvold, T. (2008) 'Monitoring Gas Production and CO_2 Injection at the Sleipner Field using Time-Lapse Gravimetry'. Geophysics 73 (6), WA155-WA161

Ambrose, W., Lakshminarasimhan, S., Holtz, M., Nunez Lopez, V., Hovorka, S., and Duncan, I. (2008) 'Geologic Factors Controlling CO_2 Storage Capacity and Permanence: Case Studies Based on Experience with Heterogeneity in Oil and Gas Reservoirs Applied to CO_2 Storage'. Environmental Geology 54 (8), 1619

Andersen, O. and Nilsen, H. M. (2018) 'Investigating Simplified Modeling Choices for Numerical Simulation of CO 2 Storage with Thermal Effects'. International Journal of Greenhouse Gas Control 72, 49-64

Andersen, O., Gasda, S. E., and Nilsen, H. M. (2015) 'Vertically Averaged Equations with Variable Density for CO_2 Flow in Porous Media'. Transport in Porous Media 107 (1), 95-127

Arts, R., Eiken, O., Chadwick, A., Zweigel, P., Van der Meer, L., and Zinszner, B. (2004) 'Monitoring of CO_2 Injected at Sleipner using Time-Lapse Seismic Data'. Energy 29 (9), 1383-1392

Bachu, S. (2015) 'Review of CO2 Storage Efficiency in Deep Saline Aquifers'. International Journal of Greenhouse Gas Control 40, 188-202

Bachu, S. (2003) 'Screening and Ranking of Sedimentary Basins for Sequestration of CO_2 in Geological Media in Response to Climate Change'. Environmental Geology 44 (3), 277-289

Bachu, S., Gunter, W., and Perkins, E. (1994) 'Aquifer Disposal of CO_2: Hydrodynamic and Mineral Trapping'. Energy Conversion and Management 35 (4), 269-279

Bachu, S. (2002) Sequestration of CO2 in Geological Media in Response to Climate Change: Road Map for Site Selection using the Transform of the Geological Space into the CO_2 Phase Space [online]. available from <http://www.sciencedirect.com/science/article/pii/S0196890401000097>

Baklid, A., Korbol, R., and Owren, G. (eds.) (1996) SPE Annual Technical Conference and Exhibition. 'Sleipner Vest CO_2 Disposal, CO_2 Injection into a Shallow Underground Aquifer': Society of Petroleum Engineers

Bandilla, K. and Celia, M. (2019) 'Numerical Modeling of Fluid Flow during Geologic Carbon Storage'. in Science of Carbon Storage in Deep Saline Formations. ed. by Anon: Elsevier, 181-208

Bandilla, K. W., Celia, M. A., and Leister, E. (2014) 'Impact of Model Complexity on CO_2 Plume Modeling at Sleipner'. Energy Procedia 63, 3405-3415

Bao, K., Lie, K., MÃ¸yner, O., and Liu, M. (2017) 'Fully Implicit Simulation of Polymer Flooding with MRST'. Computational Geosciences 21 (5), 1219-1244

Beauheim, R. L. and Roberts, R. M. (2002) 'Hydrology and Hydraulic Properties of a Bedded Evaporite Formation'. Journal of Hydrology 259 (1-4), 66-88

Behzadi, H., Alvarado, V., and Lynds, R. (2012) 'Modeling CO_2 Saturation Distribution in Eolian Systems'. International Journal of Greenhouse Gas Control 11, 110-116

Benson, S., Cook, P., Anderson, J., Bachu, S., Nimir, H., Basu, B., Bradshaw, J., Deguchi, G., Gale, J., and von Goerne, G. (2005) 'Underground Geological Storage: IPCC Special Report on Carbon Dioxide Capture and Storage'. Ed.Metz, B., Davidson, O., Coninck, H., Loos, M., Meyer, L

Bickle, M., Chadwick, A., Huppert, H. E., Hallworth, M., and Lyle, S. (2007) 'Modelling Carbon Dioxide Accumulation at Sleipner: Implications for Underground Carbon Storage'. Earth and Planetary Science Letters 255 (1-2), 164-176

Bjørnarå, T. I., Mathias, S. A., Nordbotten, J. M., Park, J., and Bohloli, B. (2014) 'Capturing the Coupled Hydro-Mechanical Processes Occurring during CO_2 Injection–example from in Salah'

Brydie, J., Jones, D., Jones, J. P., Perkins, E., Rock, L., and Taylor, E. (2014) 'Assessment of Baseline Groundwater Physical and Geochemical Properties for the Quest Carbon Capture and Storage Project, Alberta, Canada'. Energy Procedia 63, 4010-4018

Bugge, T., Knarud, R., and Mørk, A. (1984) 'Bedrock Geology on the Mid-Norwegian Continental Shelf'. in Petroleum Geology of the North European Margin. ed. by Anon: Springer, 271-283

Bui, M., Adjiman, C. S., Bardow, A., Anthony, E. J., Boston, A., Brown, S., Fennell, P. S., Fuss, S., Galindo, A., and Hackett, L. A. (2018) 'Carbon Capture and Storage (CCS): The Way Forward'. Energy & Environmental Science 11 (5), 1062-1176

Buscheck, T. A., White, J. A., Carroll, S. A., Bielicki, J. M., and Aines, R. D. (2016) 'Managing Geologic CO 2 Storage with Pre-Injection Brine Production: A Strategy Evaluated with a Model of CO 2 Injection at Snøhvit'. Energy & Environmental Science 9 (4), 1504-1512

Carman, P. C. (1937) 'Fluid Flow through Granular Beds'. Trans.Inst.Chem.Eng. 15, 150-166

Cavanagh, A. J., Haszeldine, R. S., and Nazarian, B. (2015) 'The Sleipner CO_2 Storage Site: Using a Basin Model to Understand Reservoir Simulations of Plume Dynamics'. First Break 33 (6), 61-68

Cavanagh, A. J. and Haszeldine, R. S. (2014) 'The Sleipner Storage Site: Capillary Flow Modeling of a Layered CO_2 Plume Requires Fractured Shale Barriers within the Utsira Formation'. International Journal of Greenhouse Gas Control 21, 101-112

Chadwick RA and Noy DJ. (eds.) (2010) Geological Society, Petroleum Geology Conference Series. 'Chadwick RA; Noy DJ. History-Matching Flow Simulations and Time-Lapse Seismic Data from the Sleipner CO_2 Plume'. held 2010 at London: Geological Society of London

Chadwick, A., Arts, R., Bernstone, C., May, F., Thibeau, S., and Zweigel, P. (eds.) (2008) Best Practice for the Storage of CO_2 in Saline Aquifers, Observations and Guidelines from the SACS and CO2STORE Projects.: British Geological Survey

Chadwick, R., Noy, D., Arts, R., and Eiken, O. (2009) 'Latest Time-Lapse Seismic Data from Sleipner Yield New Insights into CO_2 Plume Development'. Energy Procedia 1 (1), 2103-2110

Chadwick, R., Arts, R., Eiken, O., Kirby, G., Lindeberg, E., and Zweigel, P. (2004) '4D Seismic Imaging of an Injected C02 Plume at the Sleipner Field, Central North Sea'. Geological Society, London, Memoirs 29 (1), 311-320

Chadwick, R. A., Noy, D., Arts, R., and Eiken, O. (2009) Latest Time-Lapse Seismic Data from Sleipner Yield New Insights into CO_2 Plume Development [online] . available from <http://www.sciencedirect.com/science/article/pii/S1876610209002756>

Chang, Y., Coats, B. K., and Nolen, J. S. (eds.) (1996) Permian Basin Oil and Gas Recovery Conference. 'A Compositional Model for CO 2 Floods Including CO 2 Solubility in Water': Society of Petroleum Engineers

Chen, C., Zeng, L., and Shi, L. (2013) 'Continuum-Scale Convective Mixing in Geological CO 2 Sequestration in Anisotropic and Heterogeneous Saline Aquifers'. Advances in Water Resources 53, 175-187

Chiaramonte, L., White, J. A., and Trainor-Guitton, W. (2015) 'Probabilistic Geomechanical Analysis of Compartmentalization at the Snøhvit CO_2 Sequestration Project'. Journal of Geophysical Research: Solid Earth 120 (2), 1195-1209

Class, H., Ebigbo, A., Helmig, R., Dahle, H. K., Nordbotten, J. M., Celia, M. A., Audigane, P., Darcis, M., Ennis-King, J., Fan, Y., Flemisch, B., Gasda, S. E., Jin, M., Krug, S., Labregere, D., Naderi Beni, A., Pawar, R. J., Sbai, A., Thomas, S. G., Trenty, L., and Wei, L. (2009) 'A Benchmark Study on Problems Related to CO_2 Storage in Geologic Formations'. Computational Geosciences 13 (4), 409

Coats, K., Dempsey, J., and Henderson, J. (1971) 'The use of Vertical Equilibrium in Two-Dimensional Simulation of Three-Dimensional Reservoir Performance'. Society of Petroleum Engineers Journal 11 (01), 63-71

Coats, K., Nielsen, R., Terhune, M. H., and Weber, A. (1967) 'Simulation of Three-Dimensional, Two-Phase Flow in Oil and Gas Reservoirs'. Society of Petroleum Engineers Journal 7 (04), 377-388

Court, B., Bandilla, K. W., Celia, M. A., Janzen, A., Dobossy, M., and Nordbotten, J. M. (2012) 'Applicability of Vertical-Equilibrium and Sharp-Interface Assumptions in CO_2 Sequestration Modeling'. International Journal of Greenhouse Gas Control 10, 134-147

Cowton, L., Neufeld, J., White, N., Bickle, M., Williams, G., White, J., and Chadwick, R. (2018) 'Benchmarking of Vertically-Integrated CO 2 Flow Simulations at the Sleipner Field, North Sea'. Earth and Planetary Science Letters 491, 121-133

De Silva, G., Ranjith, P., and Perera, M. (2015) 'Geochemical Aspects of CO_2 Sequestration in Deep Saline Aquifers: A Review'. Fuel 155, 128-143

Deng, H., Bielicki, J. M., Oppenheimer, M., Fitts, J. P., and Peters, C. A. (2017) 'Leakage Risks of Geologic CO_2 Storage and the Impacts on the Global Energy System and Climate Change Mitigation'. Climatic Change 144 (2), 151-163

Dice, L. R. (1945) 'Measures of the Amount of Ecologic Association between Species'. Ecology 26 (3), 297-302

Doughty, C. (2010) 'Investigation of CO_2 Plume Behavior for a Large-Scale Pilot Test of Geologic Carbon Storage in a Saline Formation'. Transport in Porous Media 82 (1), 49-76

Doughty, C. and Pruess, K. (2004) 'Modeling Supercritical Carbon Dioxide Injection in Heterogeneous Porous Media'. Vadose Zone Journal 3 (3), 837-847

Dumont, M., Marée, R., Wehenkel, L., and Geurts, P. (2009) Fast Multi-Class Image Annotation with Random Subwindows and Multiple Output Randomized Trees.

Ennis-King, J. and Paterson, L. (eds.) (2003) Greenhouse Gas Control Technologies-6th International Conference. 'Rate of Dissolution due to Convective Mixing in the Underground Storage of Carbon Dioxide'. Pergamon: Elsevier

Ennis-King, J. and Paterson, L. (2005) 'Role of Convective Mixing in the Long-Term Storage of Carbon Dioxide in Deep Saline Formations'

Espinoza, D. N. and Santamarina, J. C. (2017) CO_2 breakthrough—Caprock Sealing Efficiency and Integrity for Carbon Geological Storage [online] . available from <http://www.sciencedirect.com/science/article/pii/S1750583617305601>

Finley, R. (ed.) (2009) 2009 Portland GSA Annual Meeting. 'An Integrated Carbon Sequestration Deployment Test at Decatur, Illinois'

Flett, M., Gurton, R., and Weir, G. (2007) 'Heterogeneous Saline Formations for Carbon Dioxide Disposal: Impact of Varying Heterogeneity on Containment and Trapping'. Journal of Petroleum Science and Engineering 57 (1-2), 106-118

Forster, A., Norden, B., Zinck-Jørgensen, K., Frykman, P., Kulenkampff, J., Spangenberg, E., Erzinger, J., Zimmer, M., Kopp, J., and Borm, G. (2006) 'Baseline Characterization of the CO_2SINK Geological Storage Site at Ketzin, Germany'. Environmental Geosciences 13 (3), 145-161

Fossen, H. (2010) 'Folds and Folding'. in Structural Geology. ed. by AnonCambridge: Cambridge University Press, 219-242

Friedmann, S. J. and Stamp, V. W. (2006) 'Teapot Dome: Characterization of a CO_2-Enhanced Oil Recovery and Storage Site in Eastern Wyoming'. Environmental Geosciences 13 (3), 181-199

Furre, A., Meneguolo, R., Ringrose, P., and Kassold, S. (2019) 'Building Confidence in CCS: From Sleipner to the Northern Lights Project'. First Break 37 (7), 83-89

Furre, A., Eiken, O., Alnes, H., Vevatne, J. N., and Kiær, A. F. (2017) '20 Years of Monitoring CO_2 Injection at Sleipner'. Energy Procedia 114, 3916-3926

Galloway, W. E. (1984) 'Reservoir Facies Architecture in a Micro-Tidal Barrier System, Frio Formation, Texas Gulf Coast'. AAPG Bulletin 68 (4), 478-478

Gammer, D., Green, A., Holloway, S., and Smith, G. (eds.) SPE Offshore Europe Oil and Gas Conference Aberdeen. 'The Energy Technologies Institute's UK CO_2 Storage Appraisal Project (UKSAP)'. held 2011: Society of Petroleum Engineers

Gasda, S. E., Nilsen, H. M., and Dahle, H. K. (2013) 'Impact of Structural Heterogeneity on Upscaled Models for Large-Scale CO_2 Migration and Trapping in Saline Aquifers'. Advances in Water Resources 62, 520-532

Gasda, S. E., Nordbotten, J. M., and Celia, M. A. (2012) 'Application of Simplified Models to CO_2 Migration and Immobilization in Large-Scale Geological Systems'. International Journal of Greenhouse Gas Control 9, 72-84

Gasda, S. E., Nordbotten, J. M., and Celia, M. A. (2009) 'Vertical Equilibrium with Sub-Scale Analytical Methods for Geological CO_2 Sequestration'. Computational Geosciences 13 (4), 469

Gasda, S., Celia, M., and Nordbotten, J. (2008) 'Upslope Plume Migration and Implications for Geological CO_2 Sequestration in Deep, Saline Aquifers'. The IES Journal Part A: Civil & Structural Engineering 1 (1), 2-16

Gasda, S. E., Nilsen, H. M., Dahle, H. K., and Gray, W. G. (2012) 'Effective Models for CO_2 Migration in Geological Systems with Varying Topography'. Water Resources Research 48 (10)

Gérard, A., Genter, A., Kohl, T., Lutz, P., Rose, P., and Rummel, F. (2006) The Deep EGS (Enhanced Geothermal System) Project at Soultz-Sous-Forêts (Alsace, France) [online] . available from <http://www.sciencedirect.com/science/article/pii/S0375650506000800>

Ghosh, R., Sen, M. K., and Vedanti, N. (2015) 'Quantitative Interpretation of CO_2 Plume from Sleipner (North Sea), using Post-Stack Inversion and Rock Physics Modeling'. International Journal of Greenhouse Gas Control [online] 32, 147-158

Goater, A. L., Bijeljic, B., and Blunt, M. J. (2013) 'Dipping Open Aquifers-the Effect of Top-Surface Topography and Heterogeneity on CO_2 Storage Efficiency'. International Journal of Greenhouse Gas Control 17, 318-331

Goldberger, J., Roweis, S., Hinton, G., and Salakhutdinov, R. (2004) Neighbourhood Components Analysis.

Grant, T., Guinan, A., Shih, C. Y., Lin, S., Vikara, D., Morgan, D., and Remson, D. (2018) Comparative Analysis of Transport and Storage Options from a CO_2 Source Perspective [online]. available from <http://www.sciencedirect.com/science/article/pii/S1750583617307120>

Grataloup, S., Bonijoly, D., Brosse, E., Dreux, R., Garcia, D., Hasanov, V., Lescanne, M., Renoux, P., and Thoraval, A. (2009) A Site Selection Methodology for CO_2 Underground Storage in Deep Saline Aquifers: Case of the Paris Basin [online]. available from <http://www.sciencedirect.com/science/article/pii/S1876610209007115>

Gregersen, U. and Johannessen, P. (2001) 'The Neogene Utsira Sand and its Seal in the Viking Graben Area, North Sea Saline Aquifer CO_2 Storage (SACS) Project, Phase 2 Task 1.7 Geology'. Geological Survey of Denmark and Greenland Report 100 (2001), 1-2

Gunter, W., Wiwehar, B., and Perkins, E. (1997) 'Aquifer Disposal of CO_2-Rich Greenhouse Gases: Extension of the Time Scale of Experiment for CO_2-Sequestering Reactions by Geochemical Modelling'. Mineralogy and Petrology 59 (1-2), 121-140

Gunter, W. D., Bachu, S., and Benson, S. (2004) 'The Role of Hydrogeological and Geochemical Trapping in Sedimentary Basins for Secure Geological Storage of Carbon Dioxide'. Geological Society, London, Special Publications 233 (1), 129-145

Gussow, W. C. (1968) 'Migration of Reservoir Fluids'. Journal of Petroleum Technology 20 (04), 353-365

Gussow, W. C. (1954) 'Differential Entrapment of Oil and Gas: A Fundamental Principle'. AAPG Bulletin 38 (5), 816-853

Haghbakhsh, R., Hayer, H., Saidi, M., Keshtkari, S., and Esmaeilzadeh, F. (2013) Density Estimation of Pure Carbon Dioxide at Supercritical Region and Estimation Solubility of Solid Compounds in Supercritical Carbon Dioxide: Correlation Approach Based on Sensitivity Analysis [online]. available from <http://www.sciencedirect.com/science/article/pii/S0378381213000058>

Haghighat, S. A., Mohaghegh, S. D., Gholami, V., Shahkarami, A., and Moreno, D. A. (eds.) (2013) SPE Annual Technical Conference and Exhibition. 'Using Big Data and Smart Field Technology for Detecting Leakage in a CO_2 Storage Project': Society of Petroleum Engineers

Han, W. S., Kim, K., Esser, R. P., Park, E., and McPherson, B. J. (2011) 'Sensitivity Study of Simulation Parameters Controlling CO_2 Trapping Mechanisms in Saline Formations'. Transport in Porous Media 90 (3), 807-829

Han, W. S. and Kim, K. (2018a) 'Evaluation of CO_2 Plume Migration and Storage Under Dip and Sinusoidal Structures in Geologic Formation'. Journal of Petroleum Science and Engineering [online] 169, 760-771

Han, W. S. and Kim, K. (2018b) Evaluation of CO_2 Plume Migration and Storage Under Dip and Sinusoidal Structures in Geologic Formation [online] . available from <http://www.sciencedirect.com/science/article/pii/S0920410518302407>

Hansen, H., Eiken, O., and Aasum, T. (2005) 'Tracing the Path of Carbon Dioxide from a Gas-Condensate Reservoir, through an Amine Plant and Back into a Subsurface Aquifer. Case Study: The Sleipner Area, Norwegian North Sea'. Society of Petroleum Engineers 96742

Hansen, O., Gilding, D., Nazarian, B., Osdal, B., Ringrose, P., Kristoffersen, J., Eiken, O., and Hansen, H. (2013) 'Snøhvit: The History of Injecting and Storing 1 Mt CO_2 in the Fluvial Tubåen Fm'. Energy Procedia 37, 3565-3573

Hassanzadeh, H., Pooladi-Darvish, M., and Keith, D. W. (2009) 'Accelerating CO_2 Dissolution in Saline Aquifers for Geological Storage・ Mechanistic and Sensitivity Studies'. Energy & Fuels 23 (6), 3328-3336

Head, M. J., Riding, J. B., Eidvin, T., and Chadwick, R. A. (2004) 'Palynological and Foraminiferal Biostratigraphy of (Upper Pliocene) Nordland Group Mudstones at Sleipner, Northern North Sea'. Marine and Petroleum Geology [online] 21 (3), 277-297

Hermanrud, C., Bolås, H. N., Teige, G., Nilsen, H., and KIær, A. (eds.) (2012) Third EAGE CO_2 Geological Storage Workshop. 'Hermanrud C, Bolås HN, Teige GM, Nilsen HM, KIær AF. History-Matching of CO_2 Flow at Sleipner–new Insight Based on Analyses of Temperature and Seismic Data'. held 2012: European Association of Geoscientists & Engineers

Hermanrud, C., Andresen, T., Eiken, O., Hansen, H., Janbu, A., Lippard, J., Bolås, H. N., Simmenes, T. H., Teige, G. M. G., and Østmo, S. (2009) Storage of CO_2 in Saline aquifers–Lessons Learned from 10 Years of Injection into the Utsira Formation in the Sleipner Area [online] . available from <http://www.sciencedirect.com/science/article/pii/S1876610209002616>

Hesse, M., Tchelepi, H., Cantwel, B., and Orr, F. (2007) 'Gravity Currents in Horizontal Porous Layers: Transition from Early to Late Self-Similarity'. Journal of Fluid Mechanics [online] 577, 363-383. available from <https://www.cambridge.org/core/article/gravity-currents-in-horizontal-porous-layers-transition-from-early-to-late-selfsimilarity/563E818F984AF6C4953A41C4BEADB856> [2017/07/04]

Hnottavange-Telleen, K., Krapac, I., and Vivalda, C. (2009) 'Illinois Basin-Decatur Project: Initial Risk-Assessment Results and Framework for Evaluating Site Performance'. Energy Procedia 1 (1), 2431-2438

Hodneland, E., Gasda, S., Kaufmann, R., Bekkvik, T. C., Hermanrud, C., and Midttømme, K. (2019) 'Effect of Temperature and Concentration of Impurities in the Fluid Stream on CO_2 Migration in the Utsira Formation'. International Journal of Greenhouse Gas Control 83, 20-28

Holloway, S., Chadwick, R., Kirby, G., Pearce, J., Gregersen, U., Johannessen, P., Kristensen, L., Zweigel, P., Lothe, A., and Arts, R. (2000) Saline Aquifer CO_2 Storage (SACS)–Final Report: Work Area 1 (Geology): BGS report, 31pp., Commercial–in confidence

Hovorka, S. D., Benson, S. M., Doughty, C., Freifeld, B. M., Sakurai, S., Daley, T. M., Kharaka, Y. K., Holtz, M. H., Trautz, R. C., and Nance, H. S. (2006) 'Measuring Permanence of CO_2 Storage in Saline Formations: The Frio Experiment'. Environmental Geosciences 13 (2), 105-121

Huang, F., Juhlin, C., Han, L., Kempka, T., Norden, B., Lüth, S., and Zhang, F. (eds.) (2015) 2015 SEG Annual Meeting. 'Application of Seismic Complex Decomposition on Thin Layer Detection of the CO_2 Plume at Ketzin, Germany': Society of Exploration Geophysicists

Jackson, C. A., Grunhagen, H., Howell, J. A., Larsen, A. L., Andersson, A., Boen, F., and Groth, A. (2010) '3D Seismic Imaging of Lower Delta-Plain Beach Ridges: Lower Brent Group, Northern North Sea'. Journal of the Geological Society 167 (6), 1225-1236

Jansen, J. (2011) 'Adjoint-Based Optimization of Multi-Phase Flow through Porous media–A Review'. Computers & Fluids 46 (1), 40-51

Jin, M., Pickup, G., Mackay, E., Todd, A., Sohrabi, M., Monaghan, A., and Naylor, M. (2012) 'Static and Dynamic Estimates of CO_2 Storage Capacity in Two Saline Formations in the UK' 17 (4), 1-8

Jing, J., Yuan, Y., Yang, Y., Wang, F., and Yang, Z. (2014) 'The Influentialstudy of Formatin Dip for CO 2 Geological Storage-Taking OrdosCCS Project for Example'. Geotechnical Investigation & Surveying 6, 39-44

Jones, R. R., McCaffrey, K. J. W., Clegg, P., Wilson, R. W., Holliman, N. S., Holdsworth, R. E., Imber, J., and Waggott, S. (2009) 'Integration of Regional to Outcrop Digital Data: 3D Visualisation of Multi-Scale Geological Models'. Computers & Geosciences 35 (1), 4-18

Juanes, R., Spiteri, E., Orr, F., and Blunt, M. (2006) 'Impact of Relative Permeability Hysteresis on Geological CO_2 Storage'. Water Resources Research 42 (12)

Kelemen, P., Benson, S. M., Pilorgé, H., Psarras, P. C., and Wilcox, J. (2019) 'An Overview of the Status and Challenges of CO_2 Storage in Minerals and Geological Formations'. Frontiers in Climate 1, 9

Kohl, A. L. and Nielsen, R. (1997) Gas Purification.: Elsevier

Korbøl, R. and Kaddour, A. (1995) 'Sleipner Vest CO_2 Disposal - Injection of Removed CO_2 into the Utsira Formation'. Energy Conversion and Management [online] 36 (6), 509-512

Kumar, A., Noh, M. H., Ozah, R. C., Pope, G. A., Bryant, S. L., Sepehrnoori, K., and Lake, L. W. (2005) 'Reservoir Simulation of CO_2 Storage in Aquifers'. SPE Journal 10 (03), 336-348

Larsen, M., Bech, N., Bidstrup, T., Christensen, N. P., Vangkilde-Pedersen, T., and Biede, O. (2007) 'Kalundborg Case Study, a Feasibility Study of CO_2 Storage in Onshore Saline Aquifers'. CO2STORE.GEUS Report 2, 2007

Leetaru, H., Couëslan, M., and McBride, J. (2009) 'Seismic Reflection Data Interpretation of the Proposed Illinois Basin-Decatur Carbon Sequestration Site Topical Report 1: An Assessment of Geological Carbon Sequestration Options in the Illinois Basin: Phase III'. Report Submitted by Illinois State Geological Survey to US DOE

Li, C., Zhang, K., Wang, Y., Guo, C., and Maggi, F. (2016) 'Experimental and Numerical Analysis of Reservoir Performance for Geological CO_2 Storage in the Ordos Basin in China'. International Journal of Greenhouse Gas Control 45, 216-232

Li, B. and Benson, S. M. (2015) Influence of Small-Scale Heterogeneity on Upward CO_2 plume Migration in Storage Aquifers [online]. available from <http://www.sciencedirect.com/science/article/pii/S0309170815001578>

Lie, K. (2019) An Introduction to Reservoir Simulation using MATLAB/GNU Octave.: Cambridge University Press

Lindeberg, E., Zweigel, P., Bergmo, P., Ghaderi, A., and Lothe, A. (2001) 'Prediction of CO_2 Distribution Pattern Improved by Geology and Reservoir Simulation and Verified by Time Lapse Seismic'. Greenhouse Gas Control Technologies 372, 377

Lothe, A. and Zweigel, P. (1999) Saline Aquifer CO_2 Storage (SACS). Informal Annual Report 1999 of SINTEF Petroleum Research's Results in Work Area 1 'Reservoir Geology'.: SINTEF Petroleum Research report 23.4300. 00/03/99, 54 p. Restricted

Lu, J., Kordi, M., Hovorka, S., Meckel, T., and Christopher, C. (2013) 'Reservoir Characterization and Complications for Trapping Mechanisms at Cranfield CO_2 Injection Site'. International Journal of Greenhouse Gas Control 18, 361-374

Lu, J., Kharaka, Y. K., Thordsen, J. J., Horita, J., Karamalidis, A., Griffith, C., Hakala, J. A., Ambats, G., Cole, D. R., and Phelps, T. J. (2012) 'CO_2–rock–brine Interactions in Lower Tuscaloosa Formation at Cranfield CO2 Sequestration Site, Mississippi, USA'. Chemical Geology 291, 269-277

Lundberg, S. M. and Lee, S. (eds.) (2017) Advances in Neural Information Processing Systems. 'A Unified Approach to Interpreting Model Predictions'

Lüth, S., Ivanova, A., and Kempka, T. (2015) 'Conformity Assessment of Monitoring and Simulation of CO_2 Storage: A Case Study from the Ketzin Pilot Site'. International Journal of Greenhouse Gas Control 42, 329-339

Maldal, T. and Tappel, I. (2004) 'CO_2 Underground Storage for Snøhvit Gas Field Development'. Energy 29 (9-10), 1403-1411

Manceau, J. and Rohmer, J. (2016) 'Post-Injection Trapping of Mobile CO_2 in Deep Aquifers: Assessing the Importance of Model and Parameter Uncertainties'. Computational Geosciences 20 (6), 1251-1267

Manceau, J. and Rohmer, J. (2014) 'Ranking Importance of Uncertainties for the Assessment of Residual and Dissolution Trapping of CO_2 on a Large-Scale Storage Site'. Energy Procedia 63, 3658-3664

Martin, J. C. (1968) 'Partial Integration of Equations of Multiphase Flow'. Society of Petroleum Engineers Journal 8 (04), 370-380

Martin, J. C. (1958) 'Some Mathematical Aspects of Two Phase Flow with Application to Flooding and Gravity Segregation'. Prod.Monthly 22 (6), 22-35

Metz, B., Davidson, O., De Coninck, H., Loos, M., and Meyer, L. (2005). IPCC Special Report on Carbon Dioxide Capture and Storage

Miall, A. D. (2013) The Geology of Fluvial Deposits: Sedimentary Facies, Basin Analysis, and Petroleum Geology.: Springer

Michael, K., Allinson, G., Golab, A., Sharma, S., and Shulakova, V. (2009) CO_2 Storage in Saline Aquifers II–Experience from Existing Storage Operations [online] . available from <http://www.sciencedirect.com/science/article/pii/S1876610209002586>

Mito, S., Xue, Z., and Ohsumi, T. (2008) 'Case Study of Geochemical Reactions at the Nagaoka CO_2 Injection Site, Japan'. International Journal of Greenhouse Gas Control 2 (3), 309-318

Morton, R. A., Jirik, L., and Galloway, W. B. (1988) Middle-Upper Miocene Depositional Sequences of the Texas Coastal Plain and Continental Shelf: Geologic Framework, Sedimentary Facies, and Hydrocarbon Plays.: Bureau of Economic Geology, University of Texas at Austin

Mountney, N. P. (2012) 'A Stratigraphic Model to Account for Complexity in Aeolian Dune and Interdune Successions'. Sedimentology 59 (3), 964-989

Mountney, N. P., Posamentier, H., and Walker, R. (eds.) (2006) Eolian Facies Models. Tulsa: SEPM (Society for Sedimentary Geology)

Møyner, O., Andersen, A., and Nilsen, H. M. (eds.) (2018) ECMOR XVI-16th European Conference on the Mathematics of Oil Recovery. 'Multi-Model Hybrid Compositional Simulator with Application to Segregated Flow'

Møyner, O. and Nilsen, H. M. (2017) 'Multiresolution Coupled Vertical Equilibrium Model for Fast Flexible Simulation of CO_2 Storage'. Computational Geosciences 23.1 (2019): 1-20.

Newell, P. and Ilgen, A. G. (2019) 'Overview of Geological Carbon Storage (GCS)'. in Science of Carbon Storage in Deep Saline Formations. ed. by Anon: Elsevier, 1-13

Nilsen, H. M., Krogstad, S., Andersen, O., Allen, R., and Lie, K. A. (2017) 'Using Sensitivities and Vertical-Equilibrium Models for Parameter Estimation of CO_2 Injection Models with Application to Sleipner Data'. Energy Procedia 114, 3476-3495

Nilsen, H. M., Lie, K. A., and Andersen, O. (2016a) 'Robust Simulation of Sharp-Interface Models for Fast Estimation of CO_2 Trapping Capacity in Large-Scale Aquifer Systems'. Computational Geosciences 20 (1), 93-113

Nilsen, H. M., Lie, K. A., and Andersen, O. (2016b) 'Fully-Implicit Simulation of Vertical-Equilibrium Models with Hysteresis and Capillary Fringe'. Computational Geosciences 20 (1), 49-67

Nilsen, H. M., Herrera, P., Ashraf, S. M., Ligaard, I. S., Iding, M., Hermanrud, C., Lie, K. A., Nordbotten, J. M., and Keilegavlen, E. (2011a) 'Field-Case Simulation of CO_2-Plume Migration using Vertical-Equilibrium Models'. Energy Procedia 4, 3801-3808

Nilsen, H. M., Herrera, P. A., Ashraf, M., Ligaarden, I., Iding, M., Hermanrud, C., Lie, K. A., Nordbotten, J. M., Dahle, H. K., and Keilegavlen, E. (2011b) Field-Case Simulation of CO_2 plume Migration using Vertical-Equilibrium Models [online] . available from <http://www.sciencedirect.com/science/article/pii/S1876610211005947>

Nilsen, H. M., Lie, K. A., and Andersen, O. (2015) 'Analysis of CO_2 Trapping Capacities and Long-Term Migration for Geological Formations in the Norwegian North Sea using MRST-Co2lab'. Computers & Geosciences 79, 15-26

Nilsen, H. M., Lie, K. A., Møyner, O., and Andersen, O. (2015) 'Spill-Point Analysis and Structural Trapping Capacity in Saline Aquifers using MRST-CO2lab'. Computers & Geosciences [online] 75, 33-43

Nilsen, H. M., Syversveen, A. R., Lie, K. A., Tveranger, J., and Nordbotten, J. M. (2012) 'Impact of Top-Surface Morphology on CO_2 Storage Capacity'. International Journal of Greenhouse Gas Control 11, 221-235

Nooner, S. L., Eiken, O., Hermanrud, C., Sasagawa, G. S., Stenvold, T., and Zumberge, M. A. (2007) 'Constraints on the in Situ Density of CO_2 within the Utsira Formation from Time-Lapse Seafloor Gravity Measurements'. International Journal of Greenhouse Gas Control 1 (2), 198-214

Nordbotten, J. M. and Celia, M. A. (2011) Geological Storage of CO_2: Modeling Approaches for Large-Scale Simulation.: John Wiley & Sons

Nordbotten, J. M., Flemisch, B., Gasda, S. E., Nilsen, H. M., Fan, Y., Pickup, G. E., Wiese, B., Celia, M. A., Dahle, H. K., Eigestad, G. T., and Pruess, K. (2012) Uncertainties in Practical Simulation of CO_2 Storage [online] . available from <http://www.sciencedirect.com/science/article/pii/S1750583612000655>

Olivier, J. G., Schure, K., and Peters, J. (2017) 'Trends in Global CO_2 and Total Greenhouse Gas Emissions'. PBL Netherlands Environmental Assessment Agency, 5

Onoja, M. U. and Shariatipour, S. M. (2018) The Impact of Gradational Contact at the Reservoir-Seal Interface on Geological CO2 Storage Capacity and Security [online] . available from <http://www.sciencedirect.com/science/article/pii/S1750583617309234>

Orr, F. M. (2009) 'Onshore Geologic Storage of CO_2'. Science 325 (5948), 1656

Perera, M. S. A., Ranjith, P. G., Airey, D. W., and Choi, S. K. (2011) Sub- and Super-Critical Carbon Dioxide Flow Behavior in Naturally Fractured Black Coal: An Experimental Study [online]. available from <http://www.sciencedirect.com/science/article/pii/S001623611100278X>

Pickup, G., Jin, M., Olden, P., Mackay, E., and Sohrabi, M. (eds.) (2011) SPE EUROPEC/EAGE Annual Conference and Exhibition. 'A Sensitivity Study on CO_2 Storage in Saline Aquifers': Society of Petroleum Engineers

Pickup, G. E., Jin, M., Olden, P., Mackay, E., Todd, A. C., Ford, J., Lawrence, D., Monaghan, A., Naylor, M., and Haszeldine, R. (2011) 'Geological Storage of CO_2: Site Appraisal and Modelling'. Energy Procedia 4, 4762-4769

Potdar, R. S. and Vishal, V. (2016) 'Trapping Mechanism of CO_2 Storage in Deep Saline Aquifers: Brief Review'. in Geologic Carbon Sequestration. ed. by Anon: Springer, 47-58

Pringle, J. K., Brunt, R. L., Hodgson, D. M., and Flint, S. S. (2010) 'Capturing Stratigraphic and Sedimentological Complexity from Submarine Channel Complex Outcrops to Digital 3D Models, Karoo Basin, South Africa'. Petroleum Geoscience 16 (4), 307-330

Pruess, K., Xu, T., Apps, J., and Garcia, J. (eds.) (2001) SPE/EPA/DOE Exploration and Production Environmental Conference. 'Pruess K, Xu T, Apps J, Garcia J. Numerical Modeling of Aquifer Disposal of CO_2': Society of Petroleum Engineers

Pruess, K. and Nordbotten, J. (2011) 'Numerical Simulation Studies of the Long-Term Evolution of a CO_2 Plume in a Saline Aquifer with a Sloping Caprock'. Transport in Porous Media 90 (1), 135-151

Pruess, K. and Zhang, K. (2008) Numerical Modeling Studies of the Dissolution-Diffusion-Convection Process during CO_2 Storage in Saline Aquifers: Lawrence Berkeley National Lab.(LBNL), Berkeley, CA (United States)

Pruess, K. and Nordbotten, J. M. (2011) 'Numerical Simulation Studies of the Long-Term Evolution of a CO_2 Plume in a Saline Aquifer with a Sloping Caprock'. Transport in Porous Media 90 (1), 135-151

Reading, H. G. (2009) Sedimentary Environments: Processes, Facies and Stratigraphy.: John Wiley & Sons

Riaz, A., Hesse, M., Tchelepi, H., and Orr, F. (2006) 'Onset of Convection in a Gravitationally Unstable Diffusive Boundary Layer in Porous Media'. Journal of Fluid Mechanics 548, 87-111

Richards, F. L., Richardson, N. J., Bond, C. E., and Cowgill, M. (2015) 'Interpretational Variability of Structural Traps: Implications for Exploration Risk and Volume Uncertainty'. Geological Society, London, Special Publications 421 (1), 7-27

Riddiford, F., Wright, I., Bishop, C., Espie, T., and Tourqui, A. (2005) 'Monitoring Geological Storage the in Salah Gas CO_2 Storage Project'. in Greenhouse Gas Control Technologies 7. ed. by Anon: Elsevier, 1353-1359

Ringrose, P. and Oldenburg, C. (2018) 'Mission Innovation Task Force Reports on Enabling Gigatonne-Scale CO_2 Storage'. First Break 36 (7), 67-72

Rodosta, T. D., Litynski, J. T., Plasynski, S. I., Hickman, S., Frailey, S., and Myer, L. (2011) U.S. Department of Energy's Site Screening, Site Selection, and Initial Characterization for Storage of CO_2 in Deep Geological Formations [online] . available from <http://www.sciencedirect.com/science/article/pii/S1876610211007065>

Sadri, M., Shariatipour, S. M., Hunt, A., and Ahmadinia, M. (2019) 'Effect of Systematic and Random Flow Measurement Errors on History Matching: A Case Study on Oil and Wet Gas Reservoirs'. Journal of Petroleum Exploration and Production Technology 9 (4), 1-10

Santi A., Furre A.K., and Ringrose P. (2020) Sleipner 2019 Benchmark Model and Supporting Documentation.: Equinor

Saripalli, P. and McGrail, P. (2002) Semi-Analytical Approaches to Modeling Deep Well Injection of CO_2 for Geological Sequestration [online]. available from <http://www.sciencedirect.com/science/article/pii/S0196890401000176>

Schieber, J., Zimmerle, W., and Sethi, P. S. (1998) 'Shales and Mudstones, Vols. I and II'

Schilling, F., Borm, G., Würdemann, H., Möller, F., Kühn, M., and CO_2 SINK Group (2009) 'Status Report on the First European on-Shore CO_2 Storage Site at Ketzin (Germany)'. Energy Procedia 1 (1), 2029-2035

Schlumberger (2017) ECLIPSE Technical Description: Schlumberger

Shariatipour, S. M., Pickup, G. E., and Mackay, E. J. (2016) 'Simulations of CO_2 Storage in Aquifer Models with Top Surface Morphology and Transition Zones'. International Journal of Greenhouse Gas Control 54, Part 1, 117-128

Shariatipour, S. M., Pickup, G. E., and Mackay, E. J. (2016) 'Investigation of CO_2 Storage in a Saline Formation with an Angular Unconformity at the Caprock Interface'. Petroleum Geoscience 22 (2), 203-210

Silva, V. L. S., Emerick, A. A., Couto, P., and Alves, J. L. D. (2017) 'History Matching and Production Optimization Under Uncertainties-Application of Closed-Loop Reservoir Management'. Journal of Petroleum Science and Engineering 157, 860-874

Singh VP, Cavanagh A, Hansen H, Nazarian B, Iding M, and Ringrose PS (eds.) (2010) SPE Annual Technical Conference and Exhibition. 'Singh VP; Cavanagh A; Hansen H;

Nazarian B; Iding M; Ringrose PS. Reservoir Modeling of CO_2 Plume Behavior Calibrated Against Monitoring Data from Sleipner, Norway'. held 2010: Society of Petroleum Engineers

Smith, M., Campbell, D., Mackay, E., and Polson, D. (2012) CO_2 Aquifer Storage Site Evaluation and Monitoring: Understanding the Challenges of CO_2 Storage: Results of the CASSEM Project.: Scottish Carbon Capture and Storage

Sørensen, T. J. (1948) A Method of Establishing Groups of Equal Amplitude in Plant Sociology Based on Similarity of Species Content and its Application to Analyses of the Vegetation on Danish Commons.: København, I kommission hos E. Munksgaard

Span, R., Eckermann, T., Herrig, S., Hielscher, S., Jager, A., and Thol, M. (2015) 'TREND. Thermodynamic Reference and Engineering Data 2.0'. Ruhr-Universitaet Bochum, Bochum, Germany

Spycher, N. and Pruess, K. (2005) 'CO_2-H_2O Mixtures in the Geological Sequestration of CO_2. II. Partitioning in Chloride Brines at 12–100 C and Up to 600 Bar'. Geochimica Et Cosmochimica Acta 69 (13), 3309-3320

Tin Kam Ho (1995) Random Decision Forests.

Torp, T. A. and Gale, J. (2004) 'Demonstrating Storage of CO_2 in Geological Reservoirs: The Sleipner and SACS Projects'. Energy [online] 29 (9), 1361-1369

Torp, T. A. and Gale, J. (2003) 'Demonstrating Storage of CO_2 in Geological Reservoirs: The Sleipner and Sacs Projects'. in Greenhouse Gas Control Technologies - 6[Th] International Conference. ed. by Gale, J. and Kaya, Y. Oxford: Pergamon, 311-316

Trevisan, L., Krishnamurthy, P., and Meckel, T. (2017) 'Impact of 3D Capillary Heterogeneity and Bedform Architecture at the Sub-Meter Scale on CO_2 Saturation for Buoyant Flow in Clastic Aquifers'. International Journal of Greenhouse Gas Control 56, 237-249

Tucker, M. E. (2011) Sedimentary Rocks in the Field: A Practical Guide.: John Wiley & Sons

UNFCCC, V. (2015) 'Adoption of the Paris Agreement'. I: Proposal by the President (Draft Decision), United Nations Office, Geneva (Switzerland) (s 32)

Vandenberghe, N., Dusar, M., Boonen, P., Fan, S. L., Voets, R., and Bouckaert, J. (2000) 'The Merksplas-Beerse Geothermal Well (17W265) and the Dinantian Reservoir'. Geol Belg 3, 349-367

Vine, J. D. and Tourtelot, E. B. (1970) 'Geochemistry of Black Shale Deposits; a Summary Report'. Economic Geology 65 (3), 253-272

Wang, F., Jing, J., Yang, Y., Liu, H., Sun, Z., Xu, T., and Tian, H. (2017) 'Impacts of Injection Pressure of a Dip-angle Sloping Strata Reservoir with Low Porosity and Permeability on CO2 Injection Amount'. Greenhouse Gases: Science and Technology 7 (1), 92-105

Wang, F., Jing, J., Xu, T., Yang, Y., and Jin, G. (2016) 'Impacts of Stratum Dip Angle on CO_2 Geological Storage Amount and Security'. Greenhouse Gases: Science and Technology 6 (5), 682-694

Warren, J. K. (2017) Salt Usually Seals, but Sometimes Leaks: Implications for Mine and Cavern Stabilities in the Short and Long Term [online]. available from <http://www.sciencedirect.com/science/article/pii/S0012825216304482>

Wei, N., Li, X., Wang, Y., Dahowski, R. T., Davidson, C. L., and Bromhal, G. S. (2013) A Preliminary Sub-Basin Scale Evaluation Framework of Site Suitability for Onshore Aquifer-Based CO_2 Storage in China [online]. available from <http://www.sciencedirect.com/science/article/pii/S1750583612002459>

White, J. C., Williams, G., Chadwick, A., Furre, A., and Kiær, A. (2018) 'Sleipner: The Ongoing Challenge to Determine the Thickness of a Thin CO_2 Layer'. International Journal of Greenhouse Gas Control 69, 81-95

White, J. C., Williams, G. A., Grude, S., and Chadwick, R. A. (2015) 'Utilizing Spectral Decomposition to Determine the Distribution of Injected CO_2 at the Snøhvit Field'. Geophysical Prospecting 63 (5), 1213-1223

White, J. A., Chiaramonte, L., Ezzedine, S., Foxall, W., Hao, Y., Ramirez, A., and McNab, W. (2014) 'Geomechanical Behavior of the Reservoir and Caprock System at the in Salah CO_2 Storage Project'. Proceedings of the National Academy of Sciences of the United States of America 111 (24), 8747-8752

White, J. C., Williams, G. A., and Chadwick, R. A. (2013) Thin Layer Detectability in a Growing CO2 Plume: Testing the Limits of Time-Lapse Seismic Resolution [online] . available from <http://www.sciencedirect.com/science/article/pii/S187661021300581X>

Williams, G. and Chadwick, A. (2012) 'Quantitative Seismic Analysis of a Thin Layer of CO_2 in the Sleipner Injection Plume'. Geophysics 77 (6), R245-R256

Wilson, I. G. (1972) 'Aeolian Bedforms—their Development and Origins'. Sedimentology 19 (3-4), 173-210

Wolfson, R. and Wissler, B. (2007) Energy, Environment, and Climate.: WW Norton & Company, Inc.

Worth, K., White, D., Chalaturnyk, R., Sorensen, J., Hawkes, C., Rostron, B., Risk, D., Young, A., and Sacuta, N. (2017) 'Aquistore: Year One–injection, Data, Results'. Energy Procedia 114, 5624-5635

Worth, K., White, D., Chalaturnyk, R., Sorensen, J., Hawkes, C., Rostron, B., Johnson, J., and Young, A. (2014) Aquistore Project Measurement, Monitoring, and Verification: From Concept to CO_2 Injection [online]. available from <http://www.sciencedirect.com/science/article/pii/S1876610214021602>

Zhang, D. and Song, J. (2014a) 'Mechanisms for Geological Carbon Sequestration'. Procedia IUTAm 10, 319-327

Zhang, D. and Song, J. (2014b) Mechanisms for Geological Carbon Sequestration [online] . available from <http://www.sciencedirect.com/science/article/pii/S2210983814000285>

Zhang, Z. and Huisingh, D. (2017) Carbon Dioxide Storage Schemes: Technology, Assessment and Deployment [online]. available from <http://www.sciencedirect.com/science/article/pii/S0959652616308861>

Zhou, Q., Birkholzer, J. T., Tsang, C., and Rutqvist, J. (2008) 'A Method for Quick Assessment of CO_2 Storage Capacity in Closed and Semi-Closed Saline Formations'. International Journal of Greenhouse Gas Control 2 (4), 626-639

Zhu, C., Zhang, G., Lu, P., Meng, L., and Ji, X. (2015) 'Benchmark Modeling of the Sleipner CO_2 Plume: Calibration to Seismic Data for the Uppermost Layer and Model Sensitivity Analysis'. International Journal of Greenhouse Gas Control 43, 233-246

Zweigel, P., Arts, R., Lothe, A. E., and Lindeberg, E. B. (2004) 'Reservoir Geology of the Utsira Formation at the First Industrial-Scale Underground CO_2 Storage Site (Sleipner Area, North Sea)'. Geological Society, London, Special Publications 233 (1), 165-180